Conectando las escalas cerebrales a través del análisis de la complejidad neural

Tesis de Doctorado en Ciencias Biológicas

Opción Neurociencias
Pedeciba Biología
UdelaR

Joaquin Gonzalez

Supervisor: Pablo Torterolo
Co-Supervisores: Ignacio Carreira, & Nicolas Rubido

Tribunal: Juan Valle-Lisboa, Jose Pedro Prieto, & Angel Caputti

Agradecimientos

A Pablo, Ignacio, y Nicolás por apoyarme durante todo este proceso. Además, quiero agradecer a Alvaro Cavana y Andres Pomi por formar parte de la CAS. Me hubiera gustado que pudieran también ser parte del tribunal.

Consciousness then is to be identified theoretically with a certain degree of complexity of phase sequence in which both central and sensory facilitation merge, the central acting to reinforce now one class of sensory stimulations, now another.

The Organization of Behavior, Donald Hebb.1949.

Abstract

La comprensión de la actividad cerebral en múltiples escalas es esencial para desentrañar las complejidades de la función neural. Desde el nivel macroscópico hasta el microscópico, el cerebro exhibe diversas dinámicas, moldeadas por miles de millones de neuronas y sus intrincadas conexiones sinápticas. Sin embargo, navegar a través de estas escalas presenta desafíos significativos debido a limitaciones técnicas y conceptuales. El análisis de la complejidad ofrece un marco prometedor para abordar estos desafíos, ofreciendo ideas sobre cómo la actividad neural se extiende a través de las escalas y cómo las alteraciones, como las inducidas por drogas, impactan en la función cerebral. Esta tesis explora la utilidad del análisis de la complejidad en el estudio de la actividad cerebral, enfatizando su papel en la navegación de las escalas neurales y en la elucidación de la compleja relación entre la dinámica neuronal microscópica y la función cerebral macroscópica. A través de esta perspectiva, nuestro objetivo es fomentar una comprensión más profunda de la complejidad cerebral y sus implicaciones para la investigación en neurociencia.

Keywords: EEG, LFP, sueño, REM, ibogaina, uretano, entropia

Introducción

Una multitud de escalas caracteriza la actividad cerebral [1–4]. El cerebro comprende miles de millones de neuronas, cada una con miles de conexiones sinápticas, formando una red vasta e interconectada [4–6]. Como resultado, la actividad cerebral abarca un rango de escalas que van desde lo macroscópico hasta lo microscópico. A nivel macroscópico, la actividad de las diferentes áreas cerebrales puede estudiarse a través de la resonancia magnética funcional (fMRI) [4,7] o la electroencefalografía (EEG) [8,9], capturando las dinámicas colectivas de grandes poblaciones de neuronas. A nivel mesoscópico, encontramos circuitos neuronales, donde diversos grupos de neuronas dan lugar a redes intrincadas que permiten que ocurran cálculos específicos [10–14]. Estas redes suelen estudiarse mediante potenciales locales de campo (LFP) [15] e imágenes de calcio [16]. Finalmente, a escala microscópica, los patrones de disparo de las neuronas individuales pueden estudiarse mediante registros de patch-clamp [17] o arrays de electrodos [18]. Estas técnicas nos permiten estudiar cómo el tiempo preciso y la frecuencia de los trenes de espigas codifican la información básica utilizada para diversos cálculos en distintas escalas.

Navegar a través de las escalas neuronales es un problema difícil [19–26]. Las dificultades surgen tanto de limitaciones técnicas como conceptuales, lo que dificulta nuestra capacidad para conectar observaciones en diferentes niveles de análisis. Si bien las técnicas imagenológicas, como la fMRI, ofrecen una excelente resolución espacial, a menudo carecen de la resolución temporal necesaria para capturar las dinámicas rápidas de la actividad neuronal individual. Por el contrario, los métodos electrofisiológicos sobresalen en el registro de las dinámicas temporales a escala de milisegundos de la actividad neuronal, pero están limitados por su cobertura espacial limitada, típicamente enfocándose en pequeñas poblaciones de neuronas o incluso células individuales. Es importante destacar que los nuevos métodos ópticos, como la imagen de calcio o de voltaje, prometen ofrecer tanto alta resolución espacial como temporal [27–30], pero estos métodos aún no se emplean tan ampliamente en el contexto de investigación y clínica como los mencionados anteriormente.

Además, el cerebro opera a través de una organización jerárquica de circuitos interconectados, donde la información se procesa e integra en múltiples niveles [33,34]. Por lo tanto, para comprender completamente el cerebro, es necesario saber cómo los cambios en la actividad a nivel de neuronas individuales se traducen en fenómenos emergentes a nivel de circuitos neuronales y dinámicas de todo el cerebro. Además, la naturaleza dinámica de la actividad cerebral añade otra capa de complejidad. La actividad neural es altamente dependiente del contexto, influenciada por factores como el estado conductual, la entrada sensorial y las señales neuromoduladoras [27,28,35–38]. Integrar estos factores dinámicos a través de las escalas presenta un desafío significativo, ya que la relación entre la actividad neural y el comportamiento puede ser no lineal y multifacética.

Dado que la actividad cerebral exhibe una amplia disposición temporal [39-41], la cual es observada a menudo en sistemas complejos [42], se han desarrollado diferentes herramientas en las últimas décadas para cuantificar directamente la complejidad de la actividad cerebral [43-45]. El uso de estas herramientas ha mostrado que la complejidad de las señales de EEG disminuye durante los estados de inconsciencia, como durante el sueño o la anestesia [45-47]. Sin embargo, estas señales macroscópicas tienen limitaciones

importantes: tienden a estar contaminadas por variables confundentes (por ejemplo, actividad muscular o movimientos oculares) y recuperar su fuente neural exacta a menudo es imposible. Por lo tanto, los patrones neuronales que causan los cambios de complejidad a lo largo de los estados de vigilia y sueño no han sido dilucidados.

Objetivos

1) Estudiar los estados cerebrales en base a la diversidad de patrones eléctricos corticales (complejidad neural).
2) Explorar cómo la actividad macroscópica cortical, registrada mediante el electrocorticograma, se relaciona con los patrones de descarga de neurona única.
3) Estudiar cómo la actividad de pequeñas poblaciones neuronales es capaz de afectar la diversidad de patrones electrográficos.

Hipotesis

La diversidad de patrones eléctricos corticales, complejidad neural, se asemeja a una cantidad conservada a distintas escalas neuronales. Es decir, los cambios en la complejidad neural en los distintos estados cerebrales (por ejemplo: vigilia, sueño) se mantiene constante independiente de que tipo de registro neuronal se emplee.

Lista de publicaciones incluidas en la tesis

1 González J, Cavelli M, Mondino A, et al. Decreased electrocortical temporal complexity distinguishes sleep from wakefulness. Sci Rep. 2019;9(1):18457. Published 2019 Dec 5. doi:10.1038/s41598-019-54788-6. **Pagina 7.**

2 González J, Cavelli M, Mondino A, et al. Electrocortical temporal complexity during wakefulness and sleep: an updated account. Sleep Science. Published online 2020. doi: 10.5935/1984-0063.20200013. **Pagina 16.**

3 González J, Cavelli M, Castro-Zaballa S, et al. EEG Gamma Band Alterations and REM-like Traits Underpin the Acute Effect of the Atypical Psychedelic Ibogaine in the Rat. ACS Pharmacol Transl Sci. 2021;4(2):517-525. Published 2021 Jan 11. doi:10.1021/acsptsci.0c00164. **Pagina 20.**

4 González J, Mateos D, Cavelli M, et al. Low frequency oscillations drive EEG's complexity changes during wakefulness and sleep. Neuroscience. 2022;494:1-11. doi:10.1016/j.neuroscience.2022.04.025. **Pagina 29.**

5 González J, Cavelli M, Tort ABL, Torterolo P, Rubido N. Sleep disrupts complex spiking dynamics in the neocortex and hippocampus. PLOS One. In press. 2023. 10.1371/journal.pone.0290146. **Pagina 40.**

6 González J, Rubido N, Carrera I, et al. Bridging the scales through the analysis of neural complexity. Preprint. 10.5281/zenodo.11003044. **Pagina 61.**

SCIENTIFIC REPORTS
nature research

OPEN

Decreased electrocortical temporal complexity distinguishes sleep from wakefulness

Joaquín González[1], Matias Cavelli[1], Alejandra Mondino[1], Claudia Pascovich[1], Santiago Castro-Zaballa[1], Pablo Torterolo[1]* & Nicolás Rubido[2]

In most mammals, the sleep-wake cycle is constituted by three behavioral states: wakefulness (W), non-REM (NREM) sleep, and REM sleep. These states are associated with drastic changes in cognitive capacities, mostly determined by the function of the thalamo-cortical system. The intra-cranial electroencephalogram or electocorticogram (ECoG), is an important tool for measuring the changes in the thalamo-cortical activity during W and sleep. In the present study we analyzed broad-band ECoG recordings of the rat by means of a time-series complexity measure that is easy to implement and robust to noise: the Permutation Entropy (PeEn). We found that PeEn is maximal during W and decreases during sleep. These results bring to light the different thalamo-cortical dynamics emerging during sleep-wake states, which are associated with the well-known spectral changes that occur when passing from W to sleep. Moreover, the PeEn analysis allows us to determine behavioral states independently of the electrodes' cortical location, which points to an underlying global pattern in the signal that differs among the cycle states that is missed by classical methods. Consequently, our data suggest that PeEn analysis of a single EEG channel could allow for cheap, easy, and efficient sleep monitoring.

The sleep-wake cycle is a critical physiological process and one of the most preserved biological rhythms through evolution[1]. This cycle is composed of different states, commonly distinguished by their electro-physiological signatures and behavioral characteristics. These states correspond to wakefulness (W), non-rapid eye movement (NREM) sleep, and rapid eye movement (REM) sleep. W and sleep are associated to different brain functional states, which can be captured by electroencephalographic (EEG) signals containing a broad frequency spectrum. Accompanying the electrocortical differences among the states, the cognitive capacities drastically change during the cycle. Fundamentally, consciousness is lost during deep NREM sleep, emerging in an altered fashion during REM sleep. Altered states of consciousness can also arise during special normal states, such as during lucid-dreams[2], or under toxic or pathological conditions, such as the states induced by psychedelic drugs or psychosis[3,4].

Cognitive states are mostly determined by the function of the thalamo-cortical system[1]. Part of this neuronal processing can be accurately measured by intra-cranial elecroencephalogram (EEG), known as electrocorticogram (ECoG). Due to the complex nature of the standard EEG and ECoG signals, traditional methods employed in neuroscience have divided the complex spectrum of the signal into frequency bands[3,5–9], and analyzed its changes during different cognitive functions[4,7], and sleep states[5,6,8]. These methods only describe particular characteristics of the recorded signals and do not account for the complex nature of the cortical electric potentials. In contrast, the field of non-linear dynamics has developed measures and models that account for the complexity of the systems and their emerging interactions[10–13]. These properties are fundamental for the characterization of the thalamo-cortical function and for the emergence of consciousness[14].

A general approach to study time-signals is the characterization of their randomness; for example, by means of the Shannon entropy (SE)[15], which measures the average unpredictability of a signal. However, SE requires a random source and an invariant probability distribution (which is typically unknown), also is affected by noise, by measurement precision, and by data length. All these elements are relevant when dealing with real-world signals. In order to find a similar non-linear measure to quantify unpredictability from real-world data, Bandt and

[1]Universidad de la República, Departamento de Fisiología de Facultad de Medicina, Av. Gral. Flores 2125, 11800, Montevideo, Uruguay. [2]Universidad de la República, Instituto de Física de Facultad de Ciencias, Iguá 4225, 11400, Montevideo, Uruguay. *email: ptortero@fmed.edu.uy

Pompe[10] introduced the Ordinal Pattern (OP) analysis, allowing to encode any signal into OPs and approximate its SE. This approximation is known as Permutation Entropy (PeEn). In contrast to other methods, PeEn is a time-series complexity measure that is simple to implement, is robust to noise and short time-series, and works for arbitrary data sets[13,16–24]. In particular, it has been shown that PeEn applied to EEG signals captures different states associated with the level of consciousness, both during anesthesia[24–27] and sleep[28,29]. Hence, in order to study the thalamo-cortical function during W and sleep, PeEn is a practical and reliable method, where results can be understood from primary principles, and can be related to the signal characteristics.

Previous works have analyzed PeEn in standard EEG recordings[25–29]. However, EEG signals have frequency limitations due to scalp-filtering, are often recorded with low sampling rates, and pre-acquisition filters are commonly applied. In addition, as the recording electrodes are placed above the scalp's skin, other sources can interfere with the cortical neural activity (e.g., muscular activity)[30]. These limitations exclude the possibility of considering high-frequency oscillations; for example, γ frequency band ($30 - 100\ Hz$), which is known to vary substantially during the sleep-wake cycle and is an active field of research in Neuroscience[3,5–9,31,32]. Thus, PeEn analysis of standard EEG signals is technically limited and is unable to assess the significance of the broad frequency spectrum in relation with the thalamo-cortical function and its cognitive counterpart. Consequently, it is still uncertain whether previous results hold when considering ECoG measurements and whether these results would depend on cortical location, frequency content, or PeEn parameters.

In the present study, we characterized the PeEn of recordings from freely moving rats during W and sleep. We found that ECoG's PeEn is maximal during W and decreases during both sleep states. Moreover, we noted that these results are independent of the cortical location (namely, the electrodes placement), pointing towards a global cortical pattern for each sleep-wake state that is captured by the PeEn analysis but is missed by classical methods.

Results

Permutation entropy during wakefulness and sleep. Figure 1a shows examples of polysomnographic recordings obtained from electrodes placed directly above the cortex of a representative rat. Electrode locations are shown on the left panel and the intra-cranial polysomnographic recordings for W (blue), NREM (green), and REM sleep (red) states are shown on the right panels, which have been distinguished by means of the standard sleep scoring criteria (see Methods). In Fig. 1b we show, for the same animal, the hypnogram (top), as well as the spectrogram (middle) and PeEn values (bottom) processed from the ECoG recorded with the V2r electrode (with a sampling rate of $1024\ Hz$ and $D = 3$ embedding dimension for the PeEn analysis; see Methods for details). The hypnogram shows the standard sleep scoring, the spectrogram shows the ECoG frequency content, and the PeEn quantifies its complexity; namely, its randomness or unpredictability. Maximal PeEn values were achieved during W, PeEN values decreased during NREM sleep and reached minimum values during REM sleep. This result states that the ECoG becomes more predictable – less random – during sleep, especially during REM sleep. More importantly, we found that PeEn is able to detect transitions between behavioral states, which are typically difficult to be noticed from raw data or from the spectrogram. For example, the power spectrum in Fig. 1b (middle panel) shows similarities between W and REM sleep, but PeEn values are drastically different between these states (W epoch at 11 to 13 minutes and REM sleep epoch at 22 to 24 minutes). The average PeEn values for all rats, behavioral states, and cortical locations are shown in Fig. 1c and Table 1, there are significant differences among behavioral states for all recorded neocortical regions; in the Olfactory Bulb (OBr, archicortex) there was a tendency to decrease ($p = 0.056$) when REM was compared to NREM sleep (first row in Table 1). Consequently, the PeEn of the ECoG characterizes and follows the state transitions regardless of the electrode's location.

Permutation entropy dependence on the embedding dimension. We characterized how PeEn reflects the ECoG temporal complexity during W and sleep. In order to do this characterization, we modified the embedding dimension D, which is the parameter that sets the ordinal pattern (OP) length encoding the ECoG signal. Specifically, each OP captures the relationship between the relative amplitudes (ranking its values) inside a D-sized non-overlapping time-window of the signal (see Methods for details on the encoding procedure). Hence, changing D modifies the time scale of the ECoG being analyzed and the resultant PeEn calculation. The larger the OP, the more details are obtained from the signal; thus, the less random the signal becomes and the smaller its PeEn value. For example, Fig. 2 shows that the PeEn values consistently decrease as we increased the embedding dimension from $D = 2$ to $D = 4$, either for W or sleep. Overall, averaged PeEn values during W were larger than during sleep for all Ds. Also, the fact that PeEn variability is minimal for $D = 2$ is because this dimension has the greatest sensitivity to random fluctuations: i.e., it mainly captures noise.

Permutation entropy relationship with the frequency spectrum. As our results show that REM sleep had the lowest temporal complexity out of all states considered, we examined whether the frequency content could be influencing our PeEn assessment. In order to associate the PeEn values with the different frequency bands, we performed successive down-samples to the ECoG signals. This process allows for the ordinal patterns to capture lower frequency components of the ECoG signal, while keeping constant the embedding dimension, D.

We down-sampled the ECoG from a sampling rate of $1024\ Hz$, halving it down to $64\ Hz$; thus, changing the maximum frequency resolution from $512\ Hz$ to $32\ Hz$. By doing this, the PeEn value changed, revealing its relationship to the frequency spectrum. Fig. 3a shows averaged PeEn using $D = 3$ for all rats and electrode locations, for W (blue), NREM (green) and REM sleep (red). The shaded areas indicate the mean $\pm$ standard error of these averages, showing that the states differentiate in average significantly (the exact statistics are exhibited in Table S1 at the Supplementary Material). Average PeEn values for the ECoGs during REM sleep are larger than NREM

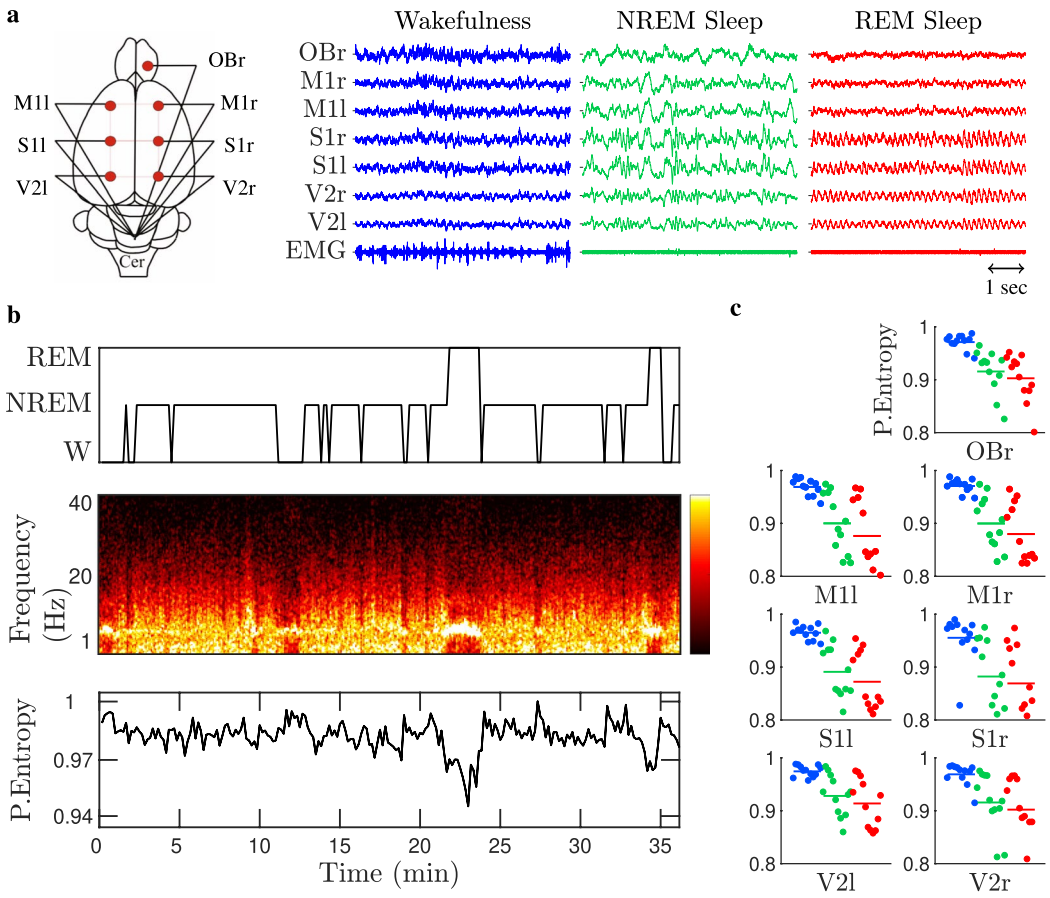

Figure 1. Permutation Entropy (PeEn) during wakefulness and sleep. Panel a shows a schematic representation of the 7 electrodes' placement across the cortex and representative ECoGs – 5 second windows referenced to the cerebellum and the neck electromyogram (EMG) for each sleep-wake state: wakefulness (blue), NREM (green), and REM sleep (red). From top to bottom, Olfactory Bulb (OBr), right and left Primary Motor (M1r/M1l), Primary Somatosensory (S1r/S1l), and Secondary Visual (V2r/V2l) cortices. Using 30 *s* sliding windows for the V2r electrode, panel b shows the hypnogram (top) with the visually scored sleep states, the power spectral density (middle) with yellow indicating high power, and PeEn analysis (bottom) for embedding dimension $D = 3$. Panel c gathers the time-averaged PeEn values (for embedding dimension $D = 3$) for 12 rats, differentiating each cortex electrode and sleep state (colour code as in panel a). Namely, each dot in panel c corresponds to the time-averaged PeEn value of each rat and cortex, where the horizontal bars are the population mean (the statistic is shown in Table 1).

Electrode	pValue	F	DF	W-NREM (pValue)	W-REM (pValue)	NREM-REM (pValue)
OBr	<0.0001	40.2	2,11	0.0003	0.0002	0.056
M1r	<0.0001	37.68	2,11	0.0005	0.0002	0.028
M1l	0.0001	29	2,11	0.0014	0.0007	0.007
S1r	<0.0001	32.1	2,11	0.0011	0.0007	0.046
S1l	<0.0001	41.18	2,11	0.0004	0.0002	0.005
V2r	<0.0001	23.09	2,11	0.0043	0.0017	0.009
V2l	<0.0001	24.92	2,11	0.0022	0.0017	0.036

Table 1. Statistical comparisons between PeEn values during sleep and wakefulness. Each row corresponds to a different cortical location, as shown in Fig. 1a. Data was evaluated by repeated ANOVA (pValue column) and Bonferroni *post-hoc* test measures (last 3 columns of the table). These results correspond to encoding the electro-corticographic signals with $D = 3$ and 1024 *Hz* sampling frequency (see Methods for details).

sleep until the maximum frequency resolution increases beyond 128 *Hz*, remaining lower than W values for all frequencies. Although Fig. 3a shows only the PeEn values for $D = 3$, we obtained similar results for larger embedding dimensions (data not shown). The relationship between the PeEn values and the sampling frequency can be

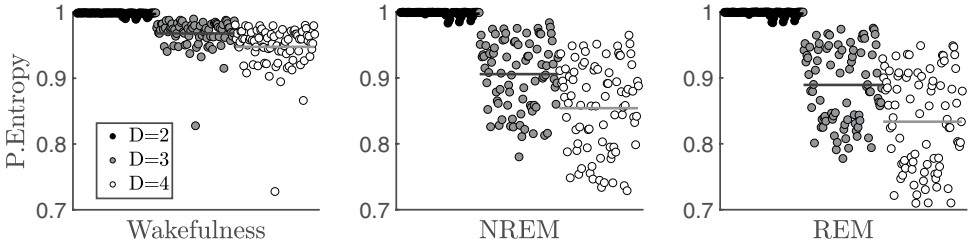

Figure 2. Permutation Entropy (PeEn) of electro-corticograms (ECoG) as a function of the embedding dimension. The PeEn values are normalized according to the maximum possible entropy for each embedding dimension, D; namely, by $\log(D!)$. From left to right, wakefulness (W), non-rapid eye movement (NREM) and rapid eye movement (REM) sleep are shown. Symbols represent each PE value for all electrode locations ($n = 7$) and animals ($n = 12$) [as shown in Fig. 1c], when using $D = 2$ (black), $D = 3$ (grey), or $D = 4$ (white) for the ordinal pattern encoding of the ECoG signals recorded at a sampling frequency of 1024 Hz. The horizontal lines represent the population and electrode location average for the respective embedding dimensions.

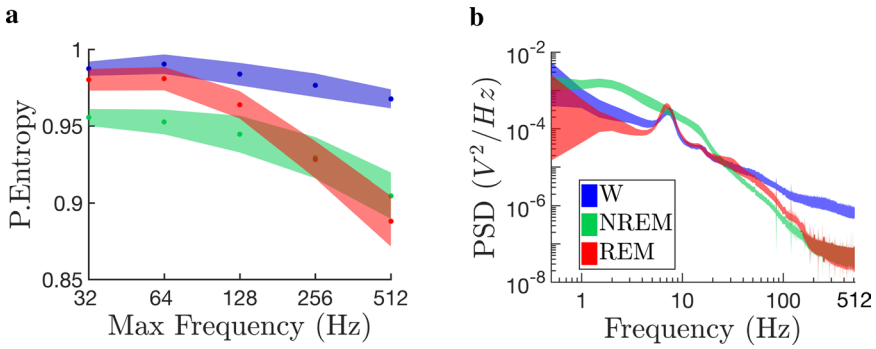

Figure 3. Permutation entropy (PeEn) relationship with frequency content and power spectrum (PSD). This figure presents the results as the average values of the 7 cortical recording sites for the 12 rats analyzed (shown in Fig. 1). Each sleep-wake state is indicated using the colour code in panel b's inset. Panel a shows the averaged PeEn values as a function of the electro-corticograms (ECoG) maximum frequency resolution. Shaded areas in this panel depict the standard error of the mean for the PeEn. The maximum frequency resolution is the ECoGs sampling frequency divided by 2, according to the Nyquist-Shannon criterion. Panel b shows the averaged PSD as a function of the frequency components. Shaded areas in this panel depict twice the standard error of the mean.

further understood by comparing these results with the power spectral density (PSD) analysis shown in Fig. 3b. In general, the PSD of a signal is the probability distribution function of its frequency content; namely, the degree of presence that each frequency component has in the signal. As we down-sampled the ECoG signals, as in Fig. 3a, the higher frequencies are cut-off from the PSD [Fig. 3b]. For the higher frequencies, i.e., >200 Hz, there is a large difference in the PSD value between W and sleep. However, when lower frequencies are considered, REMs PSD increased above NREMs. Note that below 200 Hz REMs lower frequencies become more relevant (Fig. 3b) and PeEn (Fig. 3a) values are larger than NREM sleep and closer to W.

Ordinal pattern probability distributions. In addition to the Entropy quantification, we considered the qualitative differences and variations appearing in the OP probability distributions during W and sleep. The OP distributions shown in Figs. 4 and 5 quantify the relative frequency of appearance that each OP has in the encoded ECoG signal; namely, the OP probability. Figure 4a shows the 6 possible OPs when the embedding dimension is $D = 3$ (top panel), and the resultant OP probability distribution we found from the ECoGs in each sleep-wake state (bottom panel). Similarly, Fig. 4b shows the OPs and OP distribution for $D = 4$. It is readily observed from both panels that the increasing or decreasing OPs (i.e., labels 1 and 6 in Fig. 4a and labels 1 and 24 in Fig. 4b) have a larger probability of occurrence, irrespective of the sleep-wake state or the embedding dimension (results hold for larger D – not shown). We note that, in spite of having qualitatively similar distributions for $D = 4$, other OPs start to emerge, such as labels 7 and 18, which are modified versions of labels 1 and 24, respectively. Nevertheless, these OPs are not statistically significant, since they fall within the null hypothesis confidence interval (signaled by the shaded grey areas in both panels). On the contrary, the OP distribution in Fig. 4a for $D = 3$ during sleep (red and green) significantly departs from the null hypothesis, which corresponds to the uniform distribution (shaded grey area).

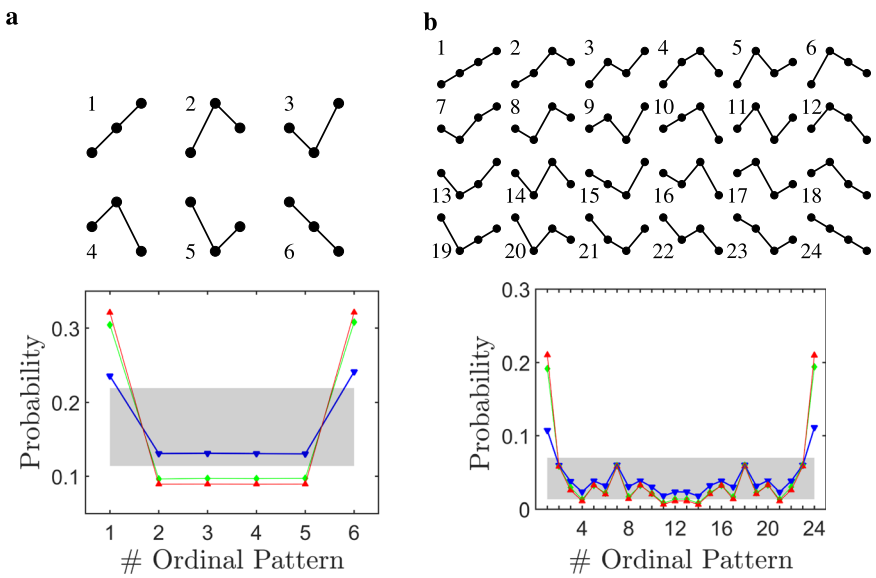

Figure 4. Ordinal Pattern (OP) probability distributions during wakefulness and sleep. The OP probability distributions shown in the bottom panels correspond to the rat population and electrode location average distributions for each sleep-wake state: Wakefulness (blue), NREM (green) and REM sleep (red). The grey areas show the null hypothesis region with a 95, 4% confidence, which correspond to the uniform OP distribution with twice the standard error of the mean (i.e., $p_{NH} \pm 2\sigma_{NH}$). Panel a [Panel b] shows the possible OPs for embedding dimension $D = 3$ [$D = 4$].

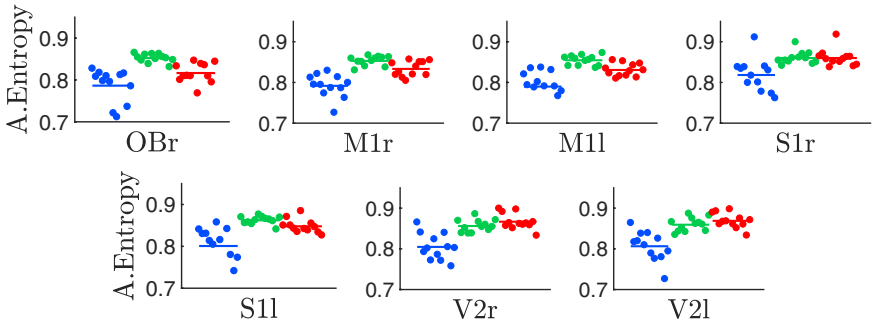

Figure 5. Amplitude entropy during wakefulness and sleep. From left to right and top to bottom, the panels show the entropy values calculated from the electro-corticographic (ECoG) histograms coming from the different cortical locations shown in Fig. 1; i.e., olfactory bulb, right and left motorsensory, somatosensory, and visual cortices, respectively. The colour code signals the sleep-wake cycle states (W, blue; NREM, green and REM sleep, red) and the symbols and horizontal lines represent the same as in Fig. 1c. The entropy values were calculated from the ECoG amplitude histograms using 18 bins. The sampling rate was 1024 *Hz*. The statistic is shown in the Supplementary Material (see Table S2).

Comparison with classical amplitude encoding. Classical analysis of time-series uses the probability distribution function of the signal; namely, the signal is encoded using a histogram of its amplitudes. This process discards the information coming from the signal's time stamps; in other words, the amplitude time-dependence. We compared the entropy values using histograms with 18 bins of the ECoG, where the results are shown in Fig. 5. As can be directly observed, there were some differences among the sleep states (either NREM or REM), but there were no consistent global pattern and no single electrode was able to differentiate between all sleep-wake states (see Table S2). Moreover, these results remain practically invariant when using larger number of bins (data not shown).

Discussion

In this work, we described that the collective cortical activity measured by ECoG in male adult rats fluctuates between periods of high temporal complexity during W, and periods of low temporal complexity during sleep (see Fig. 1b,c). These ECoG complexity variations reflect the differences in the thalamo-cortical function between sleep-wake states. Consequently, our results strongly support and extend studies in human that carried out PeEn analyses and other complexity measures in standard EEG recordings[25–29,33].

We also showed that PeEn profile during W and sleep did not change according to the cortical recording site, reflecting a common micro-structure motif and a dynamical behavior which are independent from the origin of the cortical signal. The average randomness of these micro-structure patterns distinguished sleep from W, regardless of the changes in the embedding dimensions employed in PeEn analysis (Fig. 2) and the sampling frequencies considered (Fig. 3a). These results suggest the use of PeEn as a quantitative tool for understanding thalamo-cortical dynamics during various physiological conditions, the influence of psychoactive drugs, or pathological conditions.

A strong benefit from PeEn analyses is that PeEn variations across states can be explained by dynamical systems theory[10,16,34]; conversely, with other techniques the tractability is lost (such as, machine-learning approaches). During NREM sleep, the neuro-modulation coming from the activating systems drastically decreases, which favors the occurrence of slow δ waves ($1 - 4\ Hz$) and sleep spindles ($9 - 12\ Hz$) in the thalamus and cortex[1]. This means that, as the animal transits from W to sleep, the higher-frequency cortical patterns (complex signals) decrease, while lower-frequency oscillations (less complex signals) rise (Fig. 3b). As a consequence, the OPs probability distribution becomes less uniform (in other words more predictable). Specifically, we found that strictly increasing or decreasing OP motifs are strongly favored in all ECoG signals, particularly during sleep (Fig. 4), making the remaining OP motifs to appear less frequently.

Surprisingly, we found that NREM's PeEn is larger than REM's PeEn, which contradicts previously reported results[28,29]. However, we showed that as the frequency content of the ECoG varies, the PeEn changes its value. For example, Fig. 3a exhibits that as we down-sampled the ECoG, REM sleep PeEn becomes larger than NREM's PeEn; these low sampling rates are similar to those used in previous studies[28,29]. Moreover, we analyzed the results from the PeEn as a function of the maximum frequency resolution (Fig. 3a) in conjunction with those from the power spectral density (PSD) of the ECoG (Fig. 3b). We observed that the rise in REM's PeEn as the frequency content decreased follows the variations in the PSD. Specifically, REM sleep presents larger power than NREM sleep around and below $120\ Hz$ corresponding to the high frequency oscillations and gamma band oscillations[5,6]. This means that when higher frequencies are cut-off, the PSD slope significantly increases approaching a more uniform frequency distribution, which corresponds to a more complex time-series. These analyses reveal that PeEn results depends on the frequency content of the signal. In particular, REMs temporal complexity resembles W when gamma oscillations are captured by the PeEn.

One of the main differences between W and sleep, is that muscle tone and movements are mainly absent during sleep (specially during REM sleep). In this regard, the power of the higher frequencies of the spectrum is significantly higher during W than during sleep. It is possible that exists a contribution of muscular activity on the ECoG (by volume conduction) on the high frequency bands ($>100\ Hz$), as supported by experimental evidence[30]. Hence, the high values of PeEn during W could be determined by the muscle electrical activity (produced mainly by the muscle tone, because epochs with movement artifacts were discarded from the analysis) that inevitably pollutes the ECoG. Nevertheless, the PeEn values remained constant during W following downsampling, in spite of the fact that higher frequencies were bypassed and the contribution from muscle tone became less relevant. Still, more research is needed in order to quantify the weight of the muscle artifact in the PeEn results.

As a final remark, sleep classification is usually performed by visual analysis, or automated spectral methods usually in research contexts. For instance, in rodents methods which employ spectral ratios (such as the theta/delta ratio) obtained from hippocampal or intra-craneal recordings in rodents, are able to distinguish sleep-wake states[35,36]. Thus, these methodologies rely heavily upon the use of narrow band characteristics of the EEG signal. In contrast, our data suggest that the sleep-wake states differ globally in their time-series complexity as assessed by PeEn. Hence, we suggest that cheap, robust, and reliable sleep monitoring could be achieved by means of PeEn analysis of a single ECoG channel.

Methods

Experimental animals. All experimental procedures were conducted in agreement with the National Animal Care Law (No. 18611) and with the "Guide to the care and use of laboratory animals" (8th edition, National Academy Press, Washington DC, 2010). Furthermore, the Institutional Animal Care Committee (ComisiÃşn de Etica en el Uso de Animales) approved the experiments (Exp. No 070153-000332-16), where 12 Wistar adult rats were maintained on a $12 - h$ light/dark cycle (lights on at 07: $00h$) with food and water freely available. The animals were determined to be in good health by veterinarians of the institution. We took adequate measures to minimise pain, discomfort, and stress in the animals, and all efforts were made to use the minimal number of animals necessary to obtain reliable scientific data.

Surgical procedures. The animals were chronically implanted with electrodes to monitor the states of sleep and W. We employed similar surgical procedures as in previous studies[5,6]. Anaesthesia was induced with a mixture of ketamine-xylazine ($90\ mg/kg$; $5\ mg/kg$ i.p., respectively). The rat was positioned in a stereotaxic frame and the skull was exposed. To record the ECoG, stainless steel screw electrodes were placed on the skull above motor, somatosensory, visual cortices (bilateral), the right olfactory bulb, and cerebellum, which was the reference electrode (see Fig. 1a and Table 2). In order to record the EMG, two electrodes were inserted into the neck muscle. The electrodes were soldered into a 12-pin socket and fixed onto the skull with acrylic cement. At the end of the surgical procedures, an analgesic (Ketoprofen, $1\ mg/kg$, s.c.) was administered. After the animals had recovered from these surgical procedures, they were left to adapt in the recording chamber for 1 week.

Experimental sessions and sleep scoring. Animals were housed individually in transparent cages ($40 \times 30 \times 20\ cm$) containing wood shaving material in a temperature-controlled ($21-24\ ^{\circ}C$) room, with water

Electrode	OBr	M1r	M1l	S1r	S1l	V2r	V2l
Antero-Posterior	$+7.5mm$	$+2.5mm$	$+2.5mm$	$-2.5mm$	$-2.5mm$	$-7.5mm$	$-7.5mm$
Lateral	$+1.25mm$	$+2.5mm$	$-2.5mm$	$+2.5mm$	$-2.5mm$	$+2.5mm$	$-2.5mm$

Table 2. Electrode Location. Schematic representation and electrode locations. All coordinates are referenced to *Bregma* (Lateral: 0, Antero-posterior: 0) according to Paxinos and Watson 2006[37].

and food *ad libitum*. Experimental sessions were conducted during the light period, between 10 AM and 4 PM in a sound-attenuated chamber with Faraday shield. The recordings were performed through a rotating connector, to allow the rats to move freely within the recording box. Polysomnographic data were amplified ($X1000$), acquired and stored in a computer using Dasy Lab Software employing 1024 Hz as a sampling frequency and a 16 bits AD converter. The states of sleep and W were determined in 10 s epochs. W was defined as low voltage fast waves in the motor cortex, a strong theta rhythm ($4-7$ Hz) in the visual cortices, and relatively high EMG activity. NREM sleep was determined by the presence of high voltage slow cortical waves together with sleep spindles in motor, somatosensory, and visual cortices associated with a reduced EMG amplitude; while REM sleep as low voltage fast frontal waves, a regular theta rhythm in the visual cortex, and a silent EMG except for occasional twitches. An aditional visual scoring was performed to discard artifacts and transitional states.

Ordinal pattern encoding. In order to quantify the EEGs' randomness, we encoded the time-series into ordinal patterns (OPs) following Bandt and Pompe method[10]. The encoding involves dividing a time-series, $\{x(t),\ t = 1, \ldots, T\}$, into $\lfloor (T - D)/D \rfloor$ non-overlapping vectors, where $\lfloor y \rfloor$ denotes the largest integer less than or equal to y and D is the vector's length, which is much shorter than the time-series length ($D \ll T$). Then, each vector is classified according to the relative magnitude of its D elements. The classification was done by determining how many permutations are needed to order its elements increasingly; namely, an OP is associated to represent the vector's permutations. For example, for $D = 2$, the time-series would be divided into vectors containing two consecutive values, such as $\{x(t_i),\ x(t_{i+1})\}$, that are non-overlapping (the next vector to $\{x(t_i),\ x(t_{i+1})\}$ is the $\{x(t_{i+2}),\ x(t_{i+3})\}$ vector, where t_i is the i-th time stamp). These vectors have only two possible OPs for any time t_i: either $x(t_i) < x(t_{i+1})$ or $x(t_i) > x(t_{i+1})$, which correspond to making 0 permutation or 1 permutation, respectively. It is worth noting that the number of possible permutations increases factorially with increasing vector length; i.e, for vectors of length D there are $D!$ possible OPs. In particular, we labeled the OPs as the number of permutations plus one; hence, our OPs are labeled by means of integers, α, that range from $\alpha = 1$ to $\alpha = D!$. For $D = 2, \alpha = 1$ or 2. Similarly, for $D = 3$, the OPs $\alpha = 1$ and $\alpha = 2$ correspond to having a vector from the time-series with 3 values ordered as $x(t_i) < x(t_{i+1}) < x(t_{i+2})$ and $x(t_i) < x(t_{i+2}) < x(t_{i+1})$, respectively, but there are 4 more possibilities (for $D = 3, \alpha = 1, \ldots, 3! = 1, \ldots, 6$). Small noise fluctuations were always introduced into the time-series in order to remove degeneracies; i.e., avoid the cases where, for example, $x(t_i) = x(t_{i+1})$.

Randomness quantification. Shannon entropy (SE) is a quantity used in Information theory to quantify the average randomness (information content) of a signal. It is defined as[15] $H(S) = -\sum_{\alpha \in S} p(\alpha)\ \log[p(\alpha)]$, where $p(\alpha)$ is the probability of finding symbol α in the signal (among the set of symbols S) and the summation is carried over all possible symbols. In other words, SE shows that $H(S)$ is the average value of $\log(1/p)$ with respect to an alphabet S. Hence, in order to find H for any real-valued time-series, we need to transform the time-series into a symbolic sequence. When using OPs, the resultant symbolic sequence has a finite number of symbols; i.e., the alphabet, which is given by the OP's length D and holds $D! = \#\{S\}$ possible symbols. For bin histograms, the number of possible symbols depends on the number of bins, N_b, used to create the time-series histogram, which is another way of encoding any bounded time-series into a finite set of values. In order to compare entropy values coming from OPs or bins, we need to set both quantities such that the probabilities involved in the summation of $H(S)$ are found with identical statistics. For example, when using non-overlapping OPs with $D = 3$, there are $D! = 6$ possibly different symbols in an encoded time-series of length T, which accounts to $\sim T/D$ total encoded symbols.

We highlight that the number of bins we chose corresponds to making an amplitude encoding that has the same statistical average as the OP encoding with dimension, D. Namely, a signal with T time-stamps, is encoded by non-overlapping OPs into a symbolic sequence of length $S = \lfloor (T - D)/D \rfloor \simeq T/D$, where $\lfloor \cdot \rfloor$ indicates the smaller integer closer to the argument. The resultant range for the symbolic sequence distribution is $D!$, which is the different OP possibilities. This means that a length T time series has an OP statistical average of $S/D! \simeq T/D \times D!$. On the other hand, the statistical average for histograms with N_b bins of the same time-series is T/N_b. Consequently, in order to have the same statistical average per bin and be able to compare the results, we need to set $N_b = D \times D!$, which for $D = 3$ corresponds to having $N_b = 3 \times 6 = 18$ bins.

Power spectral density and statistical analysis. The power spectral densities were performed using the *pwelch* function on MATLAB by employing the following parameters: window $= 30s$, noverlap $= []$, fs $= 1024$, nfft $= 1024$. These parameters correspond to 30 second sliding windows with half windows overlap, a $f_s = 1024$ Hz sampling frequency and a frequency resolution of $1Hz$.

On the other hand, the statistics for each ECoG PeEn calculations were based on non-overlapping windows of size $D \times D! \times N_S$, where $N_S = 200$ is the statistical average we use for our null-hypothesis. Namely, our null-hypothesis is a Bernoulli process where each ordinal pattern of size D has an equal probability of appearance, $p_{NH} = 1/D!$, and a standard error of the mean $\sigma_{NH} = \sqrt{p_{NH}\ (1 - p_{NH})/N_S}$. For example, for ordinal patterns with $D = 3$, the non-overlapping windows contained $3 \times 6 \times 200 = 3600$ data points, which accounts to approximately 3.5 seconds at a $f_s = 1024\ Hz$ sampling frequency. The null-hypothesis in this case has an average probability $p_{NH} = 1/3! = 1/6 \simeq 0.167$ and a standard error of the mean $\sigma_{NH} = \sqrt{p_{NH}\ (1 - p_{NH})/N_S}$ $\simeq 2.64 \times 10^{-2}$, which makes its confidence interval $p_{NH} \pm 2\sigma_{NH}$ narrow and the statistical significance of the PE results robust. In general, given an embedding dimension D, any time-series with T data points is analysed using non-overlapping windows with $D \times D! \times N_S$ data points. OP probabilities – as well as the corresponding PeEn value – are found for each of the $T/D \times D! \times N_S$ data windows and then averaged (namely, results are time-averaged).

For the state comparisons, we verified that PeEn distributes normally through Lilliefors test, and then applied a repeated measures ANOVA together with the Bonferroni *post-hoc* test and $p < 0.05$ in order for the result to be considered significant.

Data availability

Data is available upon reasonable request to the authors.

Received: 10 July 2019; Accepted: 6 November 2019;
Published online: 05 December 2019

References

1. Carskadon, M. A., Dement, W. C. Principles and Practice of Sleep Medicine (Sixth Edition), Chapter 2 - Normal Human Sleep: An Overview, Pages 15– 24.e3.Editor(s): Meir Kryger, Thomas Roth, William C. Dement. Elsevier (2017).
2. Dresler, M. *et al*. Neural correlates of dream lucidity obtained from contrasting lucid versus non-lucid REM sleep: a combined EEG/fMRI case study. *Oxford University Press* **35**(7), 1017–1020 (2012).
3. Uhlhaas, P. J. High-frequency oscillations and the neurobiology of schizophrenia. *Dialogues Clin Neurosci* **15**(3), 301–313 (2013).
4. Carhart-Harris, R. L. *et al*. The entropic brain: a theory of conscious states informed by neuroimaging research with psychedelic drugs. *Front. Hum. Neurosci.* **8**, 20 (2014).
5. Cavelli, M.*et al*.Absence of EEG gamma coherence in a local activated cortical state: a conserved trait of REM sleep, Translational Brain Rhythmicity, 21132017.
6. Cavelli, M.*et al*.Power and coherence of cortical high-frequency oscillations during wakefulness and sleep.*European Journal of Neuroscience* (2017).
7. Rodriguez, E. *et al*. Perception's shadow: long-distance synchronization of human brain activity. *Nature* **397**, 430–433 (1999).
8. Castro, S., Falconi, A., Chase, M. & Torterolo, P. Coherent neocortical 40-Hz oscillations are not present during REM sleep. *European Journal of Neuroscience* **37**, 1330–1339 (2013).
9. Buzsáki, G. & Schomburg, E. W. What does gamma coherence tell us about inter-regional neural communication? *Nat. Neurosci.* **18**(4), 484–489 (2015).
10. Bandt, C. & Pompe, B. Permutation Entropy: A Natural Complexity Measure for Time Series. *Phys. Rev. Lett.* **88**(17), 174102 (2002).
11. Bak, P., Tang, C. & Wiesenfeld, K. Self-organized criticality: An explanation of the 1/f noise. *Phys. Rev. Lett.* **59**(4), 381 (1987).
12. Peng, C. K., Shlomo Havlin, H., Stanley, E. & Goldberger, A. L. Quantification of scaling exponents and crossover phenomena in nonstationary heartbeat time series. *Chaos* **5**, 82 (1995).
13. Kulp, C. W., Zunino, L., Osborne, T. & Zawadzki, B. Using missing ordinal patterns to detect nonlinearity in time series data. *Phys. Rev. E* **96**(2), 022218 (2017).
14. Oizumi, M., Albantakis, L. & Tononi, G. From the Phenomenology to the Mechanisms of Consciousness: Integrated Information Theory 3.0. *PLoS Comput. Biol.* **10**(5), e1003588 (2014).
15. Shannon, C. E. A mathematical theory of communication (parts I and II). *Bell System Tech. J.* **27**, 379–423 (1948).
16. Amigó, J. M.*Permutation Complexity in Dynamical Systems-Ordinal Patterns, Permutation Entropy, and All That* (Springer Verlag, Berlin, 2010).
17. Parlitz, U. *et al*. Classifying cardiac biosignals using ordinal pattern statistics and symbolic dynamics. *Computers in Biology and Medicine* **42**, 319–327 (2012).
18. Keller, K., Unakafov, A. & Unakafova, V. Ordinal patterns, entropy, and EEG. *Entropy* **16**(12), 6212–6239 (2014).
19. Amigó, J. M., Keller, K. & Unakafova, V. A. Ordinal symbolic analysis and its application to biomedical recordings. *Philosophical Transactions of the Royal Society* **373**(2034), 20140091 (2015).
20. Zunino, L., Soriano, M. C., Fischer, I., Rosso, O. A. & Mirasso, C. R. Permutation-information-theory approach to unveil delay dynamics from time-series analysis. *Physical Review E* **82**(4), 046212 (2010).
21. Aragoneses, A., Perrone, S., Sorrentino, T., Torrent, M. C. & Masoller, C. Unveiling the complex organization of recurrent patterns in spiking dynamical systems. *Scientific reports* **4**, 4696 (2014).
22. Masoliver, M. & Masoller, C. Sub-threshold signal encoding in coupled FitzHugh-Nagumo neurons. *Scientific reports* **8**(1), 8276 (2018).
23. Quintero-Quiroz, C. *et al*. Differentiating resting brain states using ordinal symbolic analysis. *Chaos* **28**(10), 106307 (2018).
24. Ouyang, G., Dang, C., Richards, D. A. & Li, X. Ordinal pattern based similarity analysis for EEG recordings. *Clinical Neurophysiology* **121**(5), 694–703 (2010).
25. Sitt, J. D. *et al*. Large scale screening of neural signatures of consciousness in patients in a vegetative or minimally conscious state. *Brain.* **137**(8), 2258–2270 (2014).
26. Jordan, D., Stockmanns, G., Kochs, E. B., Pilge, S. & Schneider, G. Electroencephalographic Order Pattern Analysis for the Separation of Consciousness and Unconsciousness: An Analysis of Approximate Entropy, Permutation Entropy Recurrence Rate, and Phase Coupling of Order Recurrence Plots. *Anesthesiology* **109**(6), 1014–1022 (2008).
27. Thul, A. *et al*. EEG entropy measures indicate decrease of cortical information processing in Disorders of Consciousness. *Clin Neurophysiol.* **127**(2), 1419–1427 (2016).
28. Bandt, C. A New Kind of Permutation Entropy Used to Classify Sleep Stages from Invisible EEG Microstructure. *Entropy* **19**(197), 1–12 (2017).
29. Nicolaou, N. & Georgiou, J. The use of permutation entropy to characterize sleep electroencephalograms. *Clinical EEG and Neuroscience* **42**, 24–28 (2011).

30. Whitham, E. M. *et al*. O.Scalp electrical recording during paralysis: Quantitative evidence that EEG frequencies above 20 Hz are contaminated by EMG. *Clin Neurophysiol* **118**, 1877–1888 (2007).
31. Buzsáki, G. & Wang, X. J. Mechanisms of Gamma Oscillations Annual. *Review of Neuroscience* **35**, 203–225 (2012).
32. Llinas, R., Ribary, U., Contreras, D. & Pedroarena, C. The neuronal basis for consciousness. *Phil.Trans.R.Soc Lond* **353**, 1841–1849 (1998).
33. Croce, P., Quercia, A. & Costa, S. Zappasodi Circadian Rhythms in Fractal Features of EEG Signals. *Frontiers in Physiology* **9**, 1567 (2018).
34. Keller, K. & Sinn, M. Ordinal analysis of time series. *Physica A* **356**(1), 114–120 (2005).
35. Gervasoni, D. *et al*. Global forebrain dynamics predict rat behavioral states and their transitions. *J. Neurosci.* **24**(49), 11137–11147 (2004).
36. Pava, M. J., Makriyannis, A. & Lovinger, D. M. Endocannabinoid Signaling Regulates Sleep Stability. *PLoS One* **11**(3), e0152473 (2016).
37. Paxinos, G. & Watson, C. The Rat Brain in Stereotaxic Coordinates. London: Academic Press. (2007).

Acknowledgements

This study was supported by the "Programa de Desarrollo de Ciencias Básicas", PEDECIBA; Agencia Nacional de investigación e innovación (ANII), (FCE_1_2017_1_136550) and the "Comisión Sectorial de Investigación Científica" (CSIC) I + D - 2016 - 589 grant from Uruguay. N.R. acknowledges the CSIC group grant "CSIC2018 - FID 13 - Grupo ID 722".

Author contributions

J.G., N.R. and P.T. designed the study. J.G., A.M. and M.C. performed the experiments and data collection. J.G. and M.C. carried out the data analysis and N.R. developed the software. J.G., M.C., A.M., S.C., C.P., P.T. and N.R. were involved in the discussion and interpretation of the results. J.G., N.R. and P.T. wrote the manuscript. P.T. and N.R. provided the financial support. All the authors participated in the critical revision of the manuscript, added important intellectual content, and approved the definitive version.

Competing interests

The authors declare no competing financial and non-financial interests.

Additional information

Supplementary information is available for this paper at https://doi.org/10.1038/s41598-019-54788-6.

Correspondence and requests for materials should be addressed to P.T.

Reprints and permissions information is available at www.nature.com/reprints.

Publisher's note Springer Nature remains neutral with regard to jurisdictional claims in published maps and institutional affiliations.

SPECIAL ISSUE

XV Latin American Symposium on Chronobiology 2019
Colonia del Sacramento - Uruguay

Electrocortical temporal complexity during wakefulness and sleep: an updated account

Joaquín González [1]
Matias Cavelli [1,2]
Alejandra Mondino [1,3]
Claudia Pascovich [1]
Santiago Castro-Zaballa [1]
Nicolás Rubido [4,5]
Pablo Torterolo [1*]

[1] Departamento de Fisiología, Facultad de Medicina, Universidad de la República, Montevideo, 11200, Uruguay.
[2] Department of Psychiatry, University of Wisconsin, Madison, WI, USA.
[3] Department of Anesthesiology, University of Michigan, Ann Arbor, MI, USA.
[4] Instituto de Física de Facultad de Ciencias, Universidad de la República, Montevideo, 11400, Uruguay.
[5] Institute for Complex Systems and Mathematical Biology, University of Aberdeen, Aberdeen, AB24 3UE, United Kingdom.

ABSTRACT

The states of sleep and wakefulness are critical physiological processes associated with different brain patterns of activity. The intracranial electroencephalogram allows us to measure these changes, thus, it is a critical tool for its study. Recently, we showed that the electrocortical temporal complexity decreased from wakefulness to sleep. Nevertheless, the origin of this complex activity remains a controversial topic due to the existence of possible artifacts contaminating the brain signals. In this work, we showed that complexity decreases during sleep, independently of the electrode configuration employed. This fact strongly suggests that the basis for the behavioral-state differences in complexity does not have an extracranial origin; i.e., generated from the brain.

Keywords: NREM; REM; Entropy; Ordinal Patterns

Corresponding author:
Pablo Torterolo
E-mail: ptortero@fmed.edu.uy

DOI: 10.5935/1984-0063.20200013

INTRODUCTION

The sleep-wake cycle is a critical physiological process and one of the most preserved biological rhythms through evolution. It is composed by the states of wakefulness (W), non-rapid eye movement (NREM) sleep, and rapid eye movement (REM) sleep[1]. These states are associated with different dynamical patterns of electric activity, which can be recorded accurately through the intracranial electroencephalogram, also known as electrocorticogram (ECoG).

In our previous work[2], we found that the ECoGs' temporal complexity decreased from wakefulness to sleep; i.e., the repertoire of dynamical motifs was reduced when the animals fell asleep (Figure 1A, B and C). Interestingly, we observed this result in several cortical locations independent of its function (motor, olfactory, somatosensorial and visual), which suggested that the loss in temporal complexity was a global motif developed in the passage from W to sleep. Nevertheless, whether this result originated because a genuine change in brain dynamics happened or was a consequence of an artefactual measurement common to all recording electrodes, remained unanswered. It is important to consider this possibility because our previous recordings[2] employed a common reference in the cerebellum, which is in close proximity to the neck muscles and could be contaminated by the muscular activity.

In order to discard this possibility, we re-referenced our data to obtain bipolar recordings, and then we measured their temporal complexity employing the same method as our previous work. Therefore, this approach removes the influence of the reference electrode and all common signals from our ECoGs, allowing us to investigate whether our previous results arise from a common background noise or were truly reflecting a global neural pattern which shifted from W to sleep.

MATERIAL AND METHODS

In this report, we re-analyzed our previous data, therefore, the methods will be explained briefly and should be consulted in[2] for a detailed description. We employed 12 Wistar adult rats maintained in a 12h light/dark cycle. All experimental procedures

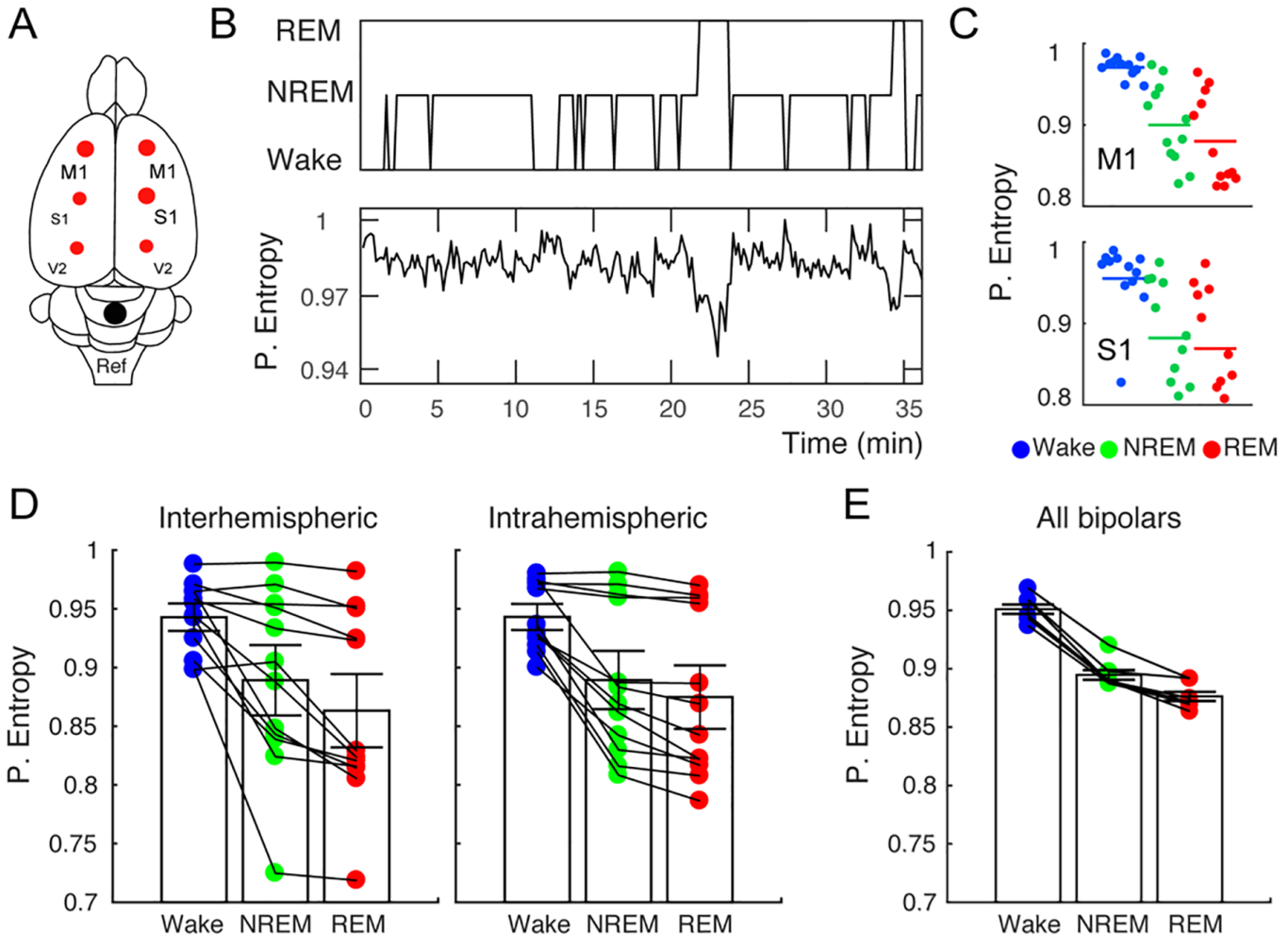

Figure 1. The ECoGs temporal complexity is independent of the electrode configuration. A Electrode localization in the rats cortex**.** The primary motor (M1; r and l, right and left) and right somatosensory (S1) cortex are shown together with the reference electrode placed above the cerebellum. **B** The hypnogram (top) from a representative animal is plotted simultaneously with the permutation entropy (bottom) from the M1r cortex as a function of time. **C** Scatter plots showing the time-average permutation entropy for each animal (12 rats) in each sleep state, blue W, green NREM and red REM. **D** The same scatter plots are now shown obtained from the bipolar configuration, interhemispheric (M1r-M1l) and intrahemispheric (M1r-S1r). **E** Permutation entropy decreases through sleep in all the bipolar configurations studied. Each dot depicts a bipolar electrode in each sleep and wake state (averaged from all the animals). 7 bipolars are plotted: M1r-M1l, M1r-S1r, M1l-S1l, S1r-S1l, S1r-V2r, S1l-V2l, V2r-V2l.

were conducted in agreement with the National Animal Care Law (No. 18611) and with the "Guide to the care and use of laboratory animals" (8th edition, National Academy Press, Washington DC, 2010). Furthermore, the Institutional Animal Care Committee (Comisión de Ética en el Uso de Animales) approved the experiments (Exp. No 070153-000332-16).

The animals were chronically implanted with electrodes to monitor the states of sleep and W. To record the ECoG, stainless steel screw electrodes were placed on the skull above motor (bilateral), somatosensory (bilateral), visual cortices (bilateral), the right olfactory bulb, and cerebellum, which was the reference electrode (see Fig. 1a and Table 2 in González et al. 2019). A neck bipolar electrode was employed to record the EMG. Experimental sessions were conducted during the light period, between 10 AM and 4 PM in a sound-attenuated chamber with Faraday shield. The recordings were performed through a rotating connector, to allow the rats to move freely within the recording box. Polysomnographic data were amplified x1000, acquired and stored in a computer using Dasy Lab Software employing 1024 as a sampling frequency and a 16 bits AD converter. The states of sleep and W were determined in 10 s epochs. W was defined as low voltage fast waves in the motor cortex, a strong theta rhythm (4-7 Hz) in the visual cortices, and relatively high EMG activity. NREM sleep was determined by the presence of high voltage slow cortical waves together with sleep spindles in motor, somatosensory, and visual cortices associated with a reduced EMG amplitude; while REM sleep as low voltage fast frontal waves, a regular theta rhythm in the visual cortex, and a silent EMG except for occasional twitches. An additional visual scoring was performed to discard artifacts and transitional states.

To assess the ECoGs temporal complexity, we employed the measure known as Permutation Entropy, which has been employed widely[3–7]. This metric is robust to noise and it is computationally efficient. The permutation entropy is calculated as follows: we encoded the ECoGs time-series into ordinal patterns (OPs) by dividing the time-series into sequences of non-overlapping vectors (each containing 3 time stamps), and classifying them according to the relative magnitude of its elements. This transforms the graded ECoG time-series into a symbolic one, which can only contain up to six symbols maximum (factorial of the number of elements in a vector). Each symbol then represents a dynamical motif found in the ECoGs.

We note that small noise fluctuations are always introduced into the time-series in order to remove degeneracies; i.e., avoid the cases where, for example x(t) = x(t+1). After the symbolic time-series is obtained, the permutation entropy is calculated applying the Shannon Entropy[8] ($SE = -\sum p(\alpha) \log[p(\alpha)]$) to the probability distribution. Where $p(\alpha)$ is the probability (relative frequency of alpha in the symbolic time-series) of the α symbol. For the statistical analysis, we employed the repeated measures ANOVA and set $p<0.05$ to be considered significant.

RESULTS

In order to discard the contribution of extracranial noise to the complexity decrease during sleep, we generated bipolar recordings by subtracting two active electrodes. As our original data came as a differential recording to a common reference, the bipolar configuration eliminates the contribution of this electrode[9–11], in our case, the cerebellum. This is especially important because of the close proximity between our reference electrode and the neck muscles.

Figure 1D shows the results we obtained employing two anatomically relevant configurations: one an interhemispheric (M1r - M1l) and the other an intrahemispheric (M1r - S1r) combination. When we analyzed this new data, we found that the temporal complexity still decreased from W to NREM sleep and reached its lowest values during REM sleep. Furthermore, this result was observed in all the bipolar recordings analyzed (Figure 1D), irrespective of being inter or intrahemispheric combinations; notice that the complexity decrease during sleep is seen in every bipolar configuration employed (Figure 1E). When we investigated the origin of this complex activity, we found that the predominant temporal patterns were the monotonically increasing or decreasing ones (Figure 2A).

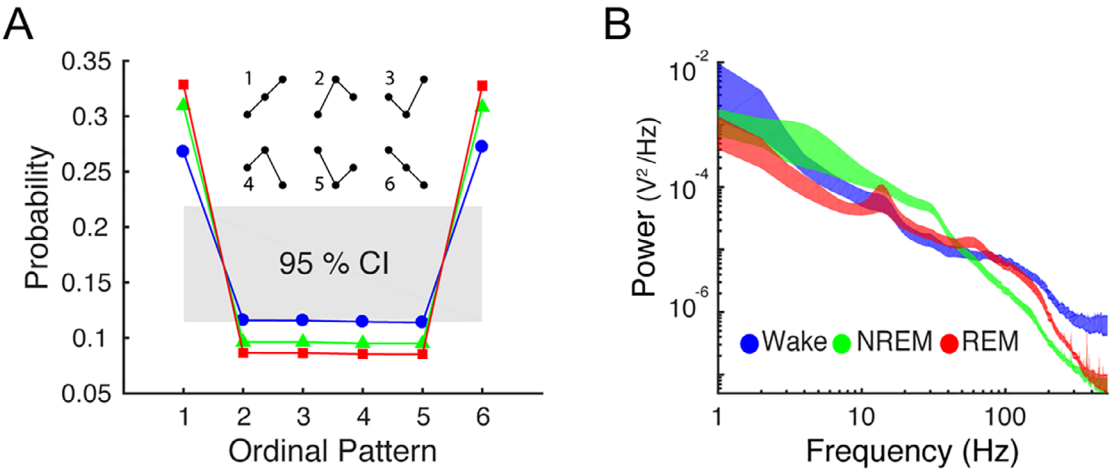

Figure 2. The dynamical characteristics of the ECoGs are preserved in the bipolar configuration . A Ordinal pattern probability distribution from the interhemispheric combination (M1r-M1l). The shaded area depicts the 95 percent confidence interval of the mean. The color code employed is the same as in panel **B. B** Average power spectral density (12 animals) during wakefulness and sleep, for the M1r-M1l bipolar configuration. The shaded areas depict the mean +/- the standard error.

This happened during W and was further overexpressed during sleep. It is worth noting that the frequency distribution of the bipolar ECoGs showed a power-law distribution which was steepened during the sleep states (Fig.2B), similar to our previous result found in monopolar electrodes (see Figure 2.B in (2)).

DISCUSSION

In the present study, we show that the loss in temporal complexity during sleep is not a consequence of a common noise entering through our reference electrode. This was evidenced by generating bipolar recordings, thus severely reducing the background noise common to all ECoG electrodes[9–12]. This is particularly relevant because our reference electrode was closely located to the neck muscles and thus could be contaminated by the changes in muscle tone during sleep. In contrast, all bipolar recordings showed a significant complexity decrease as sleep progressed and reached its lowest values during REM. This means that our initial findings were independent on the electrode configuration employed (bipolar vs monopolar), and are less likely to simply reflect the changes in muscle activity during the sleep-wake cycle. Furthermore, the bipolar recordings retained a similar frequency and ordinal pattern distribution to what we had observed by the monopolar configuration, implying that these new changes in complexity arise from the same dynamic profile as in the monopolar case. Taken together, our results confirm that the electrocortical temporal complexity decreases from W to sleep, and this fact is not a consequence of a muscle artifact recorded through the reference electrode.

REFERENCES

1. Carskadon MA, Dement WC. Chapter 2 – Normal Human Sleep: An Overview. 2011;21.
2. González J, Cavelli M, Mondino A, Pascovich C, Castro-Zaballa S, Torterolo P, et al. Decreased electrocortical temporal complexity distinguishes sleep from wakefulness. Sci Rep. 2019 Dec 5;9(1):18457.
3. Bandt C, Pompe B. Permutation entropy: a natural complexity measure for time series. Phys Rev Lett. 2002 Apr 29;88(17):174102.
4. Bandt C. A New Kind of Permutation Entropy Used to Classify Sleep Stages from Invisible EEG Microstructure. Entropy. 2017 May;19(5):197.
5. Parlitz U, Berg S, Luther S, Schirdewan A, Kurths J, Wessel N. Classifying cardiac biosignals using ordinal pattern statistics and symbolic dynamics. Comput Biol Med. 2012 Mar 1;42(3):319–27.
6. Keller K, Unakafov AM, Unakafova VA. Ordinal Patterns, Entropy, and EEG. Entropy. 2014 Dec;16(12):6212–39.
7. Amigó JM, Keller K, Unakafova VA. Ordinal symbolic analysis and its application to biomedical recordings. Philos Trans R Soc Math Phys Eng Sci. 2015 Feb 13;373(2034):20140091.
8. Shannon CE. A Mathematical Theory of Communication. Bell Syst Tech J. 1948;27(3):379–423.
9. Nunez PL, Srinivasan R. Electric fields of the brain: the neurophysics of EEG. 2nd ed. Oxford; New York: Oxford University Press; 2006. 611 p.
10. Nunez PL, Srinivasan R, Westdorp AF, Wijesinghe RS, Tucker DM, Silberstein RB, et al. EEG coherency: I: statistics, reference electrode, volume conduction, Laplacians, cortical imaging, and interpretation at multiple scales. Electroencephalogr Clin Neurophysiol. 1997 Nov 1;103(5):499–515.
11. Nunez PL, Silberstein RB, Shi Z, Carpenter MR, Srinivasan R, Tucker DM, et al. EEG coherency II: experimental comparisons of multiple measures. Clin Neurophysiol Off J Int Fed Clin Neurophysiol. 1999 Mar;110(3):469–86.
12. Li G, Jiang S, Paraskevopoulou SE, Wang M, Xu Y, Wu Z, et al. Optimal referencing for stereo-electroencephalographic (SEEG) recordings. NeuroImage. 2018 Dec 1;183:327–35.

ACS Pharmacology & Translational Science

pubs.acs.org/ptsci

Article

EEG Gamma Band Alterations and REM-like Traits Underpin the Acute Effect of the Atypical Psychedelic Ibogaine in the Rat

Joaquín González, Matias Cavelli, Santiago Castro-Zaballa, Alejandra Mondino, Adriano B. L. Tort, Nicolás Rubido, Ignacio Carrera,* and Pablo Torterolo*

Cite This: https://dx.doi.org/10.1021/acsptsci.0c00164

Read Online

ABSTRACT: Ibogaine is a psychedelic alkaloid that has attracted large scientific interest because of its antiaddictive properties in observational studies in humans as well as in animal models. Its subjective effect has been described as intense, vivid dream-like experiences occurring while awake; hence, ibogaine is often referred to as an oneirogenic psychedelic. While this unique dream-like profile has been hypothesized to aid the antiaddictive effects, the electrophysiological signatures of this psychedelic state remain unknown. We previously showed in rats that ibogaine promotes a waking state with abnormal motor behavior along with a decrease in NREM and REM sleep. Here, we performed an in-depth analysis of the intracranial electroencephalogram during "ibogaine wakefulness". We found that ibogaine induces gamma oscillations that, despite having larger power than control levels, are less coherent and less complex. Further analysis revealed that this profile of gamma activity compares to that of natural REM sleep. Thus, our results provide novel biological evidence for the association between the psychedelic state and REM sleep, contributing to the understanding of the brain mechanisms associated with the oneirogenic psychedelic effect of ibogaine.

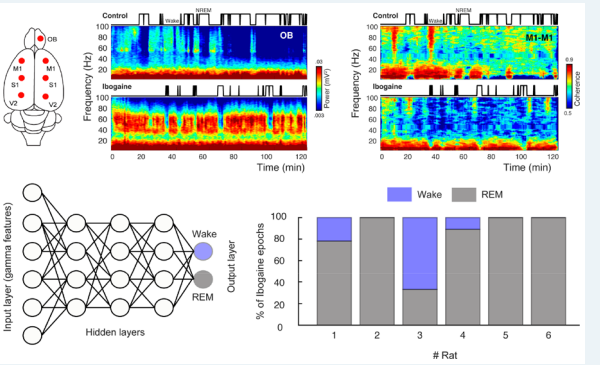

KEYWORDS: *ibogaine, intracranial electroencephalogram, computational neuroscience, sleep-wake cycle, psychedelics*

Ibogaine is a potent psychedelic alkaloid that has attracted scientific interest because of its long-lasting antiaddictive properties,[1] evidenced in anecdotal and observational studies in humans,[2−5] and in extensive preclinical work in rodents.[6−14] Subjective reports portray the ibogaine experience as entering into an intense dream-like episode while awake, involving memory retrieval and prospective imagination, without producing the typical interferences in thinking, identity distortions, and space−time alterations produced by classical psychedelics (e.g., DMT, LSD, psilocybin).[15−18] Thus, ibogaine is often referred to as an oneirogenic psychedelic.[16,18]

In spite of the vast amount of preclinical research regarding the antiaddictive effects of ibogaine, the biological substrate of its unique oneiric effects remains elusive. Although seemingly unrelated, the oneirogenic effects of ibogaine have been hypothesized to aid its antiaddictive properties.[1,19] Taking into account that most vivid dreams occur during REM sleep, the dream-like experiences would be the manifestation of a REM sleep-like brain state, which in turn could favor the antiaddictive effects through an increase in neural plasticity and memory reconsolidation, similar to previously reported functions of natural REM sleep.[20] Therefore, if this conjecture is true, we should expect to find REM sleep characteristics in the electrocortical activity following the administration of ibogaine.

In our previous work,[21] we showed in rats that ibogaine promotes a wakefulness state with abnormal motor behaviors in a dose dependent manner. These effects were accompanied by a decrease in NREM sleep and a profound REM sleep suppression. Nevertheless, as the analysis relied on visual inspection, we were not able to answer which features characterize the waking state induced by ibogaine. Therefore, in the present work we performed a state-of-the-art computational analysis of the intracranial electroencephalogram (iEEG), employing a set of electrodes distributed across the cortex bilaterally, to analyze effects of ibogaine during the first 2 h after its intraperitoneal administration. Upon analyzing the data, we found a unique iEEG profile during wakefulness, which is compatible with a REM-like brain state. Hence, our results provide the first electrophysiological evidence of a wakefulness dream-like brain state produced by ibogaine.

Special Issue: Psychedelics

Received: October 6, 2020

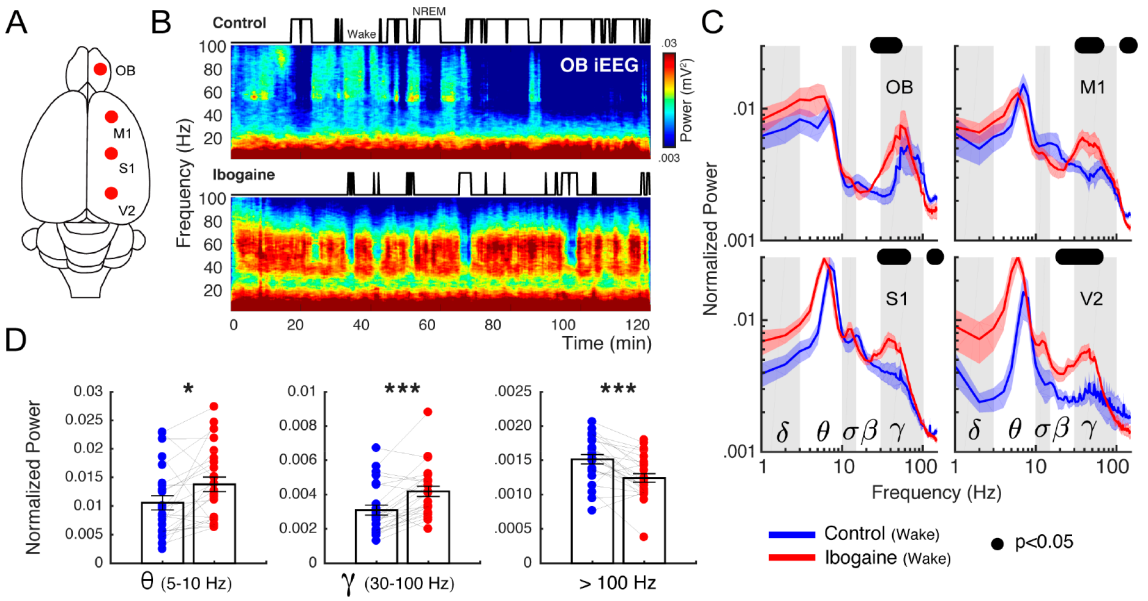

Figure 1. Ibogaine significantly alters iEEG frequency distribution. (A) Location of the analyzed intracranial electrodes in the right hemisphere (OB, olfactory bulb; M1, primary motor cortex; S1, primary somatosensory cortex; V2, secondary visual cortex). (B) Spectrograms from a representative animal following the administration of saline (control) and ibogaine (40 mg/kg). The hypnograms are plotted on top. (C) Normalized power spectra during wakefulness (see Methods for normalization details). The solid line represents the mean (n = 6 animals) for the first 2 h postinjection; the shaded area depicts the standard error of the mean (S.E.M.). The black dots mark the statistically significant frequencies ($p < 0.05$) corrected by a cluster-based permutation test. The traditional frequency bands (Greek letters) are delimited by gray and white boxes in each plot. The differences between hemispheres were minimal (see Figure S2). (D) Mean power for theta, gamma, >100 Hz (up to 512 Hz) frequency bands. Each point corresponds to an electrode of a single animal; bars show mean ± S.E.M. *$p < 0.05$, *** $p < 0.001$, paired t test.

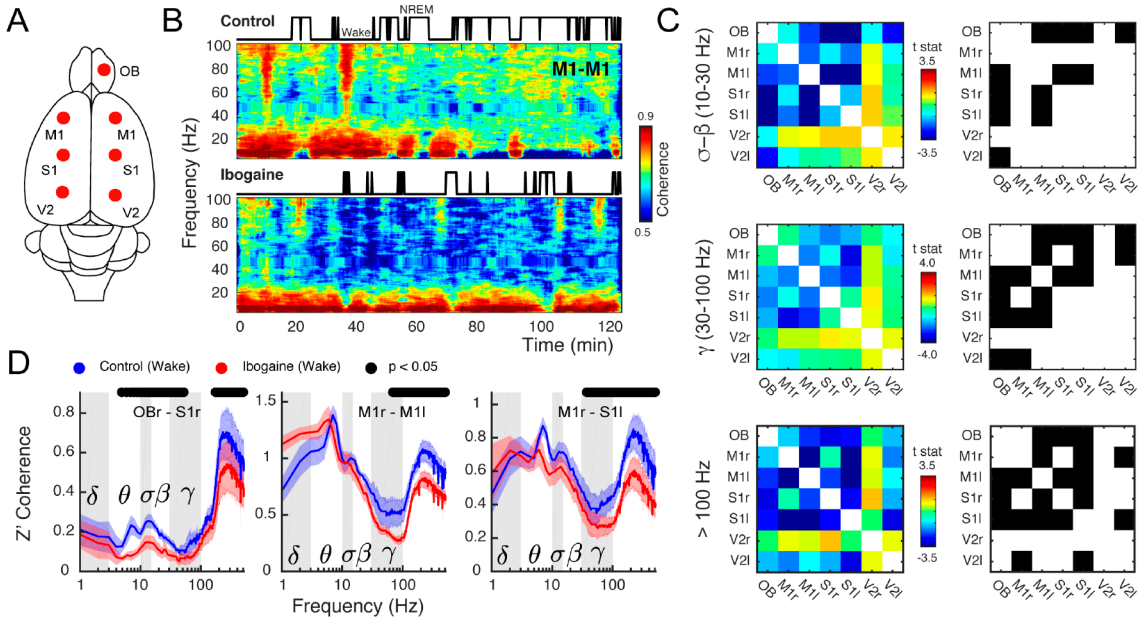

Figure 2. Ibogaine decreases long-range phase synchronization. (A) Location of the analyzed intracranial electrodes. (B) Coherogram following saline (control) and ibogaine (same animal and epoch as in Figure 1B). The hypnograms are plotted on top. This plot shows the phase coherence between the right and left primary motor cortex as a function of time and frequency. (C) The left column shows the t-statistic (t-stat) of the pairwise coherence difference matrix (i.e., the average difference is divided by the S.E.M.) for three frequency bands (sigma-beta, gamma and >100 Hz, up to 512 Hz). The right column shows the electrode pairs with a significant difference ($p < 0.05$, corrected cluster-based permutation test; r, right; l, left). (D) Z′ coherence as a function of frequency of three representative combinations of electrodes (same labels, statistical analysis, and wakefulness epochs as in Figure 1C).

RESULTS

Ibogaine Alters iEEG Oscillatory Components. To understand the acute effects of ibogaine on the rat brain, we recorded iEEG signals following its intraperitoneal administration (40 mg/kg). Electrodes were located above the olfactory bulb (OB), primary motor (M1), primary somatosensory (S1) and secondary visual cortex (V2), allowing us to monitor the dynamical and regional effects of ibogaine (Figure 1A). As a

https://dx.doi.org/10.1021/acsptsci.0c00164
ACS Pharmacol. Transl. Sci. XXXX, XXX, XXX−XXX

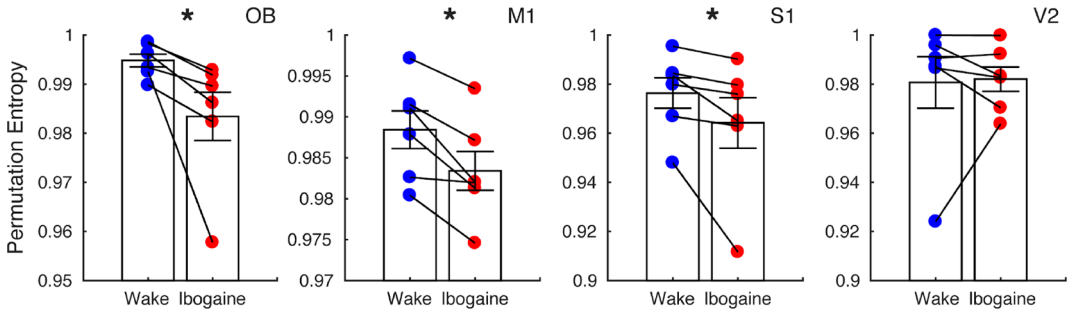

Figure 3. Ibogaine decreases iEEG complexity. Permutation entropy is employed to quantify the iEEG temporal complexity in normal (blue) and ibogaine (red) wake states (same electrodes as in Figure 1). Each dot shows the average permutation entropy of an animal ($n = 6$). Bars represent mean ± S.E.M. *$p < 0.05$, paired t test.

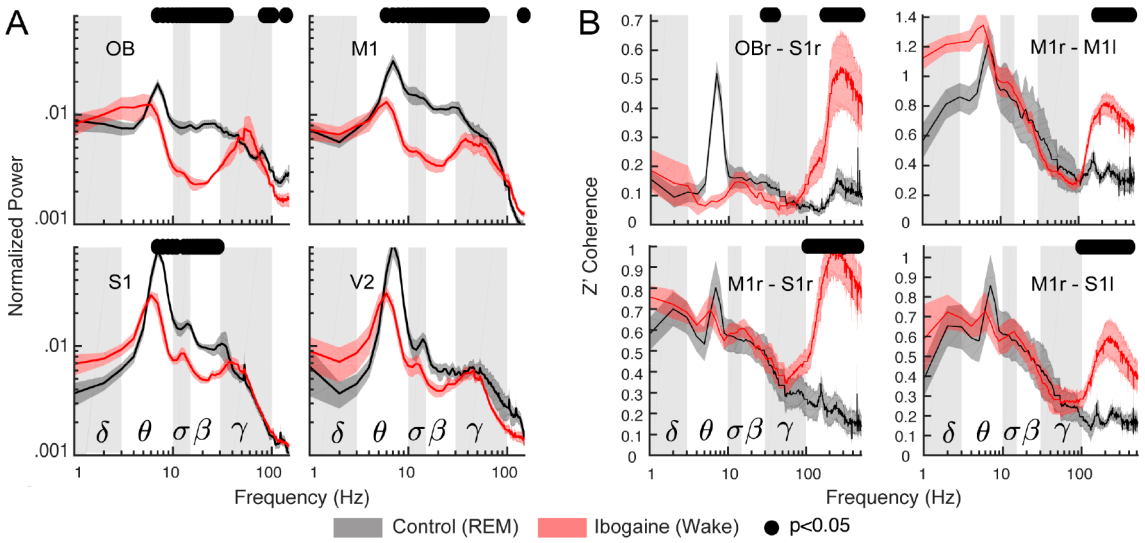

Figure 4. The ibogaine wakefulness shows REM sleep features in the gamma band. (A) Power spectrum comparison between REM sleep (black) and the ibogaine wakefulness (red); only the right hemisphere is shown. The solid line represents the mean ($n = 6$ animals); the shaded area depicts the S.E.M. (B) Coherence comparisons between REM sleep and ibogaine. The black dots mark the statistically significant frequencies ($p < 0.05$) corrected by a cluster-based permutation test.

working example, Figure 1B shows the OB time-frequency response after we administered saline (control) and ibogaine; time zero corresponds to the moment of injection. Compared to control, gamma oscillations (30−80 Hz) increased following the administration of ibogaine; this increase lasted for at least 2 h. Note that this higher gamma power occurred associated with a longer time the animal spent awake (shown in the hypnogram). To analyze ibogaine effects at the group level, we considered only the wakefulness episodes in experimental and control conditions (Figure 1)C. In comparison to control, ibogaine significantly increased gamma oscillations in the OB, M1, S1, and V2 areas (Figure 1C, and summarized in Figure 1D).

Along with the changes in gamma frequencies, the mean theta power increased (Figure 1D), while also decreasing its peak frequency from 9 to 8 Hz (readily observed in S1 and V2 cortices because of their proximity to the hippocampus, Figure S1). Additionally, the high-frequency power (>100 Hz and up to 512 Hz) decreased in M1, S1, and V2 (see Figure 1C,D), though the lack of a spectral peak suggests this result arises from changes in muscular activity produced by the drug.[22]

Ibogaine Decreases Inter-regional Synchronization. Since ibogaine significantly altered the oscillatory power content of the iEEG, we next quantified its impact on long-range synchronization of brain areas within and across hemispheres (Figure 2A). Figure 2B shows an example of interhemispheric coherence between M1 cortices as a function of time (same animal as in Figure 1B). Interestingly, as opposed to its effect on gamma power, ibogaine strongly decreased inter-regional gamma synchronization.

Figure 2C shows a group level analysis separated by frequency bands by means of pairwise electrode matrices (left column), which depict coherence differences (t-statistic) between conditions (saline vs ibogaine) in pseudocolor scale for each electrode pair (blue indicates a coherence decrease while red an increase). The electrode pairs with significant differences are also indicated in the right column. Ibogaine decreased phase coherence at the sigma-beta, gamma, and high-frequency bands in multiple cortical areas, including the OB, M1, and S1 (Figure 2C,D). In particular, inter-regional gamma coherence decreased in 9 of the 21 electrode pairs, including between right OB and right S1 cortex (Figure 2D, left panel), two areas that had an increase in their gamma power (Figure 1C). The same gamma coherence reduction occurred in the interhemispherical M1−M1 and M1−S1 electrode combination, but not in the intrahemispherical M1−S1 (see Figure 2D and Figure S3).

Ibogaine Decreases iEEG Temporal Complexity. In the previous sections, we showed that ibogaine promoted local gamma oscillations which were uncoupled between areas. This

https://dx.doi.org/10.1021/acsptsci.0c00164
ACS Pharmacol. Transl. Sci. XXXX, XXX, XXX−XXX

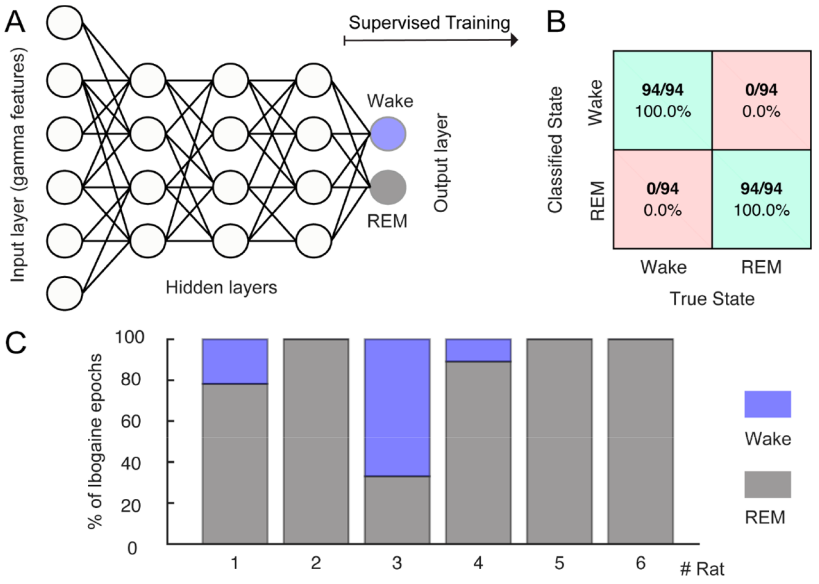

Figure 5. The ibogaine-induced brain state is considered a REM-like state by an automatic sleep scoring algorithm. (A) Schematic representation of the neural network employed to classify the states of wakefulness and REM sleep. The network contains one input layer which receives the gamma features (power and coherence of the OB, M1, and S1 electrodes), and 10 hidden layers (only three of them are shown in the picture). The network has one output layer with two nodes (wake and REM). (B) Confusion matrix for an individual animal. (C) Bar plots showing how ibogaine wakefulness epochs were classified. Each animal is shown separately and was tested with its own control network.

activity resembles gamma oscillations that naturally occur during REM sleep[23−25] (Figure S4), suggesting that the awake state under ibogaine exhibits similar REM sleep characteristics. To delve further into this matter, we tested the resemblance between states in their temporal complexity. This is important because the temporal complexity during REM sleep is significantly lower than during wakefulness, which can be observed independent of the cortical area and for a wide range of time-scales.[26]

To assess the temporal complexity, we down-sampled the original signals to 128 Hz (avoiding muscular contamination) and measured the permutation entropy of the time-series. This metric quantifies the diversity of dynamical motifs in the iEEG (larger values mean the signal has higher diversity, hence more complexity) and is robust to the presence of noise and short time measurements (see Material and Methods and.[27] Figure 3 shows the average permutation entropy for each cortical electrode. Interestingly, in comparison to normal (control) wakefulness, ibogaine wakefulness displayed significantly lower levels of dynamical complexity in OB, M1 and S1 cortex. Note that these areas are the ones with most prominent changes in power and coherence. No significant changes were observed in V2. We should also point out that by virtue of downsampling, the gamma band oscillations are the only relevant frequencies contained in our complexity estimate.

Ibogaine Wakefulness and REM Sleep Have Similar iEEG Gamma Activity. The previous section showed that the ibogaine awake state differs from normal wakefulness. We next compared the ibogaine-induced brain state with physiological REM sleep (Figure 4A). We found that theta, sigma, and beta power were lower during ibogaine wakefulness than in REM sleep. On the other hand, the high-frequency component (>100 Hz) had significantly higher power, likely due to muscular activity. Noteworthy, the power of gamma oscillations was similar between both states and minor statistically significant differences were found in the OB and M1 with larger gamma power during REM (Figure 4A). Furthermore, we also found similar levels of gamma coherence in the ibogaine wakefulness and REM sleep, even for electrode combinations which showed significant changes between physiological and ibogaine wakefulness (compare Figure 2B with Figure 4C). In contrast, the high-frequency spectrum was more coherent during ibogaine wakefulness than during REM sleep, probably as a consequence of the absence of muscle activity during REM sleep.

We also found that the temporal complexity during the ibogaine wakefulness was close to that of REM sleep (Figure S5); it was only significantly larger during ibogaine wakefulness in the M1 cortex. Overall, the data show that iEEG complexity during ibogaine wakefulness is between normal wakefulness and REM sleep. Thus, although there are differences between ibogaine wakefulness and REM sleep, the power, complexity, and inter-regional synchronization of gamma oscillations are comparable.

Finally, we directly tested whether the ibogaine wakefulness was closer to a REM-like state or to physiological wakefulness. For this purpose, we trained an artificial neural network to automatically classify the states of wakefulness and REM sleep. Figure 5A shows a schematic representation of the network, which is fed with the levels of gamma power, and coherence of single 10-s artifact free epochs (input layer) and the output were the behavioral states (wake or REM, output layer). After supervised training, the network successfully distinguished between wakefulness and REM (the confusion matrix for a representative animal is shown in Figure 5B). Then, the network was fed with ibogaine wakefulness data, these epochs were mostly classified as being REM sleep instead of wakefulness (Figure 5C). In fact, in 5 out of 6 animals the majority of the ibogaine epochs were classified as REM sleep, and in 3 animals all ibogaine epochs were classified as such. Therefore, these results show that the gamma oscillations induced by ibogaine have convincing REM sleep-like features.

https://dx.doi.org/10.1021/acsptsci.0c00164
ACS Pharmacol. Transl. Sci. XXXX, XXX, XXX−XXX

DISCUSSION

In the present study, we found that intraperitoneal administration of ibogaine in male rats induces a waking brain state that has electrocortical REM sleep traits. These traits appear in the form of high-power local gamma oscillations in the OB, M1, S1 areas, which are less coherent and less complex than in normal wakefulness. These features of gamma oscillations are similar to the ones present during REM sleep (Figures 4 and 5 and Figure S4). Therefore, by measuring an important neurophysiological trait, our results support previous oneirogenic conjectures of ibogaine's induced psychedelic state.[1,19] Interestingly, some of these traits were dragged into NREM sleep; compared to physiological NREM sleep, ibogaine NREM sleep showed gamma power increase circumscribed to the OB, and lower gamma coherence in several derivations (Figure S6). It should be noted, however, that our results only suggest the oneirogenic nature of the ibogaine state, but do not provide further evidence of the relationship between this oneiric state and the antiaddictive properties of ibogaine.

The relationship between this unique wakefulness promoted by ibogaine and the antiaddictive properties is speculative, as another experimental design should be employed to address this matter. However, considering that it had been reported by several ibogaine users that the dream-like experiences helped them change their addictive behaviors, and our findings showing that ibogaine induces a wakefulness state showing REM-like traits (i.e., a dissociate state), it is likely that this unique wakefulness state could be related to its antiaddictive properties. Nevertheless, we cannot rule out that the suppression of REM sleep by itself, could be also related to the antiaddictive effect induced by ibogaine.

When comparing our results to the effects elicited by other psychedelics, the lack of previous reports involving quantitative iEEG analysis of the psychedelic state in rodents forces us to compare our results to previous literature in human beings. For instance, the administration of 5-HT_{2A} agonist (e.g., LSD, psilocybin, DMT) in humans reduces alpha (8−12 Hz) and beta band power and decreases their functional connectivity.[28−32] Similarly, our results show that ibogaine also reduced the connectivity at sigma and beta bands (10−30 Hz). Additionally, it is worth noting that we found significant changes in the OB, while in humans the predominant effects of traditional psychedelics are observed in the visual cortex.[29] Thus, both psychedelic effects involve major sensory areas relevant to each species. Furthermore, complementary analyses show that the gamma coupling to other frequencies is not affected by ibogaine in any of the cortical locations (Figure S7). As the slow OB oscillations (1−4 Hz) reflect the slow respiratory potentials,[33,34] our results suggest that sensory information is still likely to reach the OB, but is later integrated in an altered way, similar to the psychedelic state in humans.[28]

In addition to the electrophysiological similarities between ibogaine and serotoninergic psychedelics, the type of cognition elicited by the latter has been described as analogous to the one present during dreams[28] (both referred as primary states of consciousness). In fact, a recent work shows that unlike other drugs (cocaine, opioids, etc.), the semantic content of psychedelic experiences is closely related to dreams.[35] Since dreams are to a large extent the cognitive correlates of REM sleep,[36] our report confirms such connection for ibogaine.

Nevertheless, as mentioned before, human subjective reports also indicate differences between the experience elicited by ibogaine and classic psychedelics. Pharmacological and behavioral data in rodents also support these differences. While classical psychedelics share the ability to interact with the 5-HT_{2A} receptor in the low nanomolar range inducing the head twitch response (HTR) in rodents,[17] ibogaine binds to this receptor in the micromolar range[37,38] without producing HTR or similar responses.[21] Also, previous drug discrimination studies in rats showed that although ibogaine may produce some of its effect via 5-HT_{2A} activation, this does not appear to be essential to the ibogaine-discriminative stimulus, since pirenperone (5-HT_{2A} antagonist) did not affect the ibogaine-appropriate response.[38,39] Further studies employing the same iEEG methodology should shed light into the electrophysiological similarities and differences between the wakefulness state induced by classical psychedelics and ibogaine.

It should be noted that ibogaine is rapidly metabolized (half-life: 1.22 hs) to produce noribogaine, which has its own pharmacological and pharmacokinetic profiles.[40,41] According to pharmacokinetic data,[42] both substances are present in the rat brain at pharmacologically relevant concentrations during the first 2 h after ibogaine 40 mg/kg i.p. administration. Non-competitive antagonism of *N*-methyl-D-aspartate receptors (NMDA-R) by ibogaine[43−48] and to a lesser extent by noribogaine[44,45] should be considered as a key factor to explain the effects on the gamma band, since ketamine (a non-competitive NMDA-R antagonist) also produces a marked increase in gamma power[49−52] while decreasing inter-regional gamma coherence.[51,52]

Nevertheless, effects on other neurotransmitter systems and receptors should be also considered. Since ibogaine and noribogaine inhibit serotonin reuptake by modulating SERT activity (noribogaine being approximately ten-times more potent than ibogaine),[53,54] the increase in serotoninergic transmission, in addition to the above-mentioned interaction of ibogaine with 5HT_{2A} receptor, could explain some of the similarities found in the electrocortical activity between ibogaine and classic psychedelics. Additionally, the potential contribution of the kappa opioid action of noribogaine[55] as a biased agonist should also be considered, as other kappa agonists induce oscillations in the theta range (4−10 Hz),[56−58] resembling our results.

As a final remark, our results show that ibogaine promotes a waking brain state with REM sleep traits. Because most dreams occur during REM sleep, this new finding accounts for the oneirogenic psychedelic effect experienced after ibogaine consumption, thus providing novel biological evidence linking psychedelics and REM sleep.

METHODS

Ibogaine. Ibogaine was obtained and purified from *T. Iboga* extracts following the procedures employed in ref 21 (see Ibogaine Supplementary Information in the Supporting Material for the purification protocol, structure elucidation, and purity profile). A 40 mg/kg dose (i.p.) was employed in this work, which is the effective dose used in the preclinical literature to obtain long lasting effects in the self-administration paradigms in rats, and that in our previous study showed to have the largest effect on the wakefulness−sleep architecture.[21] Dissolution of ibogaine−HCl to prepare the samples for intraperitoneal (i.p.) injection was carried out using warm saline that was previously degassed by nitrogen bubbling (~17 mg of ibo-HCl/mL of saline).

https://dx.doi.org/10.1021/acsptsci.0c00164
ACS Pharmacol. Transl. Sci. XXXX, XXX, XXX−XXX

Experimental Animals. Six Wistar male adult rats were maintained on a 12-h light/dark cycle (lights on at 07.00 h).

Although to analyze only one gender is a limitation of the study, we took it as a first approach to explore the effects of ibogaine on electrocortical activity. Food and water were freely available. The animals were determined to be in good health by veterinarians of the institution. All experimental procedures were conducted in agreement with the National Animal Care Law (No. 18611) and with the "Guide to the Care and Use of Laboratory Animals" (8th edition, National Academy Press, Washington, DC. 2010). Furthermore, the Institutional Animal Care Committee approved the experimental procedures (Exp. No. 070153-000332-16). Adequate measures were taken to minimize pain, discomfort, or stress of the animals, and all efforts were made to use the minimal number of animals necessary to obtain reliable scientific data. Each animal received the ibogaine and the vehicle dose in different days, and was therefore its own control.

Surgical Procedures. The animals were chronically implanted with electrodes to monitor the states of sleep and wakefulness. We employed similar surgical procedures as in our previous studies.[21,24,25] Anesthesia was induced with a mixture of ketamine−xylazine (90 mg/kg; 5 mg/kg i.p., respectively). The rat was positioned in a stereotaxic frame and the skull was exposed. To record the iEEG, stainless steel screw electrodes were placed in the skull above motor, somatosensory, visual cortices (bilateral), the right olfactory bulb, and cerebellum, which was the reference electrode (see Table S1). To record the electromyogram (EMG), two electrodes were inserted into the neck muscle. The electrodes were soldered into a 12-pin socket and fixed onto the skull with acrylic cement. At the end of the surgical procedures, an analgesic (ketoprofen, 1 mg/kg, s.c.) was administered. After the animals had recovered from these surgical procedures, they were left to adapt in the recording chamber for 1 week.

Experimental Sessions. Animals were housed individually in transparent cages (40 × 30 × 20 cm^3) containing wood shaving material in a temperature-controlled room (21−24 °C), with water and food *ad libitum*. Experimental sessions were conducted during the light period, between 10 AM and 4 PM during the light phase in a sound-attenuated chamber with Faraday shield. Before the beginning of the recordings, animals were injected with a 40 mg/kg ibogaine dose or vehicle i.p. The recordings were performed through a rotating connector, to allow the rats to move freely within the recording box. Polysomnographic data were acquired and stored in a computer using the Dasy Lab Software employing 1024 Hz as a sampling frequency and a 16 bits AD converter.

Sleep Scoring. The states of sleep and wakefulness were determined in 10-s epochs. Wakefulness was defined as low-voltage fast waves in the motor cortex, a noticeable theta rhythm (4−7 Hz) in the somatosensory and visual cortices, and relatively high EMG activity. NREM sleep was determined by the presence of high-voltage slow cortical waves together with sleep spindles in frontal, parietal, and occipital cortices associated with a reduced EMG amplitude; REM sleep as low-voltage fast frontal waves, a regular theta rhythm in the occipital cortex, and a silent EMG except for occasional twitches. Artifacts and transitional epochs were removed employing visual supervision.

Data Analysis. To evaluate the ibogaine effect on iEEG activity, we selected the first 2 h following its i.p. administration (10 AM to 12 AM) since almost continuous wakefulness and abnormal motor and autonomic effects (tremor, piloerection) were only evident during this period.[21] From the first 2 h, only artifact-free wake epochs were analyzed from both the control and ibogaine experiments. NREM sleep epochs were selected from the entire 6 h due to the reduced time of this state after ibogaine i.p. administration. Additionally, REM sleep epochs from control experiments were also examined. REM sleep following ibogaine administration was not considered due to the lack of this state in several animals.

Power Spectrum. The power spectrum was obtained by means of the *pwelch* built-in function in Matlab (parameters: window = 1024, noverlap = [], fs = 1024, nfft = 1024), which corresponds to 1-s sliding windows with half-window overlap, and a frequency resolution of 1 Hz. The time-frequency spectrograms were obtained employing the function *mtspecgramc* from the Chronux toolbox[59] (available at: http://chronux.org), using five tapers and a time-bandwidth product of 5. All spectra were whitened by multiplying the power at each frequency by the frequency itself, thus counteracting the 1/f trend. In addition, the spectra were normalized to obtain the relative power by dividing the power value of each frequency by the sum across frequencies. The traditional frequency bands depicted in the figures were taken as delta (1−4 Hz), theta (5−10 Hz), sigma (11−14 Hz), beta (15−29 Hz), and gamma (30−100 Hz).

Spectral Coherence. To measure synchronization between electrodes, we employed the magnitude squared coherence using the *mscohere* built-in function in Matlab (parameters: window = 1024, noverlap = [], fs = 1024, nfft = 1024), which corresponds to 1-s sliding windows with half-window overlap, and a frequency resolution of 1 Hz. The time-frequency coherograms were obtained employing the function *cohgramc* from the Chronux toolbox, using 10 tapers and a time-bandwidth product of 100.

Cluster-Based Permutation Test. To obtain statistical thresholds for group comparisons of power and coherence, we employed a data-driven approach comparing empirical clusters of frequencies instead of comparing traditionally defined frequency bands. The method consisted of first comparing individual frequencies (512 frequencies) in each condition by means of paired *t* tests ($\alpha = 0.05$). Once we obtained the *p* values for each frequency, all consecutive significant frequencies were grouped into empirical clusters (defining a minimum cluster size of four frequency points), and a new statistic was formed by summing the *t*-statistic of each frequency inside the cluster. To assess whether a given cluster was significant, a null hypothesis distribution of cluster statistics was constructed by randomizing labels (control and ibogaine) and repeating the cluster construction method for a total of 10 000 randomizations. The *p* values of the empirical clusters were obtained by comparing each cluster statistic to the randomized cluster statistic distribution (X). We employed two-tailed comparisons for the power spectrum and permutation entropy ($p_{value} = 2\min(P(X > X_{obs})), P(X < X_{obs}))$, and one-tailed for the coherence comparisons ($p_{value} = P(X < X_{obs})$).

Permutation Entropy. Prior to quantifying the permutation entropy, the iEEGs were down-sampled to 128 Hz. The framework consisted of 2 main steps. In the first step, we encoded the time-series into ordinal patterns (OP) following the Bandt and Pompe method.[27] The encoding involves dividing a time-series $\{x(t), t = 1, \cdots, T\}$ into $\lfloor (T - D)/D \rfloor$ nonoverlapping vectors, where $\lfloor y \rfloor$ denotes the largest integer less than or equal to y and D is the vector length, which is much shorter than the

https://dx.doi.org/10.1021/acsptsci.0c00164
ACS Pharmacol. Transl. Sci. XXXX, XXX, XXX−XXX

time-series length ($D \ll T$). Then, each vector is classified according to the relative magnitude of its D elements. Namely, we determined how many permutations between neighbors are needed to sort its elements in increasing order; then, an OP represents the vector permutations. The second step consists in applying the Shannon entropy to quantify the average randomness (information content) of the OP distribution. Shannon entropy is defined as $H = -\sum p(\mathrm{OP}) \log[p(\mathrm{OP})]$, where $p(\mathrm{OP})$ is the probability of finding a given OP in the signal (among the set of all OPs), and the summation is carried over all possible OPs. To assess the statistical significance between conditions, we employed paired two-tailed t tests with $\alpha = 0.05$.

Gamma-Band Sleep Scoring Neural Network. A multilayer perceptron (10 hidden layers) was employed to distinguish between the states of wakefulness and REM sleep.

We used the built-in classification network *patternnet* in Matlab. The input to the network consists of values of gamma power (OB, M1r, M1l, S1r) and coherence (the nine significant pairs in Figure 2C). The network was trained through a supervised scheme employing the visually scored states in the control condition (either Wake or REM). The training was performed employing the scaled conjugate gradient backpropagation algorithm (*trainscg* built-in function in Matlab), and the performance of the network was evaluated by the cross-entropy algorithm (*crossentropy* built-in function in Matlab).

Phase-Amplitude Coupling. To measure coupling between frequencies within a same region, we employed the modulation index method.[60] Briefly, the raw signal was filtered between 1 and 15 Hz in 1-Hz steps and 3-Hz bandwidth (*eegfilt* function in EEGLAB;[61] to obtain the slow frequency components, and then the phase time series were extracted from their analytical representation based on the Hilbert transform (*hilbert* built-in function in Matlab). In addition, the same raw signal was also filtered between 40 and 180 Hz in 10 Hz steps (bandwidth 10 Hz) to obtain the faster frequency components, and their amplitude time series are also obtained from the analytical representation. Then, phase-amplitude distributions were computed between all slow-fast frequency combinations. Finally, the modulation index was obtained as $\mathrm{MI} = (H_{\max} - H)/H_{\max}$, where $H_{\max}$ is the maximum possible Shannon entropy for a given distribution (log(number of bins)) and H is the actual entropy. The MI value of each slow-fast frequency combination was plotted in pseudocolor scale to obtain the comodulation maps. To assess the statistical significance between conditions, we employed paired two-tailed t tests with $\alpha = 0.05$.

■ ASSOCIATED CONTENT

Supporting Information

The Supporting Information is available free of charge at https://pubs.acs.org/doi/10.1021/acsptsci.0c00164.

> Electrode location; ibogaine's effect on theta oscillations; ibogaine's effect on right and left hemispheres; coherence between all electrodes; power and coherence during wakefulness and REM sleep; permutation entropy during REM; ibogaine's effects on NREM sleep; ibogaine's effect on cross-frequency coupling; ibogaine chemical supplemental information (PDF)

■ AUTHOR INFORMATION

Corresponding Authors

Pablo Torterolo − *Departamento de Fisiología, Facultad de Medicina, Universidad de la República, Montevideo 11200, Uruguay*; Email: ptortero@fmed.edu.uy

Ignacio Carrera − *Departamento de Química Orgánica, Facultad de Química, Universidad de la República, Montevideo, Uruguay*; orcid.org/0000-0002-6053-3162; Email: icarrera@fq.edu.uy

Authors

Joaquín González − *Departamento de Fisiología, Facultad de Medicina, Universidad de la República, Montevideo 11200, Uruguay*; orcid.org/0000-0002-8721-4292

Matias Cavelli − *Departamento de Fisiología, Facultad de Medicina, Universidad de la República, Montevideo 11200, Uruguay; Department of Psychiatry, University of Wisconsin, Madison, Wisconsin 53558, United States*

Santiago Castro-Zaballa − *Departamento de Fisiología, Facultad de Medicina, Universidad de la República, Montevideo 11200, Uruguay*

Alejandra Mondino − *Departamento de Fisiología, Facultad de Medicina, Universidad de la República, Montevideo 11200, Uruguay; Department of Anesthesiology, University of Michigan, Ann Arbor, Michigan 48103, United States*

Adriano B. L. Tort − *Brain Institute, Federal University of Rio Grande do Norte, Natal, Rio Grande do Norte 59056, Brazil*

Nicolás Rubido − *Aberdeen Biomedical Imaging Centre, University of Aberdeen, Aberdeen AB25 2ZG, United Kingdom; Instituto de Física de Facultad de Ciencias, Universidad de la República, Montevideo 11400, Uruguay*

Complete contact information is available at: https://pubs.acs.org/10.1021/acsptsci.0c00164

Author Contributions

J.G., M.C., I.C., and P.T. designed the experiments; J.G., M.C., and A.M., conducted the experiments; J.G. and N.R., wrote analysis software; J.G. analyzed the data; J.G., M.C., A.M., S.C., N.R., A.B.L.T., I.C., and P.T. were involved in the discussion and interpretation of the results; J.G., A.B.L.T., I.C., and P.T. wrote the manuscript. All the authors participated in the critical revision of the manuscript, added important intellectual content, and approved the final version.

Notes

The authors declare no competing financial interest.

Data and code availability. Data is available under request to the authors. The codes to obtain power and coherence spectra can be found in the Chronux toolbox and standard Matlab toolboxes. The code to perform the correction for multiple comparisons based on cluster-based permutation tests and to compute permutation entropy is freely available at https://github.com/joaqgonzar/Ibogaine_analysis_2020. In addition, the specific code employed in the multilayer perceptron is also available upon request.

■ ACKNOWLEDGMENTS

This study was supported by the Programa de Desarrollo de Ciencias Básicas, PEDECIBA; Agencia Nacional de Investigación e Innovación (ANII), (FCE-1-2017-1-136550) and the Comisión Sectorial de Investigación Científica (CSIC) I+D-2016-589 grant from Uruguay. J.G. was supported by CAP (Comisión Académica de Posgrado) and CSIC Iniciación. N.R.

acknowledges the CSIC group Grant CSIC2018-FID 13-Grupo ID 722. A.B.L.T. was supported by Conselho Nacional de Desenvolvimento Científico e Tecnológico (CNPq) and Coordenacao de Aperfeicoamento de Pessoal de Nível Superior (CAPES), Brazil.

REFERENCES

(1) Alper, K. R. (2001) Ibogaine: A Review. *Alkaloids Chem. Biol. 56*, 1−38.
(2) Brown, T. K., and Alper, K. (2018) Treatment of Opioid Use Disorder with Ibogaine: Detoxification and Drug Use Outcomes. *Am. J. Drug Alcohol Abuse 44* (1), 24−36.
(3) Mash, D. C., Duque, L., Page, B., and Allen-Ferdinand, K. (2018) Ibogaine Detoxification Transitions Opioid and Cocaine Abusers Between Dependence and Abstinence: Clinical Observations and Treatment Outcomes. *Front. Pharmacol. 9*, 529.
(4) Noller, G. E., Frampton, C. M., and Yazar-Klosinski, B. (2018) Ibogaine Treatment Outcomes for Opioid Dependence from a Twelve-Month Follow-up Observational Study. *Am. J. Drug Alcohol Abuse 44* (1), 37−46.
(5) Schenberg, E. E., de Castro Comis, M. A., Chaves, B. R., and da Silveira, D. X. (2014) Treating Drug Dependence with the Aid of Ibogaine: A Retrospective Study. *J. Psychopharmacol. 28* (11), 993−1000.
(6) Dzoljic, E. D., Kaplan, C. D., and Dzoljic, M. R. (1988) Effect of Ibogaine on Naloxone-Precipitated Withdrawal Syndrome in Chronic Morphine-Dependent Rats. *Arch. Int. Pharmacodyn. Ther. 294*, 64−70.
(7) Glick, S. D., Rossman, K., Steindorf, S., Maisonneuve, I. M., and Carlson, J. N. (1991) Effects and Aftereffects of Ibogaine on Morphine Self-Administration in Rats. *Eur. J. Pharmacol. 195* (3), 341−345.
(8) Glick, S. D., Rossman, K., Rao, N. C., Maisonneuve, I. M., and Carlson, J. N. (1992) Effects of Ibogaine on Acute Signs of Morphine Withdrawal in Rats: Independence from Tremor. *Neuropharmacology 31* (5), 497−500.
(9) Cappendijk, S. L., and Dzoljic, M. R. (1993) Inhibitory Effects of Ibogaine on Cocaine Self-Administration in Rats. *Eur. J. Pharmacol. 241* (2−3), 261−265.
(10) Glick, S. D., Kuehne, M. E., Raucci, J., Wilson, T. E., Larson, D., Keller, R. W., and Carlson, J. N. (1994) Effects of Iboga Alkaloids on Morphine and Cocaine Self-Administration in Rats: Relationship to Tremorigenic Effects and to Effects on Dopamine Release in Nucleus Accumbens and Striatum. *Brain Res. 657* (1−2), 14−22.
(11) Dworkin, S. I., Gleeson, S., Meloni, D., Koves, T. R., and Martin, T. J. (1995) Effects of Ibogaine on Responding Maintained by Food, Cocaine and Heroin Reinforcement in Rats. *Psychopharmacology (Berl.) 117* (3), 257−261.
(12) Rezvani, A. H., Overstreet, D. H., and Leef, Y. W. (1995) Attenuation of Alcohol Intake by Ibogaine in Three Strains of Alcohol-Preferring Rats. *Pharmacol., Biochem. Behav. 52* (3), 615−620.
(13) Pearl, S. M., Hough, L. B., Boyd, D. L., and Glick, S. D. (1997) Sex Differences in Ibogaine Antagonism of Morphine-Induced Locomotor Activity and in Ibogaine Brain Levels and Metabolism. *Pharmacol., Biochem. Behav. 57* (4), 809−815.
(14) He, D.-Y., McGough, N. N. H., Ravindranathan, A., Jeanblanc, J., Logrip, M. L., Phamluong, K., Janak, P. H., and Ron, D. (2005) Glial Cell Line-Derived Neurotrophic Factor Mediates the Desirable Actions of the Anti-Addiction Drug Ibogaine against Alcohol Consumption. *J. Neurosci. 25* (3), 619−628.
(15) Brown, T. K., Noller, G. E., and Denenberg, J. O. (2019) Ibogaine and Subjective Experience: Transformative States and Psychopharmacotherapy in the Treatment of Opioid Use Disorder. *J. Psychoact. Drugs 51* (2), 155−165.
(16) Naranjo, C. (1974) *The Healing Journey: New Approaches to Consciousness*, Pantheon Books, New York.
(17) Nichols, D. E. (2016) Psychedelics. *Pharmacol. Rev. 68* (2), 264−355.
(18) Schenberg, E. E., de Comis, M. A. C., Alexandre, J. F. M., Tófoli, L. F., Chaves, B. D. R., and da Silveira, D. X. (2017) A Phenomenological Analysis of the Subjective Experience Elicited by Ibogaine in the Context of a Drug Dependence Treatment. *J. Psychedelic Stud. 1* (2), 74−83.
(19) Goutarel, R., Gollnhofer, O., and Salinas, R. (1993) Pharmacodynamics and Therapeutic Applications of Iboga and Ibogaine. *Psychedelic Monogr. Essays 6*, 70.
(20) Izawa, S., Chowdhury, S., Miyazaki, T., Mukai, Y., Ono, D., Inoue, R., Ohmura, Y., Mizoguchi, H., Kimura, K., Yoshioka, M., Terao, A., Kilduff, T. S., and Yamanaka, A. (2019) REM Sleep-Active MCH Neurons Are Involved in Forgetting Hippocampus-Dependent Memories. *Science 365* (6459), 1308−1313.
(21) González, J., Prieto, J. P., Rodríguez, P., Cavelli, M., Benedetto, L., Mondino, A., Pazos, M., Seoane, G., Carrera, I., Scorza, C., and Torterolo, P. (2018) Ibogaine Acute Administration in Rats Promotes Wakefulness, Long-Lasting REM Sleep Suppression, and a Distinctive Motor Profile. *Front. Pharmacol. 9*, 374.
(22) Whitham, E. M., Pope, K. J., Fitzgibbon, S. P., Lewis, T., Clark, C. R., Loveless, S., Broberg, M., Wallace, A., DeLosAngeles, D., Lillie, P., Hardy, A., Fronsko, R., Pulbrook, A., and Willoughby, J. O. (2007) Scalp Electrical Recording during Paralysis: Quantitative Evidence That EEG Frequencies above 20 Hz Are Contaminated by EMG. *Clin. Neurophysiol. 118* (8), 1877−1888.
(23) Castro, S., Falconi, A., Chase, M. H., and Torterolo, P. (2013) Coherent Neocortical 40-Hz Oscillations Are Not Present during REM Sleep. *Eur. J. Neurosci. 37* (8), 1330−1339.
(24) Cavelli, M., Castro, S., Schwarzkopf, N., Chase, M. H., Falconi, A., and Torterolo, P. (2015) Coherent Neocortical Gamma Oscillations Decrease during REM Sleep in the Rat. *Behav. Brain Res. 281*, 318−325.
(25) Cavelli, M., Castro-Zaballa, S., Mondino, A., Gonzalez, J., Falconi, A., and Torterolo, P. (2017) Absence of EEG Gamma Coherence in a Local Activated Cortical State: A Conserved Trait of REM Sleep. *Transl. Brain Rhythm. 2*, No. 115, DOI: 10.15761/TBR.1000115.
(26) González, J., Cavelli, M., Mondino, A., Pascovich, C., Castro-Zaballa, S., Torterolo, P., and Rubido, N. (2019) Decreased Electrocortical Temporal Complexity Distinguishes Sleep from Wakefulness. *Sci. Rep. 9* (1), 18457.
(27) Bandt, C., and Pompe, B. (2002) Permutation Entropy: A Natural Complexity Measure for Time Series. *Phys. Rev. Lett. 88* (17), 174102.
(28) Carhart-Harris, R. L., Leech, R., Hellyer, P. J., Shanahan, M., Feilding, A., Tagliazucchi, E., Chialvo, D. R., and Nutt, D. (2014) The Entropic Brain: A Theory of Conscious States Informed by Neuroimaging Research with Psychedelic Drugs. *Front. Hum. Neurosci. 8*, 20.
(29) Carhart-Harris, R. L., Muthukumaraswamy, S., Roseman, L., Kaelen, M., Droog, W., Murphy, K., Tagliazucchi, E., Schenberg, E. E., Nest, T., Orban, C., Leech, R., Williams, L. T., Williams, T. M., Bolstridge, M., Sessa, B., McGonigle, J., Sereno, M. I., Nichols, D., Hellyer, P. J., Hobden, P., Evans, J., Singh, K. D., Wise, R. G., Curran, H. V., Feilding, A., and Nutt, D. J. (2016) Neural Correlates of the LSD Experience Revealed by Multimodal Neuroimaging. *Proc. Natl. Acad. Sci. U. S. A. 113* (17), 4853−4858.
(30) Pallavicini, C., Vilas, M. G., Villarreal, M., Zamberlan, F., Muthukumaraswamy, S., Nutt, D., Carhart-Harris, R., and Tagliazucchi, E. (2019) Spectral Signatures of Serotonergic Psychedelics and Glutamatergic Dissociatives. *NeuroImage 200*, 281−291.
(31) Timmermann, C., Roseman, L., Schartner, M., Milliere, R., Williams, L. T. J., Erritzoe, D., Muthukumaraswamy, S., Ashton, M., Bendrioua, A., Kaur, O., Turton, S., Nour, M. M., Day, C. M., Leech, R., Nutt, D. J., and Carhart-Harris, R. L. (2019) Neural Correlates of the DMT Experience Assessed with Multivariate EEG. *Sci. Rep. 9* (1), 16324.
(32) Pallavicini, C., Cavanna, F., Zamberlan, F., de la Fuente, L. A., Perl, Y. S., Arias, M., Romero, C., Carhart-Harris, R., Timmermann, C., and Tagliazucchi, E. (2020) Neural and Subjective Effects of Inhaled DMT in Natural Settings, v 1, *bioRxiv*, DOI: 10.1101/2020.08.19.258145.

https://dx.doi.org/10.1021/acsptsci.0c00164
ACS Pharmacol. Transl. Sci. XXXX, XXX, XXX−XXX

(33) Lockmann, A. L. V., Laplagne, D. A., Leão, R. N., and Tort, A. B. L. (2016) A Respiration-Coupled Rhythm in the Rat Hippocampus Independent of Theta and Slow Oscillations. *J. Neurosci. 36* (19), 5338−5352.
(34) Tort, A. B. L., Brankačk, J., and Draguhn, A. (2018) Respiration-Entrained Brain Rhythms Are Global but Often Overlooked. *Trends Neurosci. 41* (4), 186−197.
(35) Sanz, C., Zamberlan, F., Erowid, E., Erowid, F., and Tagliazucchi, E. (2018) The Experience Elicited by Hallucinogens Presents the Highest Similarity to Dreaming within a Large Database of Psychoactive Substance Reports. *Front. Neurosci. 12*, 7.
(36) Siclari, F., Baird, B., Perogamvros, L., Bernardi, G., LaRocque, J. J., Riedner, B., Boly, M., Postle, B. R., and Tononi, G. (2017) The Neural Correlates of Dreaming. *Nat. Neurosci. 20* (6), 872−878.
(37) Glick, S. D., Maisonneuve, I. M., Hough, L. B., Kuehne, M. E., and Bandarage, U. K. (2006) (±)-18-Methoxycoronaridine: A Novel Iboga Alkaloid Congener Having Potential Anti-Addictive Efficac. *CNS Drug Rev. 5*, 27 DOI: 10.1111/j.1527-3458.1999.tb00084.x.
(38) Helsley, S., Fiorella, D., Rabin, R. A., and Winter, J. C. (1998) Behavioral and Biochemical Evidence for a Nonessential 5-HT2A Component of the Ibogaine-Induced Discriminative Stimulus. *Pharmacol., Biochem. Behav. 59* (2), 419−425.
(39) Helsley, S., Rabin, R. A., and Winter, J. C. (1997) The Effects of Noribogaine and Harmaline in Rats Trained with Ibogaine as a Discriminative Stimulus. *Life Sci. 60* (9), PL147−153.
(40) Mash, D. C., Staley, J. K., Baumann, M. H., Rothman, R. B., and Hearn, W. L. (1995) Identification of a Primary Metabolite of Ibogaine That Targets Serotonin Transporters and Elevates Serotonin. *Life Sci. 57* (3), PL45−50.
(41) Baumann, M. H., Rothman, R. B., Pablo, J. P., and Mash, D. C. (2001) In Vivo Neurobiological Effects of Ibogaine and Its O-Desmethyl Metabolite, 12-Hydroxyibogamine (Noribogaine), in Rats. *J. Pharmacol. Exp. Ther. 297* (2), 531−539.
(42) Rodríguez, P., Urbanavicius, J., Prieto, J. P., Fabius, S., Reyes, A. L., Havel, V., Sames, D., Scorza, C., and Carrera, I. (2020) A Single Administration of the Atypical Psychedelic Ibogaine or Its Metabolite Noribogaine Induces an Antidepressant-like Effect in Rats. *ACS Chem. Neurosci. 11*, 1661.
(43) Chen, K., Kokate, T. G., Donevan, S. D., Carroll, F. I., and Rogawski, M. A. (1996) Ibogaine Block of the NMDA Receptor: In Vitro and in Vivo Studies. *Neuropharmacology 35* (4), 423−431.
(44) Layer, R. T., Skolnick, P., Bertha, C. M., Bandarage, U. K., Kuehne, M. E., and Popik, P. (1996) Structurally Modified Ibogaine Analogs Exhibit Differing Affinities for NMDA Receptors. *Eur. J. Pharmacol. 309* (2), 159−165.
(45) Mash, D. C., Staley, J. K., Pablo, J. P., Holohean, A. M., Hackman, J. C., and Davidoff, R. A. (1995) Properties of Ibogaine and Its Principal Metabolite (12-Hydroxyibogamine) at the MK-801 Binding Site of the NMDA Receptor Complex. *Neurosci. Lett. 192* (1), 53−56.
(46) Popik, P., Layer, R. T., and Skolnick, P. (1994) The Putative Anti-Addictive Drug Ibogaine Is a Competitive Inhibitor of [3H]MK-801 Binding to the NMDA Receptor Complex. *Psychopharmacology (Berl.) 114* (4), 672−674.
(47) Popik, P., Layer, R. T., Fossom, L. H., Benveniste, M., Geter-Douglass, B., Witkin, J. M., and Skolnick, P. (1995) NMDA Antagonist Properties of the Putative Antiaddictive Drug, Ibogaine. *J. Pharmacol. Exp. Ther. 275* (2), 753−760.
(48) Staley, J. K., Ouyang, Q., Pablo, J., Hearn, W. L., Flynn, D. D., Rothman, R. B., Rice, K. C., and Mash, D. C. (1996) Pharmacological Screen for Activities of 12-Hydroxyibogamine: A Primary Metabolite of the Indole Alkaloid Ibogaine. *Psychopharmacology (Berl.) 127* (1), 10−18.
(49) Ahnaou, A., Huysmans, H., Biermans, R., Manyakov, N. V., and Drinkenburg, W. H. I. M. (2017) Ketamine: Differential Neurophysiological Dynamics in Functional Networks in the Rat Brain. *Transl. Psychiatry 7* (9), No. e1237.
(50) Caixeta, F. V., Cornélio, A. M., Scheffer-Teixeira, R., Ribeiro, S., and Tort, A. B. L. (2013) Ketamine Alters Oscillatory Coupling in the Hippocampus. *Sci. Rep. 3*, 2348.
(51) Castro-Zaballa, S., Cavelli, M. L., Gonzalez, J., Nardi, A. E., Machado, S., Scorza, C., and Torterolo, P. (2019) EEG 40 Hz Coherence Decreases in REM Sleep and Ketamine Model of Psychosis. *Front. Psychiatry 9*, 766.
(52) Manduca, J. D., Thériault, R.-K., Williams, O. O. F., Rasmussen, D. J., and Perreault, M. L. (2020) Transient Dose-Dependent Effects of Ketamine on Neural Oscillatory Activity in Wistar-Kyoto Rats. *Neuroscience 441*, 161.
(53) Coleman, J. A., Yang, D., Zhao, Z., Wen, P.-C., Yoshioka, C., Tajkhorshid, E., and Gouaux, E. (2019) Serotonin Transporter-Ibogaine Complexes Illuminate Mechanisms of Inhibition and Transport. *Nature 569* (7754), 141−145.
(54) Jacobs, M. T., Zhang, Y.-W., Campbell, S. D., and Rudnick, G. (2007) Ibogaine, a Noncompetitive Inhibitor of Serotonin Transport, Acts by Stabilizing the Cytoplasm-Facing State of the Transporter. *J. Biol. Chem. 282* (40), 29441−29447.
(55) Maillet, E. L., Milon, N., Heghinian, M. D., Fishback, J., Schürer, S. C., Garamszegi, N., and Mash, D. C. (2015) Noribogaine Is a G-Protein Biased κ-Opioid Receptor Agonist. *Neuropharmacology 99*, 675−688.
(56) Young, G. A., and Khazan, N. (1984) Differential Neuropharmacological Effects of Mu, Kappa and Sigma Opioid Agonists on Cortical EEG Power Spectra in the Rat. Stereospecificity and Naloxone Antagonism. *Neuropharmacology 23* (10), 1161−1165.
(57) Coltro Campi, C., and Clarke, G. D. (1995) Effects of Highly Selective Kappa-Opioid Agonists on EEG Power Spectra and Behavioural Correlates in Conscious Rats. *Pharmacol., Biochem. Behav. 51* (4), 611−616.
(58) Tortella, F. C., Rose, J., Robles, L., Moreton, J. E., Hughes, J., and Hunter, J. C. (1997) EEG Spectral Analysis of the Neuroprotective Kappa Opioids Enadoline and PD117302. *J. Pharmacol. Exp. Ther. 282* (1), 286−293.
(59) Bokil, H., Andrews, P., Kulkarni, J. E., Mehta, S., and Mitra, P. P. (2010) Chronux: A Platform for Analyzing Neural Signals. *J. Neurosci. Methods 192* (1), 146−151.
(60) Tort, A. B. L., Komorowski, R., Eichenbaum, H., and Kopell, N. (2010) Measuring Phase-Amplitude Coupling Between Neuronal Oscillations of Different Frequencies. *J. Neurophysiol. 104* (2), 1195−1210.
(61) Delorme, A., and Makeig, S. (2004) EEGLAB: An Open Source Toolbox for Analysis of Single-Trial EEG Dynamics Including Independent Component Analysis. *J. Neurosci. Methods 134* (1), 9−21.

https://dx.doi.org/10.1021/acsptsci.0c00164
ACS Pharmacol. Transl. Sci. XXXX, XXX, XXX−XXX

NEUROSCIENCE
RESEARCH ARTICLE

J. González et al. / Neuroscience 494 (2022) 1–11

Low frequency oscillations drive EEG's complexity changes during wakefulness and sleep

Joaquín González, [a1] **Diego Mateos,** [b,c,d1] **Matias Cavelli,** [e,a] **Alejandra Mondino,** [f,a] **Claudia Pascovich,** [a,g] **Pablo Torterolo** [a] **and Nicolás Rubido** [h,i*]

[a] *Universidad de la República, Departamento de Fisiología de Facultad de Medicina, 11200 Montevideo, Uruguay*

[b] *Consejo Nacional de Investigaciones Científicas y Técnicas, Buenos Aires, Argentina*

[c] *Universidad Autónoma de Entre Ríos (UADER), Entre Ríos, Argentina*

[d] *Instituto de Matemática Aplicada del Litoral (IMAL-CONICET-UNL), Santa Fe, Argentina*

[e] *Department of Psychiatry, University of Wisconsin, Madison, WI, USA*

[f] *Department of Clinical Sciences, North Carolina State University, NC, USA*

[g] *University of Cambridge, Department of Psychology, Consciousness and Cognition Laboratory, CB2 3EB Cambridge, United Kingdom*

[h] *University of Aberdeen, King's College, Institute for Complex Systems and Mathematical Biology, AB24 3UE Aberdeen, United Kingdom*

[i] *Universidad de la República, Instituto de Física de Facultad de Ciencias, 11400 Montevideo, Uruguay*

Abstract—Recently, the sleep-wake states have been analysed using novel complexity measures, complementing the classical analysis of EEGs by frequency bands. This new approach consistently shows a decrease in EEG's complexity during slow-wave sleep, yet it is unclear how cortical oscillations shape these complexity variations. In this work, we analyse how the frequency content of brain signals affects the complexity estimates in freely moving rats. We find that the low-frequency spectrum – including the Delta, Theta, and Sigma frequency bands – drives the complexity changes during the sleep-wake states. This happens because low-frequency oscillations emerge from neuronal population patterns, as we show by recovering the complexity variations during the sleep-wake cycle from micro, meso, and macroscopic recordings. Moreover, we find that the lower frequencies reveal synchronisation patterns across the neocortex, such as a sensory-motor decoupling that happens during REM sleep. Overall, our works shows that EEG's low frequencies are critical in shaping the sleep-wake states' complexity across cortical scales.

Key words: EEG, sleep-wake cycle, low frequency oscillations.

1. INTRODUCTION

The sleep-wake cycle is one of the most prevalent biological rhythms in the animal kingdom, being crucial to regulate physiological functions. The cycle is divided into 3 main states: wakefulness (Wake), rapid-eye movement (REM), and non rapid-eye movement sleep (NREM). At the neocortical level, Wake is characterised by asynchronous and irregular neuronal activity (Evarts, 1964; Vyazovskiy et al., 2009; Watson et al., 2016b). REM sleep is strikingly similar to Wake's activity, with the difference that muscular activity is absent (Chase and Morales, 1983; Chase et al., 1989). In contrast, NREM exhibits neuronal synchronous silences that conform the nominative slow waves recorded in electroencephalograms (EEG) (Evarts, 1964; Vyazovskiy et al., 2009; Watson et al., 2016b; Nir et al., 2011; Todorova and Zugaro, 2019).

In order to understand cortical function during the sleep-wake cycle, classical analysis divides EEG oscillations into specific frequency bands (Buzsáki and Draguhn, 2004). These divisions stem from the oscillations being: 1) state-dependent, i.e., happen in relation to specific sleep-wake states, 2) related to different physiological functions, and 3) produced by distinct neuronal circuits. For example, frequencies up to 12 Hz contain the Delta (1-4 Hz), Theta (4-8 Hz), and Sigma (8-12 Hz) bands, which have been associated to state-dependent oscillations (Gervasoni et al., 2004; Watson et al., 2016b). On the other hand, higher frequencies, like Beta (15-30 Hz) or Gamma (30-150 Hz), have been predominantly associated to cognitive functions (Kisley and Cornwell, 2006; Kanayama et al., 2007; Bastos et al., 2015; Richter et al., 2017; Bastos et al., 2020; Wiesman et al., 2020) – even during sleep (Carr et al., 2012; Valderrama et al., 2012; Eichenlaub et al., 2020).

*Corresponding author.
[1] Equal contributions.

https://doi.org/10.1016/j.neuroscience.2022.04.025
0306-4522/

Recently, the classical analysis of EEG per frequency bands has been complemented by the study of EEG's complexity (Jordan et al., 2008; Ouyang et al., 2010; Nicolaou and Georgiou, 2011; Sitt et al., 2014; Abásolo et al., 2015; Sarasso et al., 2015; Bandt, 2017; González et al., 2019; González et al., 2020; Varley et al., 2020; Hou et al., 2021; Mateos et al., 2021; Varley et al., 2021; González et al., 2021); Sarasso et al., 2021 provides a up-to-date literature review. Complexity analyses usually focus on the EEG signal as a whole, instead of its frequency components (or bands). Under this framework, it has been shown that EEG's complexity changes according to the behavioural state, but irrespective of the animal species (including mice, rats, cats, monkeys, and humans). In particular, it has been consistently reported (Nicolaou and Georgiou, 2011; Abásolo et al., 2015; Bandt, 2017; González et al., 2019; González et al., 2020; Mateos et al., 2021; Varley et al., 2021; González et al., 2021; Pascovich et al., 2021) that Wake is a highly complex state, that complexity decreases during NREM when consciousness is lost, and that it increases during REM sleep when a state of altered consciousness emerges, i.e., dreams. However, it is still unclear how these complexity results are related to the classical frequency bands during the sleep-wake states.

Here, we study intracranial EEG (ECoG) complexity during the states of Wake, NREM, and REM sleep by dividing the ECoG recordings into low and high frequency-bands. We find that the low frequency band – including the classic Delta, Theta, and Sigma bands – contains most of the information that determines the state's complexity. Importantly, we show that this low frequency-band preserves information across neuronal scales, from the activity of neuronal ensembles, up to the local field potentials and ECoGs. This means that our division effectively denoises ECoG signals, revealing the underlying neural oscillations. Moreover, we find novel synchronization patterns across the cortex. In particular, we find that although Wake and REM sleep have similar complexity values at the local level, cortical sensory-motor integration is severely compromised during REM sleep. Overall, our work supports classical EEG analyses that focus on the low-frequency oscillations in order to study the sleep-wake cycle, since these frequency bands contain highly relevant information.

2. RESULTS

The complexity of a signal can be quantified by means of its information content, for example, by finding the signal's Shannon Entropy (Shannon, 1948). However, for finite and real-valued signals, such as an electro-corticogram (ECoG), estimating the Shannon Entropy is challenging. Instead, we encode the ECoG signal into a finite alphabet using Ordinal Patterns (OPs), and then find the entropy – known as Permutation Entropy (Bandt and Pompe, 2002; Zanin et al., 2012). This quantification depends on the OP dimension, D (number of data points), and embedding delay, τ (resampling). In order to increase differences between close OP distributions, we use the Permutation Minimum-Entropy (PME) instead of its classical value (Zunino et al., 2015).

2.1. Frequency bands affect the complexity of sleep-wake states differently

We study the effects that ECoG's low and high frequency bands have on the PME of brain signals for Wake, REM, NREM sleep. We divide the recordings from 12 rats (under freely moving conditions through their sleep-wake cycle) into a frequency band $\leqslant 12\,Hz$ and frequency band $> 12\,Hz$. This division separates the classic frequencies commonly employed to visually classify sleep-wake states from the higher frequencies, which are prone to noise contamination. In particular, the low frequency-band contains different sub-bands, such as the Delta band (i.e., $\delta = \{1, 4\}\,Hz$) related to slow-wave activity, the Theta band (i.e., $\theta = \{4, 8\}\,Hz$) related to exploratory behaviour and cognitive functions during REM sleep, and the Sigma band (i.e., $\sigma = \{8, 12\}\,Hz$) related to sleep spindles and memory.

Fig. 1A shows the rat's brain, where we record the activity from the primary motor cortex (M1), primary somatosensory cortex (S1) and secondary visual cortex (V2). As it can be seen from Fig. 1B, the ECoG in each cortex changes as a function of the behavioural state, from an asynchronous state during Wake and REM sleep, to a synchronous slow-wave activity during NREM sleep. We analyse the PME [Eq. (3)] per frequency band during each sleep-wake state (Fig. 1B), finding the optimal temporal scale for encoding the frequency bands into OPs. Namely, we find a state-dependent embedding delay, $\tau^{\star}$, for the OP encoding of each band [Eq. (5)].

Resultant PME values for low and high-frequency bands are respectively shown in Fig. 1C and D. We can see that these values are similar across cortical areas, suggesting that PME is a cortical-area independent measurement. In particular, we find that Wake is the most complex state (regardless of the frequency band), while NREM sleep shows significantly lower complexity values for both frequency bands. Interestingly, REM's PME strongly depends on the frequency content, showing Wake-like PME values for the lower frequencies, and NREM-like PME values for the higher frequencies.

We also show that the low-frequency band's PME robustly differentiates the sleep-wake states even when the frequency cutoff is changed – as can be seen in Fig. 1E, where we set a range of cut-off frequencies from 8 to 20 Hz. For example, when the frequency cut-off is 8 Hz, the PME values in Fig. 1E for the frequencies $\leqslant 8\,Hz$ are similar to those from Fig. 1C. As the cut-off is increased, higher frequencies are included in the low-frequency band, affecting the PME values and revealing a cortical dependence, where S1 and V2 behave similarly (middle and bottom panels in Fig. 1E) approaching an intermediate PME value between Wake and NREM sleep.

Overall, these results suggest that the low frequency-band contains most of the relevant information of sleep-wake states and their raw ECoG signals (i.e., before

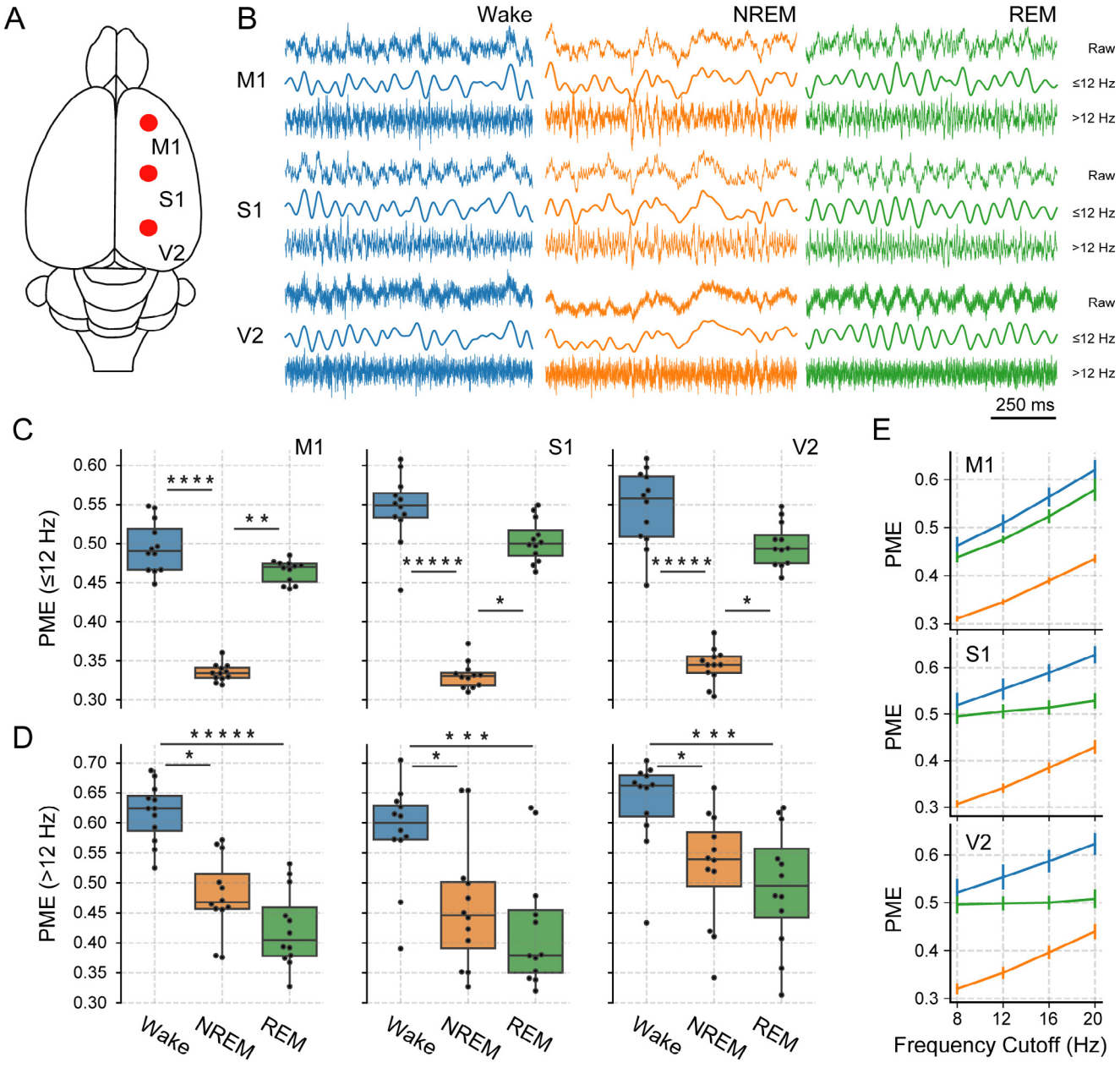

Fig. 1. Permutation Minimum-Entropy (PME) for different sleep-wake states, cortical locations, and frequency bands. **(A)** Cortical locations for the ECoG sensors: primary Motor cortex (M1), primary Somato-sensory cortex (S1), and secondary Visual cortex (V2). **(B)** Examples of ECoG recordings for wakefulness (Wake), rapid-eye-movement sleep (REM), and non-REM sleep (NREM). Top traces correspond to the raw ECoG signal and bottom traces show the respective low- and high-frequency oscillations ($\leqslant 12\,Hz$ and $> 12\,Hz$, respectively). Box plots show population PME values (12 rats) for the low (panel **C**) and high (panel **D**) frequency-bands at the M1, S1, and V2 cortical locations according to the sleep-wake state. PME [Eq. (3)] values obtained by encoding the ECoG signals with ordinal-patterns of dimension $D = 5$ and embedding delay, $\tau^{\star}$ (Bandt and Pompe, 2002), where $\tau^{\star} = 25$ for Wake, $\tau^{\star} = 21$ for REM, and $\tau^{\star} = 17$ for NREM low frequency bands and $\tau^{\star} = 1$ for all states in the high frequency band. (**E**) Population average PME (error bars represent the 95% confidence interval) for each state and cortical location as a function of the maximum frequency included in the low-frequency band (frequency cut-off) for the $\tau^{\star}$ in panel **C**. * $p < 0.05$, ** $p < 0.01$, **** $p < 0.0001$, ***** $p < 0.00001$.

filtering). In particular, we find that in this band, Wake and REM sleep show similar PME values, which aligns with previous results by González et al., 2019 using PE. On the contrary, the high frequency-band PME variations correlate to the changes in muscular activity during sleep (Fig.S1). Consequently, for the following analysis we focus on the low-frequency band.

2.2. Dependence of the embedding delay on the frequency band

A signal's information-content changes when looking at different frequency bands. This implies that the encoding needs to take into account the signal's frequency content by adjusting the encoding parameters. In our work, when encoding an ECoG

signal with ordinal patterns (OPs), we need to analyse the resultant PME [see Eq. (3)] as a function of the embedding delay, τ, for each frequency band. In Fig. 2 we show the results of finding the optimal embedding delay, $\tau^{\star}$ [see Eq. (5)], for the ECoG's low frequency-band across the sleep-wake states and cortical locations.

Fig. 2A shows ECoG's power spectra. We find that Wake and REM sleep have similar low-frequency content (shaded rectangle) in all neocortical areas, with a peak in the Theta range ($\theta = [4, 8]\,Hz$). On the other hand, NREM sleep shows more power at the sleep-spindles ($\sigma = [8, 12]\,Hz$) and slow-wave range ($\delta = [1, 4]\,Hz$). In Fig. 2B we show how the PME changes as we increase τ from 1 (OP constructed with consecutive data points) to 35 (OP constructed with data taken every 35 points) for the low frequency-band. We note increasing complexity values for all sleep-wake states – independently of the neocortical area. However, the growth is non-monotonic, as Fig. 2C reveals by the PME rates [see Eq. (4)]; that is, the PME tangents.

At the maximum PME rate, the encoding captures the optimal information content generated by the low frequencies. From Fig. 2C, we can see that this is obtained by an optimal embedding delay, $\tau^{\star}$ [see Eq. (5)], which depends on the behavioural state (coloured curves) but is independent of the cortical location (panels). In particular, we find that Wake's PME rate peaks at $\tau^{\star} = 25$, NREM's at $\tau^{\star} = 17$, and REM's at $\tau^{\star} = 21$. We note that during REM sleep, we cannot statistically differentiate between PME Rate($\tau = 21$) and PME Rate($\tau = 25$) in the M1 area (left panel in Fig. 2C), so we set $\tau^{\star} = 21$ to match the other neocortical sites. These $\tau^{\star}$ values are the ones used in Fig. 1C. We then conclude that the optimal temporal scale to study ECoG dynamics solely depends on the behavioural state of the low frequencies. On the other hand, doing the same analysis to the high frequency band results in $\tau^{\star} = 1$ for all sleep-wake states and cortical locations (Fig.S2), since at this band entropy is generally driven by the high frequencies, which require a high sampling rate (i.e., that of the raw signal).

2.3. ECoG's lower frequencies contain neuronal information across recording scales

Our findings show that Wake and REM sleep ECoG's low frequency-bands have larger PME than NREM sleep. Now we analyse whether these PME values are conserved across cortical scales; that is, if Local-Field Potentials (LFP) and neuronal spiking activity has the same complexity features according to the animal's behavioural state. In addition, we use the spiking activity binary signals to construct synthetic LFP (sLFP), which we generate by making convolutions with a decreasing exponential and then taking a population average. The resultant signal is similar to an LFP, which mainly originates from the spatial average of excitatory post-synaptic potentials (Buzsáki et al., 2012). We then perform the same analysis as in Fig. 2 to LFP and sLFP signals focusing on their low frequency-bands ($\leqslant 12\,Hz$).

From top to bottom, Fig. 3A shows low-frequency band signals for an M1 ECoG of our experiments on 12 freely-moving rats (Cavelli et al., 2017; Cavelli et al., 2018) and a frontal cortex LFP, sLFP, and spike trains (units) of the data-set with 11 rats from the work by Watson et al., 2016b. Fig. 3B shows box plots of the resultant PME values from our analysis of these recording scales in all animals, where the top panel is the same as the left panel in Fig. 1C. Here, we can see that NREM's PMEs are significantly smaller than Wake's and REM's PMEs across cortical scales; that is, our findings are consistent for ECoG, LFP, and sLFPs. We also find that PME grows with increasing τ for all recording scales (Fig. 3C), which we previously observed in Fig. 2B for the ECoG signals. Similarly, PME rates in Fig. 3D for ECoGs, LFPs, and sLFPs exhibit comparable behaviours, where we note that $\tau^{\star}$ values are always larger during Wakefulness or REM sleep than during NREM sleep. Consequently, our findings show that low frequency-bands contain state-dependent information that stems from the spiking activity, which is conserved across the recording scales.

2.4. Sensory-motor integration is compromised during REM sleep

Having shown that the low-frequency ECoG band contains state-dependent spiking information, we now study how this activity is integrated across the neocortex. We do this by quantifying the Permutation Minimum-Mutual-Information (PMMI) between the low-frequency ECoG recordings of every pair of cortical locations, where we encode each ECoG signal into ordinal patterns (Bandt and Pompe, 2002) of length $D = 5$ and optimal embedding delay $\tau^{\star}$ for each sleep-wake state (i.e., $\tau^{\star} = 25$ for Wake, $\tau^{\star} = 21$ for REM, and $\tau^{\star} = 17$ for NREM, as it can be seen from Fig. 2C).

Fig. 4A shows the low-frequency ECoG signals during each sleep-wake state. During Wake (left panel in Fig. 4A), we note synchronous θ oscillations on M1 (primary motor), S1 (primary somato-sensory), and V2 (secondary visual) cortical regions. During NREM sleep (middle panel in Fig. 4A), slow waves appear almost synchronously in all cortices. On the other hand, we note that during REM sleep (right panel in Fig. 4A), the M1 cortex decouples from the rest, while S1 and V2 exhibit synchronous θ rhythms that resemble Wake.

In line with these observations, PMMI values [see Eq. (6)] between cortical areas show a dependence on both the distance between cortices and the sleep-wake state (Fig. 4B). The inter-electrode distance for S1-V2 and M1-S1 is $\simeq 5mm$, but is $\simeq 10mm$ for the M1-V2 combination. In particular, Fig. 4B shows that PMMI is significantly higher for cortical pairs that are $\simeq 5mm$ apart in comparison to those that are $\simeq 10mm$, regardless of the sleep-wake state. However, we find a significant decrease in PMMI during REM sleep when comparing the equidistant pairs S1-V2 and M1-S1, which is absent during Wake or NREM sleep. These results point to a loss in sensory-motor integration during REM sleep that is not emerging because of cortical distances.

When comparing PMMI from different sleep-wake states, we find that REM's M1-S1 and M1-V2 PMMI are significantly smaller than those from Wake. For

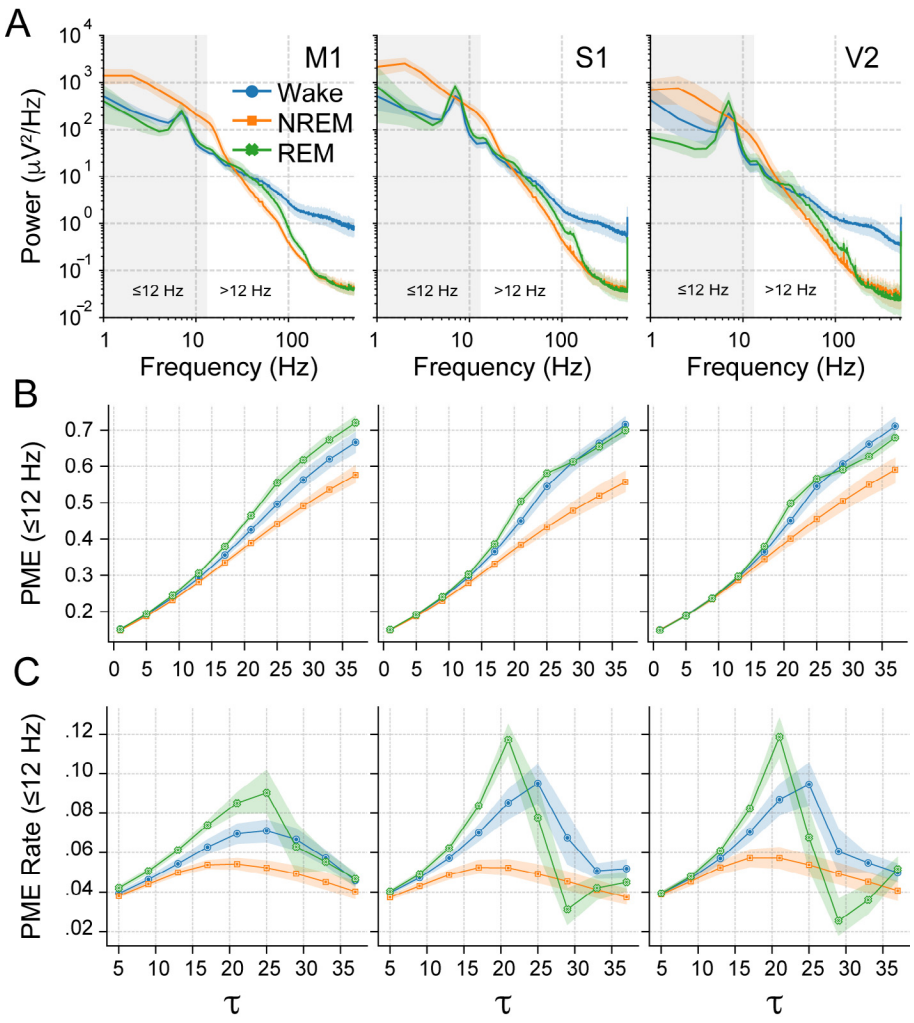

Fig. 2. Power spectra and entropy variations for wakefulness (Wake), rapid-eye movement (REM) and non-REM (NREM) sleep. (**A**) Power spectral densities for different cortical locations and sleep-wake states. Shaded rectangular areas signal the low frequency band ($\leqslant 12\,Hz$). (**B**) Permutation Minimum-Entropy (PME) values for the EEG's low frequency-band as the embedding delay, τ, of the ordinal pattern (OP) is increased (i.e., data sampled at increasing steps) in each cortical location from Fig. 1A. (**C**) Corresponding PME rates [Eq. (4)] from panel **B**, i.e., PME tangents as a function of τ. OP dimension in panels **B** and **C** is $D = 5$ data points (as in Fig. 1C). All panels show population averages (solid curves) with their 95% confidence interval (coloured shading) after 1000 bootstrap samples.

example, REM's and Wake's population-averaged PMMI between M1 and V2 is 0.09 and 0.12 (normalised units), respectively. We highlight that this decrease in PMMI between M1 and V2 low frequencies happens even though their PME values for Wake and REM are similar (Fig. 1C). On the contrary, the decrease in PMMI values happening during NREM sleep between M1-V2 in comparison to Wake can be explained from the significantly smaller PME values that NREM shows in all cortical areas (Fig. 1C).

3. DISCUSSION

Complex neural dynamics are thought to be necessary for consciousness (Tononi and Edelman, 1998; Oizumi et al., 2014). Different reports show that cortical activity exhibits complex patterns during Wakefulness, that are reduced during deep NREM sleep (Ouyang et al., 2010; Nicolaou and Georgiou, 2011; Abásolo et al., 2015; Schartner et al., 2017(1):niw022; Bandt, 2017; González et al., 2019; González et al., 2020; Hou et al., 2021; Mondino et al., 2021; Mateos et al., 2021) or anesthesia (Jordan et al., 2008; Sitt et al., 2014; Sarasso et al., 2015; Fagerholm et al., 2016; Thul et al., 2016; Varley et al., 2020; Varley et al., 2021). However, it was unclear how the different frequency bands contribute to the observed complexity changes in EEG analyses.

3.1. Low-frequency oscillations drive complexity changes during the states of wake and sleep

In this work, we show that the intracranial EEG (ECoG) frequencies up to $12\,Hz$ are sufficient to reproduce the complexity variations that are typically observed across the sleep-wake states. According to our findings (Figs. 1C and 2), Delta, Theta, and Sigma bands are the most important frequencies contributing to the state's complexity and its decrease during NREM sleep. Thus, our work highlights the fact that EEG complexity critically depends on the modulation of the thalamocortical loops (Llinás et al., 1999; Llinás et al., 2005), particularly in the orchestration of the slow-wave activity (1-4 Hz) during NREM sleep (Pigorini et al., 2015; D'Andola et al., 2018; Rosanova et al., 2018; Dasilva et al., 2021; Sarasso et al., 2021; González et al., 2021). Consistent with these results, we have shown that population DOWN states trap cortical activity into recurrent dynamics (González et al., 2021), explaining why slow-oscillations – caused by DOWN states and synchronised by the thalamus (Steriade et al., 1993; Vyazovskiy et al., 2009; Nir et al., 2011; Todorova and Zugaro, 2019; Hay et al., 2021) – reduce the complexity of cortical activity during sleep.

Our present results also suggest that ECoG's high frequencies ($> 12\,Hz$) contain muscular information, which we can explain as follows. On the one hand, REM sleep shows the least complex EEG signals in the high frequency range (Fig. 1D), in spite of having neuronal activity resembling that of wakefulness (Abásolo et al., 2015; González et al., 2021). The fact that

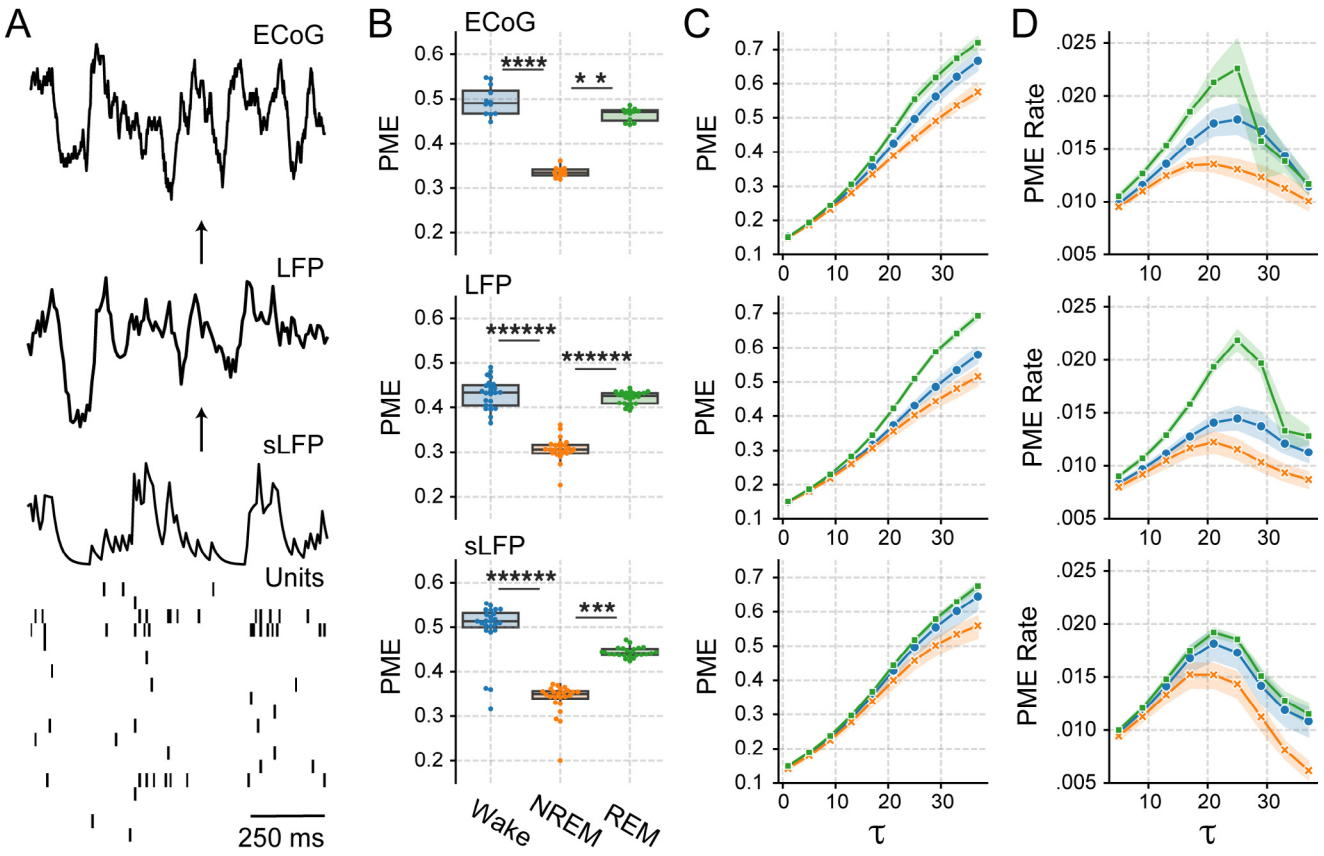

Fig. 3. Permutation Minimum-Entropy (PME) across recording scales. (**A**) Brain recordings at different scales. From top to bottom, electrocorticograms (ECoG), local field potential (LFP), synthetic LFP (obtained by the convolution of the spike trains and a decreasing exponential kernel), and units (spikes from individual neurons recorded from the extracellular medium). ECoG data comes from our experiments, as in Figs. 1 and 2, but the other recordings come from the work by Watson et al., 2016b (data-set available at: CRCNS.org). We note that we inverted both LFP and ECoG recordings for representation purposes. (**B**): Box plots show PME values for the ECoGs (from Fig. 1C), LFPs, and sLFPs data-sets.* $p < $ **C** PME as a function of τ (delay embedding); as in Fig. 2B. (**C**) PME Rate as a function of τ; as in Fig. 2**C**. The solid lines show the population average values and the shaded areas their 95% confidence interval.* $p < 0.05$, ** $p < 0.01$, **** $p < 0.0001$, ****** $p < 0.000001$.

muscular tone is absent during REM sleep (Fig.S1) can explain this discrepancy between neuronal activity and ECoG's complexity values. On the other hand, we find that the optimal delay embedding for encoding high-frequency signals is always $\tau^{\star} = 1$ (Fig.S2) for all sleep-wake states and cortical locations. This $\tau^{\star} = 1$ implies that the ordinal patterns can encode most of the information coming from frequencies in the range $1024\,Hz/5 \sim 200\,Hz$ up to $512\,Hz$ – according to Eq. (1). This range is higher than any up-to-date physiological frequency band, making the high-frequency band analysis with ordinal patterns prone to capture extra-neural sources, such as electrical muscular activity.

Because muscular activity is intrinsically random and our approach is to maximise the entropy rates, we could be missing relevant information from the frequencies contained in the 12 to $200\,Hz$ when analysing the high-frequency range. This limitation in our high-frequency band analysis could require the inclusion of an intermediate band of frequencies. Such intermediate frequencies could contain the Beta (15-30 Hz) and Gamma (30-150 Hz) bands, potentially capturing complementary information to our present work; but outside of its current scope. Nevertheless, our results remain practically unchanged when we choose a different cut-off frequency to define the low and high frequency bands (Fig. 1E), exploring cut-off values between 8 to $20\,Hz$.

3.2. Frequency Content of an Ordinal Pattern

When trying to measure the content of information from an ECoG signal, we need to tune the encoding to match the relevant frequencies of the signal under study. In our case, the Ordinal Pattern (OP) encoding has the embedding dimension, D, and delay, τ parameters, which set the number of points to be taken as a single OP and at which sampling rate. Consequently, depending on their values, an OP can see different frequencies, ν. Specifically, we can estimate the OP frequency range by

$$\frac{\nu_s}{D\tau^{\star}} \lesssim \nu \lesssim \frac{\nu_s}{2\tau^{\star}}, \tag{1}$$

where ν_s is the sampling frequency of the signal (in our case, $\nu_s = 1024\,Hz$), D is the OP's embedding dimension, and $\tau^{\star}$ is the optimum embedding delay from Eq. (5).

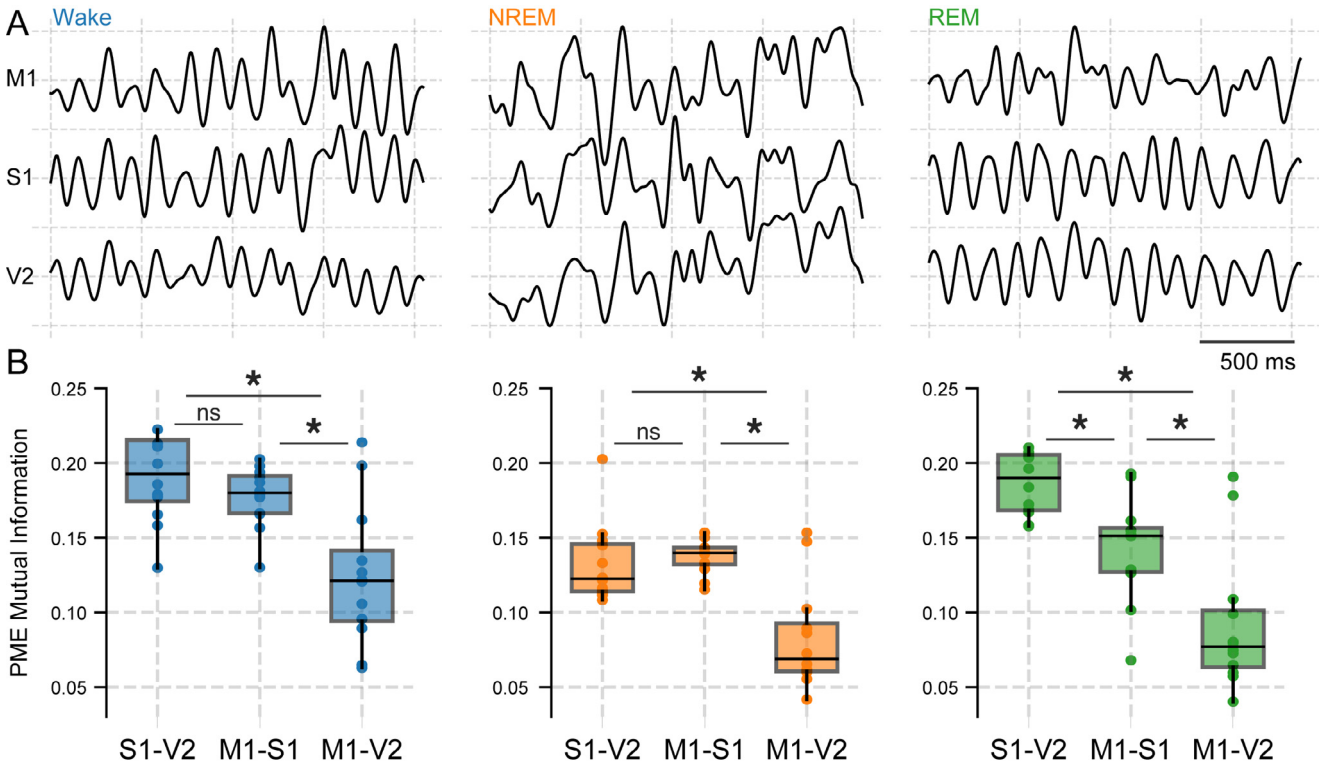

Fig. 4. Permutation Minimum Mutual Information (PMMI) for Wakefulness, NREM and REM sleep. (**A**) Standardised ECoG recordings of the primary Motor cortex (M1), primary Somato-sensory cortex (S1), and secondary Visual cortex (V2) in each sleep-wake state. (**B**) Box-plots with the pair-wise PMMI values [Eq. (6)] between the 3 neocortical areas during each of the sleep-wake states. $*$ signals a $P < 0.05$ Wilcoxon signed-rank test with a Benjamini-Hochberg multiple comparisons correction.

Eq. (1) implies that for our low frequency-band ECoG analysis ($\leq 12\,Hz$), when we have $D = 5$ and $\tau^{\star} = 25$ (corresponding to wakefulness), the OP lower and upper frequency limits are approximately equal to $8\,Hz$ and $20\,Hz$, respectively. This means that the $D = 5$ OP encoding will be quantifying the information content from a signal mostly within 8 and $20\,Hz$. However, we note that for different D and sleep-wake states, we find different $\tau^{\star}$ – although independently of the cortical location. The optimal $\tau^{\star}$ of the low frequency band for each sleep-wake states can be seen in Fig. 2C. On the other hand, for the high frequency-band ECoG analysis ($> 12\,Hz$), we find $\tau^{\star}(D) = 1$ independently of the embedding dimension or sleep-wake state (see Fig. S2C). In this case, the OP has an upper limit of $512\,Hz$, coinciding with the Nyquist-Shannon criterion, but a lower limit that depends on D, being $256\,Hz$ if $D = 4$ and approximately $200\,Hz$ if $D = 5$.

It is worth noting that, although Eq. (1) sets a frequency range that an OP can capture for a given D and $\tau^{\star}$, this range only considers part of the information that an OP captures. Specifically, frequencies ν that are smaller than the lower bound, $\nu_s/D\tau^{\star}$, are still captured by the OP. For example, a slow wave oscillation would constitute monotonically increasing or decreasing OPs, which would (strictly) have insufficient data-points to represent the slow-wave's period, but still contain local information about the signal and contribute to differentiate it to other frequencies.

3.3. Low-frequency ECoG oscillations recover neuronal dynamics

We find that we can bridge several cortical scales by focusing on the lower ECoG frequencies (Fig. 3). We note that decoding specific neuronal firing patterns from a field recording, such as an ECoG, is an ill-posed problem, but we can approximate (to a degree) the amount of information that neuronal populations generate during each sleep-wake state. In this sense, our analysis shows that Wake and REM's neuronal dynamics and field recordings are complex across scales (Fig. 3B). In contrast, the appearance of DOWN states in neuronal populations and slow-waves in field recordings make NREM activity more predictable and less complex (González et al., 2021).

We note that although our frequency band division is a simple procedure, invariant complexity across scales disappears when considering the whole ECoG signal frequency content. In particular, if we include the high frequencies, extra-neural contamination likely confounds the complexity results and brakes the scale invariance we are finding in this work. Moreover, extra-neural sources of contamination above $20\,Hz$ are already reported by Whitham (Whitham et al., 2007) for scalp EEG, which supports our decision to use a division at $12\,Hz$ – making it available for scalp EEG analysis.

3.4. Low-frequency synchronization reveals cortical sensory-motor decoupling during REM sleep

Finally, our mutual information analysis of the low frequency band reveals particular synchronization patterns between neocortical areas during REM sleep. We find that the motor cortex decouples from sensory and visual cortices (Fig. 4), in spite of the different cortical areas maintaining complex patterns of activity. Given that the activity of these lower frequencies correlates with true neuronal dynamics (Fig. 3B), it seems unlikely that the sensory-motor decoupling is spurious. Because REM sleep is characterized by muscle atony and a decreased proprioceptive sensory entrance (Chase and Morales, 1983; Chase et al., 1989; Soja et al., 1993), a reduction in the mutual information between the motor cortex and the rest of the brain is expected (Fig. 4B). We argue that a possible cause for this sensory-motor decoupling (i.e., less information sharing between motor areas and the rest of the neocortex), is because motor feedback signals are unable to synchronize the sensory cortices with the motor areas due to motor pathways being inhibited.

4. EXPERIMENTAL PROCEDURES

Experimental procedures are in agreement with the National Animal Care Law (No. 18611) and with the "Guide to the care and use of laboratory animals" (8th Edition, National Academy Press, Washington DC, 2010), and approved by the Institutional Animal Care Committee, Uruguay (Exp. No 070153–000332-16). The experiments involve 12 Wistar adult rats, sustaining a controlled 12 h light/dark cycle (light comes on at 07:00 UYT) with unrestricted access to food and water. Veterinarians of the institution determined the animals were all in good health and we took extra care to minimise pain, discomfort, and stress in the animals. Also, we made an effort to use the minimum number of animals necessary to obtain reliable data.

Surgical procedures imply chronically implanting electrodes to the animals, where we follow procedures carried in previous studies by Cavelli et al., 2017,Cavelli et al., 2018. Anaesthesia is induced by a mixture of ketamine-xylazine (90 mg/kg and 5 mg/kg i.p., respectively), the rat is then positioned in a stereotactic frame, and the skull is exposed to attach 8 stainless-steel screw-electrodes, which record the intra-cranial EEG. 6 electrodes are placed bilaterally above motor (M1), somato-sensory (S1), and visual (V2) cortices. Remaining electrodes are placed in the right olfactory bulb (OB) and cerebellum (taken as the reference electrode). EMG registration is done by inserting 2 electrodes into the neck muscle. All electrodes are soldered into a 12-pin socket and fixed onto the skull with acrylic cement. At the end of the surgical procedures, an analgesic (Ketoprofen, 1 mg/kg, s.c.) is administered. After the animals recover from these surgical procedures, they are left to adapt in separate transparent cages ($40 \times 30 \times 20\,cm$) for 1 week before data is collected. Cages contain wood-shaving material in a temperature-controlled room (set to 21–24 °C), with water and food *ad libitum.*

Experimental sessions are conducted during the light period, between 10AM and 4PM UYT. Data from each rat is collected individually in a sound-attenuated recording chamber with a Faraday shield by a rotating connector that allows free movement within the cage. Polysomnographic recordings are amplified ($\times 1000$), acquired (by a 16 bits AD converter set at a 1024 Hz sampling frequency), and stored using DASY LAB SOFTWARE – recordings available upon request. The states of REM, NREM and Wake are determined in 10 s epochs. Wake is defined by low-voltage fast-waves in M1, strong theta-rhythm (4–7 Hz) in V2, and relatively high EMG activity. REM sleep is defined by low-voltage fast-frontal-waves, a regular theta-rhythm in V2, and a silent EMG (except for occasional twitches). NREM sleep is determined by the presence of high-voltage slow-cortical-waves (1–4 Hz), sleep spindles in M1, S1, and V2, and a reduction in EMG amplitudes. Additionally, a visual scoring is performed to discard artifacts and transitional states.

Frontal cortex data-set We also employ the data-set from Watson et al., 2016b,Watson et al., 2016a to study population dynamics and local field potentials in the frontal cortex; freely available at CRCNS.org. For these recordings, silicon probes were implanted in frontal cortical areas of 11 male Long-Evans rats. Recording sites include the medial prefrontal cortex (mPFC), anterior cingulate cortex (ACC), pre-motor cortex/M2, and orbito-frontal cortex (OFC). Recordings took place during light hours in the home cage, including 25 sessions with mean duration of 4.8hs $\pm$ 2.2 std, at a 20 kHz sampling frequency. We exclude *BWRat19_032413* from our analyses because the recording lack REM sleep data. We extract Local-Field Potentials (LFPs) by applying low-pass filters to the recordings and resampling at 1250 Hz. We extract neuronal spikes by applying a high-pass filter at 800 Hz and then by detecting threshold crossings. Spike sorting is carried by means of the KLUSTAKWIK open-source software. Sleep-wake states are identified by means of Principal Component (PC) analysis. In particular, SWS exhibits high LFP PC1 (power in the low $< 20\,Hz$) and low EMG. REM sleep shows high Theta with low EMG cluster, and a diffuse cluster of low broadband LFP with high EMG. Wake has a diffuse cluster of low broadband LFP with higher EMG, and a range of Theta oscillations.

5. DATA ANALYSIS

Pre-processing of field recordings is done by a 1st-order Finite-duration Impulse Response (FIR1) band-pass $[0.1, 450]\,Hz$. We divide these signals into Low-Frequency Oscillations (LFO) by a $[0.1, 12]\,Hz$ FIR1 band-pass and High-Frequency Oscillations (HFO) by a $[13, 450]\,Hz$ FIR1 band-pass, which corresponds to making a division according to the classical polysomnographic frequency bands (Buzsáki and Draguhn, 2004). Then, we fix the total signal length, T, to a range between 3×10^5 to 3×10^6 data points for all cortical locations and sleep-wake states. This means that

the shortest [largest] signals last $T\Delta t = 3 \times 10^5/1024\,Hz \simeq 5$ minutes [$T\Delta t \simeq 50$ minutes].

Encoding of signals into Ordinal Patterns (OPs) [Bandt and Pompe, 2002] is done to quantify the signals' randomness and how it changes during the sleep-wake states. This encoding involves dividing a signal, $X = \{x(t) : t = 0, \ldots, (T-1)\,\Delta t\}$ (where $1/\Delta t$ is the sampling frequency of the signal), into sliding vectors with D data-points (such that $D \ll T$) at a new sampling τ, where $D \geqslant 2$ is known as the embedding dimension and τ as the delay embedding. For example, $\{x(t), x(t+\tau), x(t+2\tau)\}$ is a vector at time t with $D = 3$ data points and sampled at $\tau \geqslant 1$ times. Each of these vectors is assigned an OP according to the relative magnitude of its D elements and how many permutations are needed to order them increasingly. In other words, an OP represents the necessary permutations needed to order the elements of the embedded vector, which has up to $D!$ possible permutations. In what follows, we set $D = 5$ (meaning there are $5! = 120$ possible OPs), and analyse how results change for different τ. We note that similar results for both the low and high-frequency bands are obtained employing $D = 4$ (see Fig.S3).

Permutation Entropy (Bandt and Pompe, 2002) (PE) quantifies the temporal randomness of a signal X after encoding it into OPs. It is defined from the probability distribution of OPs ($P_{(D,\tau)}(\alpha\{X\})$, with $\alpha = 1, \ldots, D!$ and τ the delay embedding) by

$$PE_X(D,\tau) = -\sum_{\alpha=1}^{D!} P_{(D,\tau)}(\alpha)\,\frac{\log_2\left[P_{(D,\tau)}(\alpha)\right]}{\log_2[D!]} = -\sum_{\alpha=1}^{D!} P_{(D,\tau)}(\alpha)\log_{D!}\left[P_{(D,\tau)}(\alpha)\right], \quad (2)$$

which depends on D and τ and is normalised by the maximum PE, $\log_2(D!)$; namely, $0 \leqslant PE_X \leqslant 1$ for any signal X, dimension D, or delay τ. In general, there are slight changes in the probability distribution of OPs when analysing different consciousness states. This means that PE values from Eq. (2) are similar and differences can be hindered in the statistical comparisons. In order to enhance these differences, we use the *Permutation Minimum-Entropy* (PME), which is the infinit limit of the Rényi entropy (Rényi et al., 1961; Rényi, 1965; Zanin et al., 2012; Zunino et al., 2015), is defined by

$$PME_X(D,\tau) = \frac{\min_\alpha\{-\log_2[p(\alpha)]\}}{\log_2[D!]} = -\log_{D!}\left[\max_\alpha\{p(\alpha)\}\right]. \quad (3)$$

Entropy Rates are the incremental variations that entropy has when a parameter is changed. In our case, a PME rate is given by changes in the delay embedding, $\tau = 1, \ldots, 40$, for a fixed embedding dimension; namely, $D = 4$ or 5. We are interested on the entropy rates because of the low and high frequency-bands, which imply different relevant frequencies. Specifically, we find the PME rate of a signal X by

$$\frac{\Delta PME_X}{\Delta\tau} = \frac{PME_X(D,\tau+\Delta\tau) - PME_X(D,\tau)}{\Delta\tau}, \quad (4)$$

where we choose $\Delta\tau = 4$ for most of the PME analysis (we also explore finer values, using $\Delta\tau = 1$; results not shown here). In particular, we optimise τ by selecting the maximum PME for each cortical location and sleep-wake state. Namely,

$$\tau^\star(D) = \left\{\tau : \max_\tau\left(\frac{\Delta PME_X}{\Delta\tau}\right)\right\}. \quad (5)$$

Mutual Information, $I(X,Y)$, is the amount of shared information between 2 random signals, X and Y. It is a non-linear measure of the correlation between the signals, found from $I(X,Y) = H(X) + H(Y) - H(X,Y)$, $H(X)$ [$H(Y)$] being the marginal entropy of signal X [Y] and $H(X,Y)$ being their joint entropy. In this work, we use the PME [Eq. (3)] to quantify the entropy of a signal, so we use this entropy to quantify a *Permutation Minimum-Mutual-Information* (PMMI) between pairs of signals. Namely,

$$PI_{X,Y}(D,\tau) = PME_X(D,\tau) + PME_Y(D,\tau) - PME_{X,Y}(D,\tau), \quad (6)$$

where $PME_{X,Y}(D,\tau)$ is the joint permutation minimum-entropy at a given D and τ (meaning that we are comparing both signals after they have been encoded into OPs).

5.1. Statistics

We present data as regular boxplots showing the median, the 1st and 3rd quartiles, and the distribution range. Because of the complexity metrics we analyse, we employ non-parametric statistics. In particular we use the Friedman test (available with the scipy.stats) to compare the results among states (Wake-NREM-REM) with the Siegel post hoc test applying the Benjamini-Hochberg false discovery rates correction (available with the scikitlearn python 3 package (https://scikit-learn.org/stable/)). We set $p < 0.05$ for a result to be considered significant.

DECLARATION OF COMPETING INTEREST

The authors declare that they have no known competing financial interests or personal relationships that could have appeared to influence the work reported in this paper.

ACKNOWLEDGEMENT

J.G. acknowledges the support of Comisión Académica de Posgrado (CAP), CSIC Iniciación and PEDECIBA. P. T. and N.R. also acknowledges the support of PEDECIBA.

REFERENCES

Abásolo D, Simons S, Morgado da Silva R, Tononi G, Vyazovskiy VV (2015) Lempel-Ziv complexity of cortical activity during sleep and waking in rats. J Neurophysiol 113(7):2742–2752.

Bandt C (2017) A new kind of permutation entropy used to classify sleep stages from invisible eeg microstructure. Entropy 19(5).

Bandt C, Pompe B (2002) Permutation entropy: a natural complexity measure for time series. Phys Rev Letters 88(17) 174102.

Bastos AM, Lundqvist M, Waite AS, Kopell N, Miller EK (2020) Layer and rhythm specificity for predictive routing. Proc Natl Acad Sci U S A 117(49):31459–31469.
Bastos AM, Vezoli J, Bosman CA, Schoffelen JM, Oostenveld R, Dowdall JR, De Weerd P, Kennedy H, Fries P (2015) Visual areas exert feedforward and feedback influences through distinct frequency channels. Neuron 85(2):390–401.
Buzsáki G, Anastassiou CA, Koch C (2012) The origin of extracellular fields and currents–EEG, ECoG. LFP and spikes. Nat Rev Neurosci 13(6):407–420.
Buzsáki G, Draguhn A (2004) Neuronal oscillations in cortical networks. Science 304(5679):1926–1929.
Carr MF, Karlsson MP, Frank LM (2012) Transient slow gamma synchrony underlies hippocampal memory replay. Neuron 75 (4):700–713.
Cavelli M, Castro-Zaballa S, Mondino A, Gonzalez J, Falconi A, Torterolo P (2017) Absence of eeg gamma coherence in a local activated cortical state: a conserved trait of rem sleep. Transl Brain Rhythmicity. 21132017.
Cavelli M, Rojas-Líbano D, Schwarzkopf N, Castro-Zaballa S, Gonzalez J, Mondino A, Santana N, Benedetto L, Falconi A, Torterolo P (2018) Power and coherence of cortical high-frequency oscillations during wakefulness and sleep. Eur J Neurosci 48(8):2728–2737.
Chase MH, Morales FR (1983) Subthreshold excitatory activity and motoneuron discharge during REM periods of active sleep. Science 221(4616):1195–1198.
Chase MH, Soja PJ, Morales FR (1989) Evidence that glycine mediates the postsynaptic potentials that inhibit lumbar motoneurons during the atonia of active sleep. J Neurosci 9 (3):743–751.
D'Andola M, Rebollo B, Casali AG, Weinert JF, Pigorini A, Villa R, Massimini M, Sanchez-Vives MV (2018) Bistability, Causality, and Complexity in Cortical Networks: An In Vitro Perturbational Study. Cereb Cortex 28(7):2233–2242.
Dasilva M, Camassa A, Navarro-Guzman A, Pazienti A, Perez-Mendez L, Zamora-López G, Mattia M, Sanchez-Vives MV (2021) Modulation of cortical slow oscillations and complexity across anesthesia levels. Neuroimage 224 117415.
Eichenlaub JB, Biswal S, Peled N, Rivilis N, Golby AJ, Lee JW, Westover MB, Halgren E, Cash SS (2020) Reactivation of Motor-Related Gamma Activity in Human NREM Sleep. Front Neurosci 14:449.
Evarts EV (1964) Temporal patterns of discharge of pyramidal tract neurons during sleep and waking in the monkey. J Neurophysiol 27(2):152–171.
Fagerholm ED, Scott G, Shew WL, Song C, Leech R, Knöpfel T, Sharp DJ (2016) Cortical Entropy, Mutual Information and Scale-Free Dynamics in Waking Mice. Cereb Cortex 26(10):3945–3952.
Gervasoni D, Lin SC, Ribeiro S, Soares ES, Pantoja J, Nicolelis MA (2004) Global forebrain dynamics predict rat behavioral states and their transitions. J Neurosci 24(49):11137–11147.
González, J., Cavelli, M., Tort, A.B., Torterolo, P., and Rubido, N. (2021). Off-periods reduce the complexity of neocortical activity during sleep. bioRxiv..
González J, Cavelli M, Mondino A, Pascovich C, Castro-Zaballa S, Torterolo P, Rubido N (2019) Decreased electrocortical temporal complexity distinguishes sleep from wakefulness. Sci Rep 9 (1):18457.
González J, Cavelli M, Mondino A, Pascovich C, Castro-Zaballa S, Torterolo P, Rubido N (2020) Electrocortical temporal complexity during wakefulness and sleep: an updated account. Sleep Sci.
Hay YA, Deperrois N, Fuchsberger T, Quarrell TM, Koerling A-L, Paulsen O (2021) Thalamus mediates neocortical down state transition via gabab-receptor-targeting interneurons. Neuron.
Hou F, Zhang L, Qin B, Gaggioni G, Liu X, Vandewalle G (2021) Changes in EEG permutation entropy in the evening and in the transition from wake to sleep. Sleep 44(4).
Jordan D, Stockmanns G, Kochs EF, Pilge S, Schneider G (2008) Electroencephalographic order pattern analysis for the separation of consciousness and unconsciousness: an analysis of approximate entropy, permutation entropy, recurrence rate, and phase coupling of order recurrence plots. Anesthesiology 109 (6):1014–1022.
Kanayama N, Sato A, Ohira H (2007) Crossmodal effect with rubber hand illusion and gamma-band activity. Psychophysiology 44 (3):392–402.
Kisley MA, Cornwell ZM (2006) Gamma and beta neural activity evoked during a sensory gating paradigm: effects of auditory, somatosensory and cross-modal stimulation. Clinical neurophysiology 117(11):2549–2563.
Llinás R, Urbano FJ, Leznik E, Ramírez RR, van Marle HJ (2005) High-speed voltage-sensitive dye imaging. Trends Neurosci 6 (28):325–333.
Llinás RR, Ribary U, Jeanmonod D, Kronberg E, Mitra PP (1999) Thalamocortical dysrhythmia: a neurological and neuropsychiatric syndrome characterized by magnetoencephalography. Proceedings of the National Academy of Sciences 96 (26):15222–15227.
Mateos DM, Gómez-Ramírez J, Rosso OA (2021) Using time causal quantifiers to characterize sleep stages. Chaos, Solitons Fractals 146(110798).
Mondino A, Hambrecht-Wiedbusch VS, Li D, York AK, Pal D, González J, Torterolo P, Mashour GA, Vanini G (2021) Glutamatergic Neurons in the Preoptic Hypothalamus Promote Wakefulness, Destabilize NREM Sleep, Suppress REM Sleep, and Regulate Cortical Dynamics. J Neurosci 41(15):3462–3478.
Nicolaou N, Georgiou J (2011) The use of permutation entropy to characterize sleep electroencephalograms. Clin EEG Neurosci 42 (1):24–28.
Nir Y, Staba RJ, Andrillon T, Vyazovskiy VV, Cirelli C, Fried I, Tononi G (2011) Regional slow waves and spindles in human sleep. Neuron 70(1):153–169.
Oizumi M, Albantakis L, Tononi G (2014) From the phenomenology to the mechanisms of consciousness: Integrated Information Theory 3.0. PLoS Comput Biol 10(5) e1003588.
Ouyang G, Dang C, Richards DA, Li X (2010) Ordinal pattern based similarity analysis for EEG recordings. Clin Neurophysiol 121 (5):694–703.
Pascovich, C., Castro-Zaballa, S., Mediano, P.A., Bor, D., Canales-Johnson, A., Torterolo, P., and Bekinschtein, T.A. (2021). Ketamine and sleep modulate neural complexity dynamics in cats. bioRxiv..
Pigorini A, Sarasso S, Proserpio P, Szymanski C, Arnulfo G, Casarotto S, Fecchio M, Rosanova M, Mariotti M, Lo Russo G, Palva JM, Nobili L, Massimini M (2015) Bistability breaks-off deterministic responses to intracortical stimulation during non-REM sleep. Neuroimage 112:105–113.
Rényi A (1965) On the foundations of information theory. Revue de l'Institut International de Statistique:1–14.
Rényi A et al (1961) On measures of entropy and information. In: Proceedings of the Fourth Berkeley Symposium on Mathematical Statistics and Probability, Volume 1: Contributions to the Theory of Statistics. The Regents of the University of California.
Richter CG, Thompson WH, Bosman CA, Fries P (2017) Top-Down Beta Enhances Bottom-Up Gamma. J Neurosci 37 (28):6698–6711.
Rosanova M, Fecchio M, Casarotto S, Sarasso S, Casali AG, Pigorini A, Comanducci A, Seregni F, Devalle G, Citerio G, Bodart O, Boly M, Gosseries O, Laureys S, Massimini M (2018) Sleep-like cortical OFF-periods disrupt causality and complexity in the brain of unresponsive wakefulness syndrome patients. Nat Commun 9 (1):4427.
Sarasso S, Boly M, Napolitani M, Gosseries O, Charland-Verville V, Casarotto S, Rosanova M, Casali AG, Brichant JF, Boveroux P, Rex S, Tononi G, Laureys S, Massimini M (2015) Consciousness and Complexity during Unresponsiveness Induced by Propofol, Xenon, and Ketamine. Curr Biol 25(23):3099–3105.
Sarasso S, Casali AG, Casarotto S, Rosanova M, Sinigaglia C, Massimini M (2021) Consciousness and complexity: a consilience of evidence. Neurosci Consciousness niab023.

Schartner, M.M., Pigorini, A., Gibbs, S.A., Arnulfo, G., Sarasso, S., Barnett, L., Nobili, L., Massimini, M., Seth, A.K., and Barrett, A.B. (2017). Global and local complexity of intracranial EEG decreases during NREM sleep. Neurosci Conscious, 2017(1):niw022..

Shannon CE (1948) A mathematical theory of communication. The Bell Syst Tech J 27(3):379–423.

Sitt JD, King JR, El Karoui I, Rohaut B, Faugeras F, Gramfort A, Cohen L, Sigman M, Dehaene S, Naccache L (2014) BrainLarge scale screening of neural signatures of consciousness in patients in a vegetative or minimally conscious state. Brain 137(Pt 8):2258–2270.

Soja PJ, Oka JI, Fragoso M (1993) Synaptic transmission through cat lumbar ascending sensory pathways is suppressed during active sleep. J Neurophysiol 70(4):1708–1712.

Steriade M, Nuñez A, Amzica F (1993) 1 Hz) neocortical oscillation and other sleep rhythms of the electroencephalogram. J Neurosci 13(8):3266–3283.

Thul A, Lechinger J, Donis J, Michitsch G, Pichler G, Kochs EF, Jordan D, Ilg R, Schabus M (2016) EEG entropy measures indicate decrease of cortical information processing in Disorders of Consciousness. Clin Neurophysiol 127(2):1419–1427.

Todorova R, Zugaro M (2019) ScienceIsolated cortical computations during delta waves support memory consolidation. Science 366 (6463):377–381.

Tononi G, Edelman GM (1998) Consciousness and complexity. Science 282(5395):1846–1851.

Valderrama M, Crépon B, Botella-Soler V, Martinerie J, Hasboun D, Alvarado-Rojas C, Baulac M, Adam C, Navarro V, Le Van Quyen M (2012) Human gamma oscillations during slow wave sleep. PLoS One 7(4) e33477.

Varley TF, Denny V, Sporns O, Patania A (2021) Topological analysis of differential effects of ketamine and propofol anaesthesia on brain dynamics. R Soc Open Sci 8(6) 201971.

Varley TF, Sporns O, Puce A, Beggs J (2020) Differential effects of propofol and ketamine on critical brain dynamics. PLoS Comput Biol 16(12) e1008418.

Vyazovskiy VV, Olcese U, Lazimy YM, Faraguna U, Esser SK, Williams JC, Cirelli C, Tononi G (2009) Cortical firing and sleep homeostasis. Neuron 63(6):865–878.

Watson, B.O., Levenstein, D., Greene, J.P., Gelinas, J.N., and Buzsáki, G. (2016a). Multi-unit spiking activity recorded from rat frontal cortex (brain regions mPFC, OFC, ACC, and M2) during wake-sleep episode wherein at least 7 minutes of wake are followed by 20 minutes of sleep. CRCNS.org..

Watson BO, Levenstein D, Greene JP, Gelinas JN, Buzsáki G (2016b) Network homeostasis and state dynamics of neocortical sleep. Neuron 90(4):839–852.

Whitham EM, Pope KJ, Fitzgibbon SP, Lewis T, Clark CR, Loveless S, Broberg M, Wallace A, DeLosAngeles D, Lillie P, Hardy A, Fronsko R, Pulbrook A, Willoughby JO (2007) Scalp electrical recording during paralysis: quantitative evidence that EEG frequencies above 20 Hz are contaminated by EMG. Clin Neurophysiol 118(8):1877–1888.

Wiesman AI, Koshy SM, Heinrichs-Graham E, Wilson TW (2020) Beta and gamma oscillations index cognitive interference effects across a distributed motor network. Neuroimage 213 116747.

Zanin M, Zunino L, Rosso OA, Papo D (2012) Permutation entropy and its main biomedical and econophysics applications: a review. Entropy 14(8):1553–1577.

Zunino L, Olivares F, Rosso OA (2015) Permutation min-entropy: An improved quantifier for unveiling subtle temporal correlations. EPL (Europhysics Letters) 109(1):10005.

APPENDIX A. SUPPLEMENTARY DATA

Supplementary data associated with this article can be found, in the online version, athttps://doi.org/10.1016/j.neuroscience.2022.04.025.

(Received 7 March 2022, Accepted 28 April 2022)
(Available online xxxx)

PLOS ONE

RESEARCH ARTICLE

Sleep disrupts complex spiking dynamics in the neocortex and hippocampus

Joaquín González[1,2], **Matias Cavelli**[3], **Adriano B. L. Tort**[2], **Pablo Torterolo**[1], **Nicolás Rubido**[4,5]*

1 Departamento de Fisiología de Facultad de Medicina, Universidad de la República, Montevideo, Uruguay, **2** Brain Institute, Federal University of Rio Grande do Norte, Natal, Brazil, **3** Department of Psychiatry, University of Wisconsin, Madison, Wisconsin, United States of America, **4** University of Aberdeen, King's College, Institute for Complex Systems and Mathematical Biology, Aberdeen, United Kingdom, **5** Instituto de Física, Facultad de Ciencias, Universidad de la República, Montevideo, Uruguay

* nicolas.rubidoobrer@abdn.ac.uk, nrubido@fisica.edu.uy

Citation: González J, Cavelli M, Tort ABL, Torterolo P, Rubido N (2023) Sleep disrupts complex spiking dynamics in the neocortex and hippocampus. PLoS ONE 18(8): e0290146. https://doi.org/10.1371/journal.pone.0290146

Editor: Jordi Garcia-Ojalvo, Universitat Pompeu Fabra, SPAIN

Received: April 28, 2023

Accepted: August 2, 2023

Published: August 17, 2023

Peer Review History: PLOS recognizes the benefits of transparency in the peer review process; therefore, we enable the publication of all of the content of peer review and author responses alongside final, published articles. The editorial history of this article is available here: https://doi.org/10.1371/journal.pone.0290146

Data Availability Statement: All relevant data for this study are publicly available from the CRCNS databases (https://crcns.org/data-sets/fcx/fcx-1 and https://crcns.org/data-sets/hc/hc-11).

Abstract

Neuronal interactions give rise to complex dynamics in cortical networks, often described in terms of the diversity of activity patterns observed in a neural signal. Interestingly, the complexity of spontaneous electroencephalographic signals decreases during slow-wave sleep (SWS); however, the underlying neural mechanisms remain elusive. Here, we analyse *in-vivo* recordings from neocortical and hippocampal neuronal populations in rats and show that the complexity decrease is due to the emergence of synchronous neuronal DOWN states. Namely, we find that DOWN states during SWS force the population activity to be more recurrent, deterministic, and less random than during REM sleep or wakefulness, which, in turn, leads to less complex field recordings. Importantly, when we exclude DOWN states from the analysis, the recordings during wakefulness and sleep become indistinguishable: the spiking activity in all the states collapses to a common scaling. We complement these results by implementing a critical branching model of the cortex, which shows that inducing DOWN states to only a percentage of neurons is enough to generate a decrease in complexity that replicates SWS.

Introduction

Cognition and behaviour drastically change across the sleep-wake cycle [1]. During wakefulness, animals are able to interact with their environment, but lose this ability as they fall asleep. During sleep, there is an alternation between slow-wave sleep (SWS), associated with diminished cognitive capacities, and rapid eye movement (REM) sleep, an active state where most dreams occur [2, 3]. The electroencephalogram (EEG) concomitantly changes along with behavior: fast and desynchronised activity appears during wakefulness and REM sleep, while slow quasi-synchronous patterns characterize SWS. Nevertheless, in spite of having well-documented, state-dependent EEG signatures, their underlying mechanisms remain to be fully understood.

In the last decade, there has been a significant rise in the use of complexity metrics (which often measure the diversity of patterns in a signal) capable of revealing hidden non-linear

Funding: J.G acknowledges the support of Comisión Académica de Posgrado (CAP), CSIC Iniciación and PEDECIBA. P.T also acknowledges the support of PEDECIBA. A.B.L.T acknowledges the support of CAPES and CNPq. N.R. acknowledges the CSIC group grant "CSIC2018 - FID 13 - Grupo ID 722. The funders had no role in study design, data collection and analysis, decision to publish, or preparation of the manuscript.

Competing interests: The authors have declared that no competing interests exist.

effects in electrophysiological recordings. These tools have repeatedly shown that the complexity of EEG signals decreases during unconscious states, such as during sleep [4–15] or anaesthesia [14, 16–23]. However, these macroscopic signals have major limitations: they tend to be contaminated by confounding variables (e.g., muscular activity or eye movements) and recovering their exact neural source is often impossible. Thus, the neural patterns driving complexity changes across the sleep-wake states have not been elucidated.

A possible mechanism causing the complexity reduction during sleep is the emergence of DOWN states, defined as synchronous periods of spiking silence [24–29] which generate the extracellular slow waves characteristic of SWS [24–31]. These states are hypothesised to disrupt neural interactions [32], and have been shown to directly alter the complexity of evoked cortical responses [33, 34]. However, no direct analysis of *in-vivo* neuronal populations has shown that DOWN states reduce the complexity of spontaneous cortical activity during sleep.

Here, we analyse *in-vivo* recordings of neuronal populations in the neocortex and hippocampus, quantifying their spontaneous ensemble dynamics in terms of their phase-space recurrences. Our analyses, along with neuronal modelling, show that DOWN states fully account for the complexity decrease during SWS, while a common spiking regime characterises all sleep-wake states in the neocortex and hippocampus.

Results

We study *in-vivo* neuronal recordings from the neocortex and hippocampus of 15 rats cycling through the states of wakefulness (Wake), slow-wave sleep (SWS), and rapid-eye movement (REM) sleep (Fig 2**A**). We analyse $\simeq$1600 neurons, corresponding to 31 independent sessions with 51±5 neurons simultaneously recorded (details in Methods: Datasets). We use recurrence quantification analysis (RQA) to characterise the evolution of the whole population firing counts in each session during each sleep-wake state, extending the characterisation of a population activity beyond a single measure (such as Hurst exponent, entropy, or fractal dimension) or an aggregate of individual neurons. We complement the RQA with coherence and entropy analyses of local field potentials (LFP), spike avalanches, and a critical branching model.

Recurrence analysis reduces high-dimensional dynamics to a 2D representation

The population activity from a cortical location at any given time is a high-dimensional variable detailing the system instantaneous state, i.e., the spiking activity of all neurons (Fig 1**A**, **left**). Its evolution gives a trajectory in the N-dimensional phase-space, which has the firing counts of each neuron as its components (Fig 1**A**, **right**). An attractor is evidenced as a manifold that attracts different trajectories of the system to the same region of the phase-space; the more convoluted (fractal) the attractor is, the higher the temporal complexity of its trajectories. The trajectory of a cortical area is typically high-dimensional, since 50 neurons from any given experimental session results in $N = 50$-dimensional phase-space. By applying Recurrence Quantification Analysis (RQA), we reduce these dimensions to the analysis of 2-dimensional recurrence plots (RP) (Fig 1**C**).

We construct a recurrence plot as follows. Let $\{\vec{x}(t_1), \vec{x}(t_2), \ldots, \vec{x}(t_n)\}$ be a trajectory, where $\vec{x}(t_i)$ is the state-vector whose components are firing counts, $x_k(t_i)$, for each neuron k in the population ($k = 1, \ldots, N$) at time t_i with $i = 1, \ldots, T$, T being the number of 50 *ms* time bins. We choose this time-bin width to match the definition of a neocortical OFF-period, i.e., a period $\geq$ 50 *ms* without spikes. Hence, our firing counts are integer variables that can range from 0 up to 50 (assuming a maximum of 1 spike per *ms*). A recurrence plot is then defined by a symmetric matrix whose entries are $R(i, j) = 1$ if $\|\vec{x}(t_i) - \vec{x}(t_j)\| < \epsilon$, or $R(i, j) = 0$ otherwise,

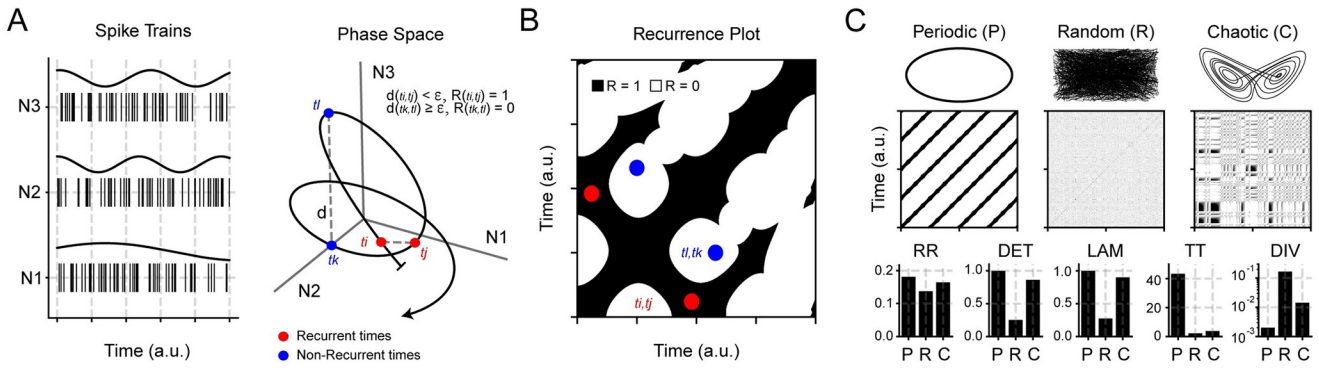

Fig 1. Recurrence example of population activity. A Left Example of spike trains for 3 neurons (N1-N3). The continuous line on top shows the firing counts of each spike train. **Right** Resultant phase-space trajectory (evolution), where the axes represent the firing counts of each neuron. For every pair of points in the trajectory, their distance (d) is computed (the dashed lines illustrate two such distances); If the distance is less than a predefined ϵ value, a recurrence between the time points is defined to occur. Two recurrent times are shown in red (ti,tj), while two non-recurrent times are shown in blue (tk, tl). **B** Recurrence plot for the trajectory shown in panel **A**. Red and blue time pairs are now depicted as coordinates in the resulting map. **C** Example recurrence plots from periodic, random, and chaotic trajectories. On top of the recurrence plot, we show the phase-space of the example; below we illustrate how the RQA metrics behave for each trajectory type. RR: Recurrence Rate, DET: Determinism, LAM: Laminarity, TT: Trapping Time, DIV: Divergence.

https://doi.org/10.1371/journal.pone.0290146.g001

with $i, j = 1, \ldots, T$ and $\epsilon > 0$ defining closeness. A recurrence happens whenever the system trajectory returns to the same region of phase-space up to ϵ. We set $\epsilon = \sigma_p$ (σ_p being the standard deviation of the population activity during wakefulness) to guarantee a sufficiently sparse plot but with sufficient points to carry statistical analyses. Nevertheless, our results are robust to changes in ϵ or time-bin width (S1 Fig).

Two generic structures appear in a recurrence plot: diagonal lines, originating from periodic trajectories, and vertical lines, originating from trapped (frozen) trajectories. These structures help to differentiate between periodic, random, or chaotic trajectories (corresponding panels in Fig 1C), which can be quantified by different metrics (see RQA in Methods). We use RQA to measure (i) Recurrence Rate (density of points), RR, (ii) Determinism (proportion of points forming diagonal lines), DET, (iii) Laminarity (proportion of points forming vertical lines), LAM, (iv) Trapping Time (average length of vertical lines), TT, and (v) Divergence (inverse of the longest diagonal line, excluding the identity line), DIV.

To illustrate how the RQA metrics behave, we compute them for the examples of Fig 1C. RR is slightly larger for the periodic system since it recurs more often into similar states than the other examples, while the chaotic trajectory recurs more than the random example. DET and LAM, on the other hand, are maximal for periodic and chaotic systems because all points form vertical and diagonal structures, while these drop near zero for the random system since recurrent times are rarely connected. Moreover, TT is larger for the periodic system since there are no isolated recurrent times (all points form small vertical structures). TT decreases in the chaotic system due to isolated recurrent times and lowers even further for the random system because recurrences occur by chance and rarely form any vertical structure. Finally, DIV is the largest for the random system since no diagonal structures are formed, while DIV plummets to near zero for the periodic system since all points form long diagonal lines. DIV lies in-between for the chaotic system since it forms short diagonal lines. Thus, predictability in the system trajectory is quantified by RR, DET, LAM, and TT, where the larger [smaller] their values, the more [less] predictable. On the other hand, randomness is quantified by DIV, where the larger [smaller] its value, the more divergent [convergent] the trajectory.

The complexity of neuronal dynamics is reduced during slow-wave sleep

Fig 2**A** shows the LFP and spike trains of frontal cortex neurons in a session for a representative animal under each sleep-wake state. The corresponding recurrence plots for 10-second trajectories are shown in Fig 2**B**. Note that SWS exhibits a denser plot than Wake or REM sleep, implying that SWS has firing patterns recurring more often than Wake or REM sleep. Also, SWS shows a distinctive square-shaped recurrence pattern, which points to the existence of time windows when the trajectory of the population activity is frozen (or practically unchanged). The RQA metrics applied to all available 10-second trajectories for all recorded sessions confirm that frontal cortex activity (∼900 neurons in total) is significantly more predictable and less random during SWS than Wake or REM sleep (Fig 2**C**; see statistics in S1 Table in S1 File).

Specifically, SWS has the largest RR, DET, LAM, and TT, indicating high predictability of the neuronal activity, whereas it has the smallest DIV, suggesting that SWS is less random than Wake or REM sleep. Noteworthy, these RQA changes during SWS correlate with the number of recorded neurons (S2 Fig), suggesting the complexity reduction is a population-level phenomena. Also note that the RQA differences across states are not due to a change of the attractor's topology (S3 Fig). Moreover, the RQA results hold true when dividing the frontal cortex into specific areas (Fig 2**D** and 2**E**) or when analysing the population activity from the hippocampus (S2 Table in S1 File). In fact, when comparing the RQA metrics among the secondary

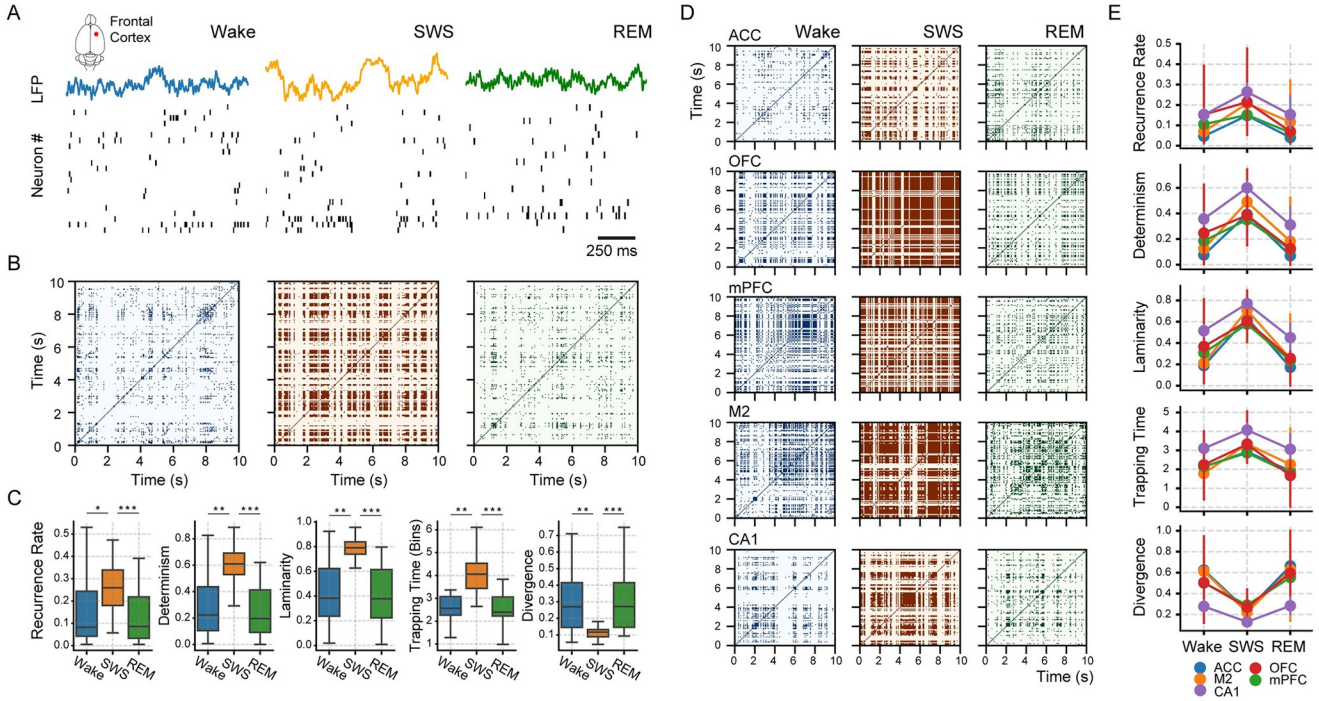

Fig 2. Recurrence quantification analysis (RQA) of *in- vivo* population activity from the frontal cortex and hippocampus. A Local field potentials (LFP) and spike-train raster plots (1*s* interval) for a representative rat during Wake (left), SWS (middle), and REM sleep (right). **B** Recurrence plots constructed from a 10*s* interval of the population activity (see Methods for details). **C** 5 RQA metrics for the sleep-wake states; boxplots show results from the pool of 24 sessions across 12 animals (outliers are not shown). $^{*}p < 0.001$, $^{**}p < 0.0001$, $^{***}p < 0.00001$ (corrected for multiple comparisons). **D** Example recurrence plots for different cortical locations sleep-wake states. ACC: anterior cingulate cortex; OFC: orbito-frontal cortex; mPFC: medial prefrontal cortex; M2: secondary motor cortex; CA1: hippocampus. **E** RQA metrics for the sleep-wake states in each cortical area shown in the previous panel.

https://doi.org/10.1371/journal.pone.0290146.g002

motor cortex (M2), medial prefrontal cortex (mPFC), orbitofrontal cortex (OFC), anterior cingulate cortex (ACC) and the CA1 hippocampus region, we find no statistical differences (Kruskal-Wallis test across cortex: RR [$p = 0.68$], DET [$p = 0.39$], LAM [$p = 0.69$], TT [$p = 0.21$] and DIV [$p = 0.46$]), suggesting that the complexity reduction in the spiking activity is conserved across brain regions. Thus, these results demonstrate that SWS is the least complex spiking state, consistent with previous reports of decreased EEG complexity during sleep [4–15] or anaesthesia [14, 16–22].

Neuronal recurrences during SWS are mainly driven by DOWN states

The square-shaped recurrences appearing during SWS in Fig 2 can be generated by two possible mechanisms. Either a subset of the neurons (or even all) remains constantly active for a period of time, or the neurons remain silent (null firing counts) corresponding to a trajectory in the origin of the phase space. Next, we show that the latter is true and is mainly due to DOWN states.

DOWN states are the neural substrate underlying slow-wave activity ($0–4Hz$) [24–26, 28, 30]. Therefore, a correlation between recurrent trajectories and DOWN states provides a physiological mechanism for the loss of complexity during sleep. For the neocortex, DOWN states can be obtained by finding OFF- periods [26, 28, 29], i.e., periods $\geq 50ms$ when almost all neurons remain silent [26] (Fig 3**A** left). For the hippocampus, we obtain DOWN states by selecting the times when less than 10% of the recorded neurons fired since hippocampal neurons maintain a minimal firing activity during DOWN states [35] (Fig 3**A** right).

The time-series of DOWN states in the neocortex match the times when the trajectory has a recurrence (see the pink and black curves in Fig 3**B** bottom panel). We find a significant correlation between these time-series ($R = 0.77 \pm 0.02$, $p < 10^{-64}$ for all sessions). This means that the majority of the SWS recurrences is due to DOWN states. We observe a similar scenario in the hippocampus (right panels in Fig 3**A** and 3**B**), where we find an even higher correlation between the time-series of DOWN states and that of the recurrences ($R = 0.84 \pm 0.01$, $p < 10^{-64}$ for all sessions).

Notably, SWS becomes more complex if we exclude DOWN states; namely, if we employ a trajectory containing only the population UP states. The corresponding recurrences and metrics are shown in Fig 3**D** and 3**E**; note that RR, DET, LAM, TT and DIV significantly change and become comparable to those of Wake and REM sleep (S4 Fig and Fig 2**C**). Overall, these results support the hypothesis that neuronal trajectories are similar in SWS UP states to Wake and REM sleep [36, 37].

Neocortical DOWN states explain the EEG complexity reduction during sleep

We next investigate how the population activity results translate to the EEG and LFP signals simultaneously recorded from the freely moving animals. To that end, we create synthetic local field potentials (sLFP) (Fig 4) from the actual excitatory spiking activity, in which we assume that each spike generates an exponentially decaying PSP. The motivation behind this method is that it allows to precisely control the sources which dictate the field potential and avoid the influence of any external variable not directly related to spiking activity (such as EMG contamination and volume-conducted signals [38]). Since LFPs primarily reflect postsynaptic potentials (PSPs) [39], we average the modelled PSPs over the population of neurons at each time in order to obtain the instantaneous sLFP (Fig 4**A**).

We find that sLFPs have asynchronous low-amplitude activity during Wake and REM sleep, but have synchronous activity during SWS with periodic high-amplitude waves (Fig 4**B**).

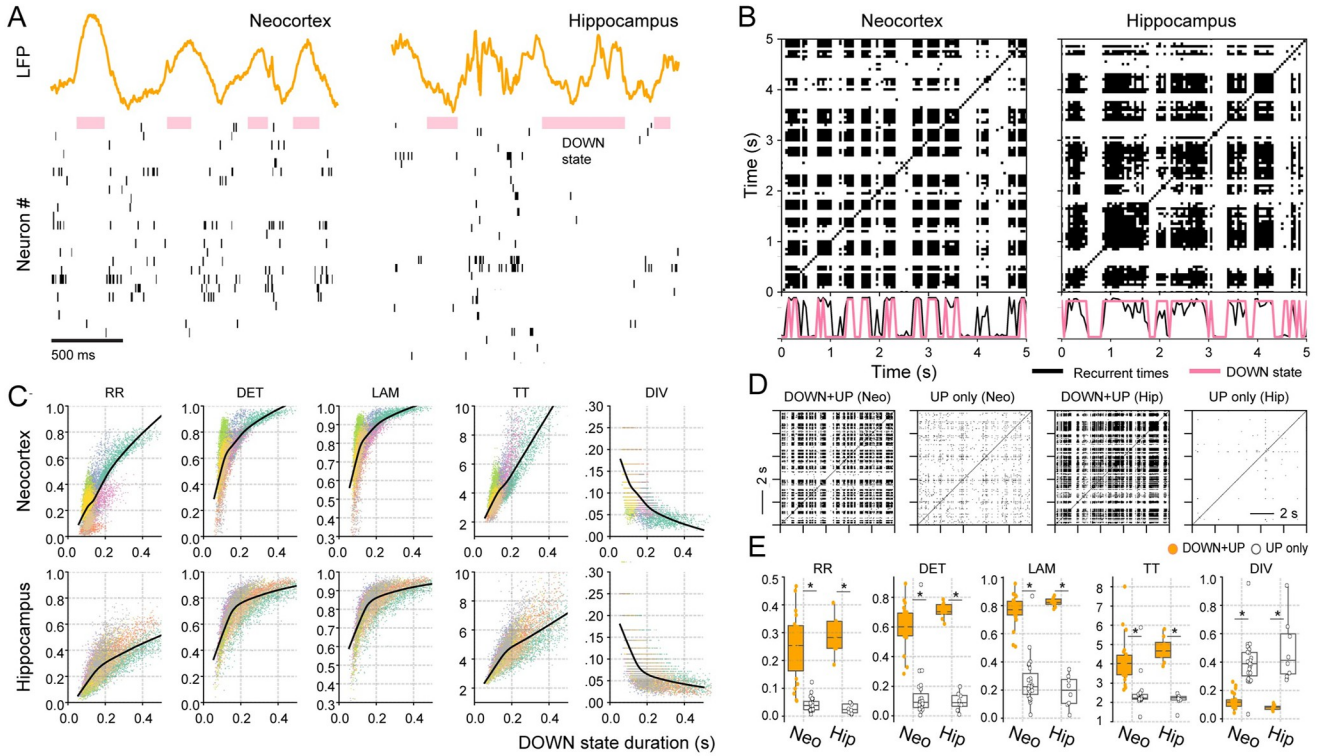

Fig 3. Correlation between recurrent spiking activity and DOWN states in the neocortex and hippocampus during SWS. A Example of LFP (different calibrations) and spiking activity in the neocortex (left) and hippocampus (right) exhibiting DOWN states during SWS. **B** Recurrence plots for the corresponding population activity. The number of recurrences per time (sum over columns) is shown in the bottom panel along with the DOWN state periods. **C** Scatter plot between RQA metrics and the average duration of the DOWN state in each recording session, the different colours depict different individual sessions; solid lines indicate the LOWESS regression estimate taking into account all sessions. **D** SWS recurrence plots computed using the whole period (DOWN + UP) or discarding the DOWN states (UP only) for the neocortex (Neo) and hippocampus (Hip). **E** Boxplots of the RQA metrics for DOWN + UP vs. UP only. Neo, $N = 24$ sessions; Hip, = 9 sessions; $^{*}p < 0.00001$.

https://doi.org/10.1371/journal.pone.0290146.g003

These waves correspond to slow-oscillations of 0–4*Hz* (Fig 4C top), coherent to the LFP activity (Fig 4C bottom). Thus, our sLFP recovers the slow-wave activity oscillatory profile present in the real LFP recordings, including a peak in the delta band particularly visible during SWS (compare Fig 4C and S5 Fig).

We then quantify the temporal-complexity of LFPs and sLFPs by using Sample Entropy (SE) [40], Permutation Entropy (PE) [41], and Lempel-Ziv Complexity (LZ) [42]. Fig 4D shows that results are independent of the chosen complexity measure. The true LFP activity is significantly less entropic during SWS than during REM or Wake (left panels in Fig 4D; S4 Table in S1 File), consistent with previous EEG and electrocorticogram (ECoG) results [4–15]. Accordingly, the sLFP exhibits similar temporal-complexity values (right panels of Fig 4D; S3 Table in S1 File), and also shows a significant decrease during SWS. Importantly, the complexity reduction during SWS is not easily observed for single units: some neurons decrease while others increase their spiking complexity (S6 Fig), suggesting that the temporal coordination among neurons is necessary for the LFP/sLFP complexity results.

Interestingly, when constructing SWS sLFP only employing UP states (i.e., excluding DOWN states) or actually excluding DOWN state periods from the LFP activity, we find that the decrease in complexity during SWS is lost (Fig 4D, S3 Table in S1 File). In fact, the SWS UP states have significantly higher levels of complexity than the SWS sLFP or LFP containing

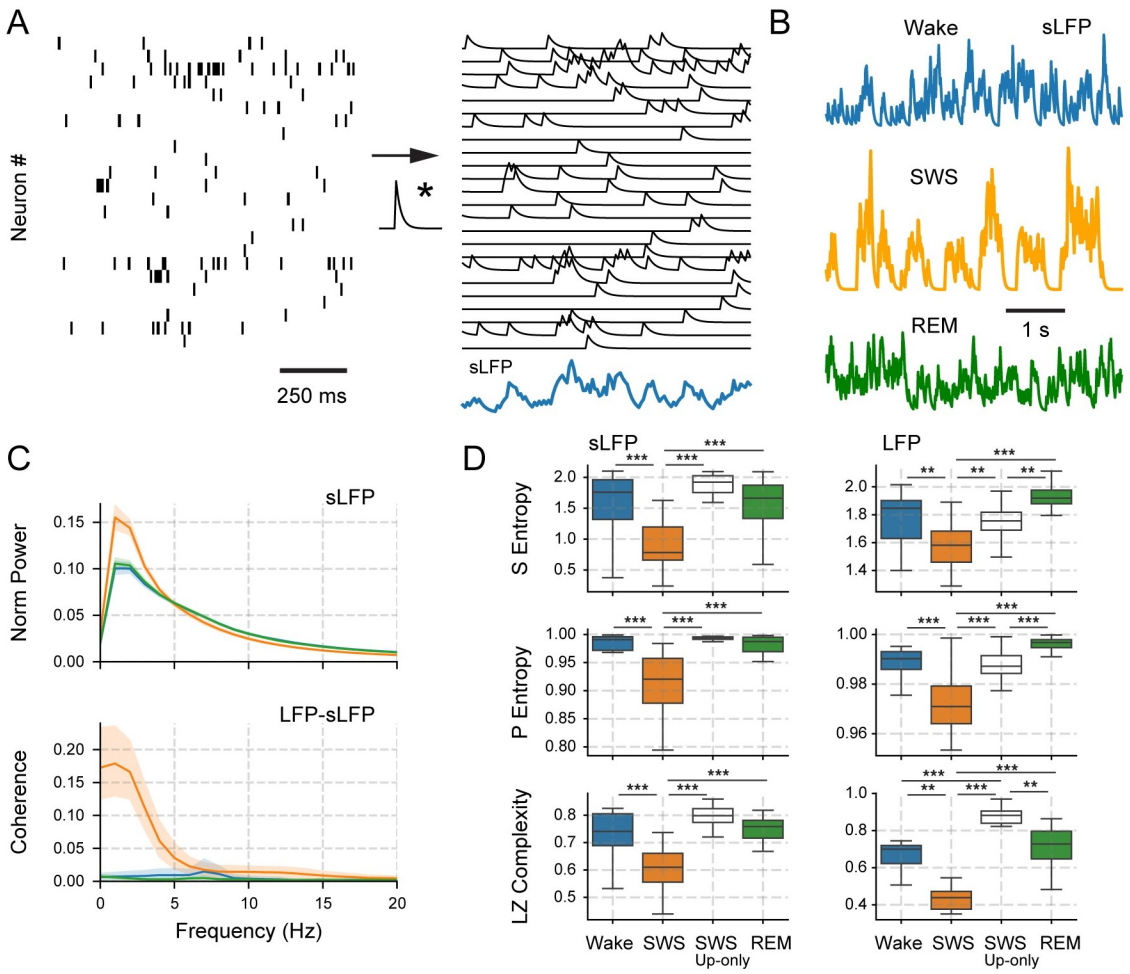

Fig 4. Construction and analysis of synthetic local fieldpotentials (sLFP) during Wake, SWS, and REM sleep. A The sLFP is defined as the average of the convolutions between spike trains and a decaying exponential function. **B** Examples of sLFP resulting from Wake, SWS, and REM sleep population activity. **C** sLFP power spectra(top) and coherence between sLFP and LFP (bottom) for the different sleep-wake states (colour coded). **D** Boxplots of Sample Entropy (top), Permutation Entropy (middle), and Lempel-Ziv Complexity (bottom) of the sLFPs and LFPs in each state ($N = 24$ sessions). $^{*}p < 0.05$, $^{**}p < 0.01$, $^{***} = p < 0.001$.

https://doi.org/10.1371/journal.pone.0290146.g004

both UP and DOWN states, reaching values comparable to those from Wake or REM states. Therefore, we conclude that DOWN states are necessary for the complexity reduction observed in field recordings since spiking periods are similar across states.

Spiking periods across states exhibit similar avalanches

Our previous results show that DOWN states disrupt population dynamics in the neocortex and hippocampus (Figs 2–4). We next complement these results by analysing spike avalanches to understand the factors underlying spiking complexity across sleep-wake states. Avalanches are cascades of activity in quiescent systems [43–50], which in our case correspond to active spiking periods within a brain region; by definition, avalanches exclude DOWN states.

Fig 5A shows a neuronal population exhibiting an avalanche, where the time bin defining its occurrence is set as the average inter-spike interval (ISI). By definition, an avalanche starts after a time bin without spikes and finishes when another empty time bin is reached. Two

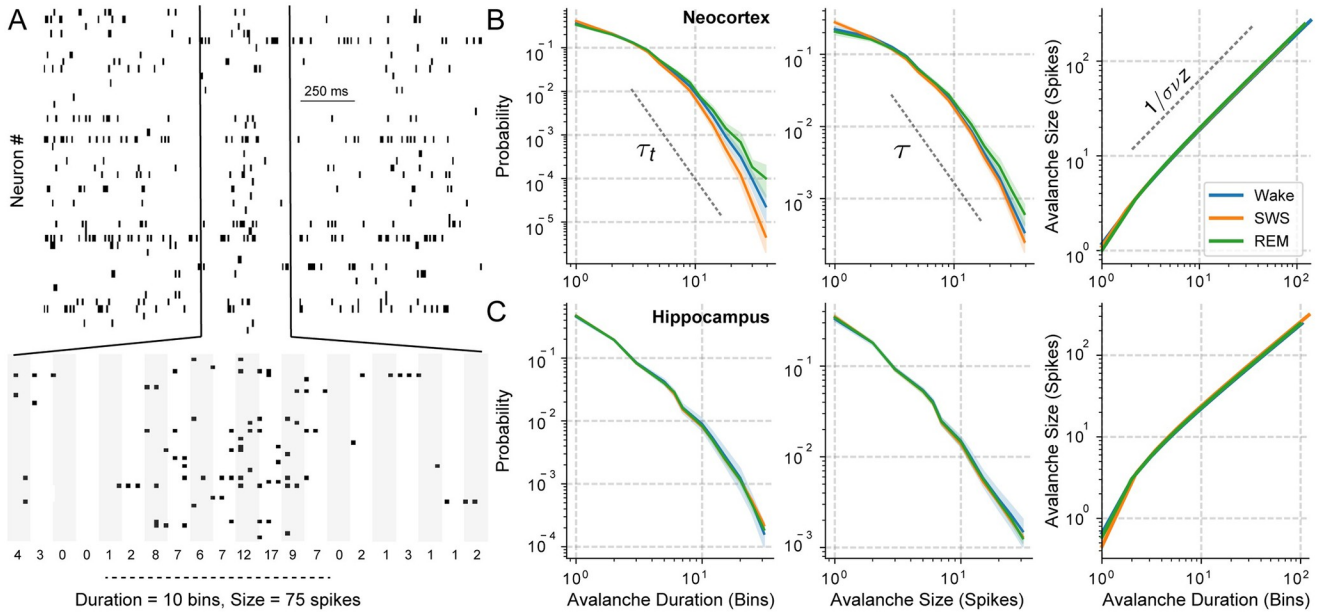

Fig 5. Avalanche distributions for Wake, SWS and REM sleep. A Example of a neuronal avalanche. The average ISI is used to bin the raster plot (shaded rectangles) and count the number of spikes per bin. **B** Avalanche statistics for the neocortex. Left: distribution of avalanche duration, used to estimate the τ_t exponent. Middle: distribution of avalanche size, used to estimate τ. Right: avalanche size as a function of its duration, from which the $\frac{1}{\sigma\nu z}$ exponent is estimated. **C** As in **B** but for hippocampal avalanches. For each state (colour coded), the mean distributions are shown in solid lines with a shaded area depicting the 95% confidence interval.

https://doi.org/10.1371/journal.pone.0290146.g005

parameters commonly characterise an avalanche: its size, i.e., the total number of spikes, and its duration, i.e., the time interval from start to finish. The avalanche statistics for each sleep-wake state are derived from the probability distribution of these parameters [44, 45].

Fig 5**B** and 5**C** show minimal differences between the probability distribution of avalanche duration and size during Wake, REM sleep, or SWS in the neocortex and hippocampus, respectively. For instance, avalanches occurring during SWS tend to be shorter due to DOWN states. The power-law exponents for the avalanche duration (τ_t) and size (τ) are related by the crackling noise relationship, $\frac{\tau_t-1}{\tau-1}$, which is a more stringent criticality statistics [45]. Considering all sleep-wake states, we get $\frac{\tau_t-1}{\tau-1} = 1.19$ (inter-quartile range, $IQR = 0.33$) for the neocortex and $\frac{\tau_t-1}{\tau-1} = 1.24$ ($IQR = 0.37$) for the hippocampus, with no significant differences across states ($p = 0.31$ and 0.68, respectively). More importantly, we find that the avalanche size and duration distributions collapse to the same scaling function resembling a power-law behaviour characterised by the exponent $1/\sigma\nu z$[45] (right panels in Fig 5**B** and 5**C**). This suggests that the spiking periods (UP states) have a common behaviour across sleep-wake states. We find that $\frac{1}{\sigma\nu z} = 1.11 (IQR = 0.05)$ for the neocortex with no significant differences across sleep-wake states ($p = 0.21$). Similarly, $\frac{1}{\sigma\nu z} = 1.20 (IQR = 0.02)$ for the hippocampus ($p = 0.09$ for state differences).

Thus, once the spiking activity is initiated, it follows a common avalanche regime irrespective of the sleep-wake state. Consequently, complexity differences in the sleep-wake states should originate from DOWN states where no spikes occur. Noteworthy, these results restrict the possible mathematical models which can describe cortical dynamics, since the model must be able to reproduce DOWN states (during SWS) and the avalanches appearing for any state during spiking activity.

Critical branching model for the spiking activity in the cortex

Here, we show that cortical spiking patterns during wakefulness and sleep can be captured by a critical branching model, known to exhibit universal behaviour [51], when implemented using exponents matching our *in-vivo* results (see Methods). The critical branching model consists of interacting discrete units whose internal state may be resting, spiking, or refractory. The units evolve in time according to the excitation coming from neighbouring units (as controlled by a branching parameter) as well as due to a noisy drive set by a Poisson distribution, which can randomly make a unit fire at any given time. The branching parameter, σ, determines the probability of a spike from unit A at time t affecting unit B at time $t + 1$. When $\sigma = 1$, the system is critical; the network exhibits a phase transition from a sub- critical quiescent state for $\sigma < 1$ (activity dies out after a small transient) to a super-critical active state for $\sigma > 1$ (activity is self-sustained). The interplay between units interacting due to branching and noise recreates a network of higher-order neurons that receives inputs from lower areas such as the thalamus [52]. To reproduce an SWS state, we add to the branching model a periodic silencing of the noisy drive for some (adjustable percentage of) units in order to model DOWN states.

Fig 6A shows an example of the resultant spike trains for the branching model without (left panel) and with (right panel) the periodic silencing. These results are obtained using 50 units (similar size to the experimental ensembles recorded) and setting the branching parameter at

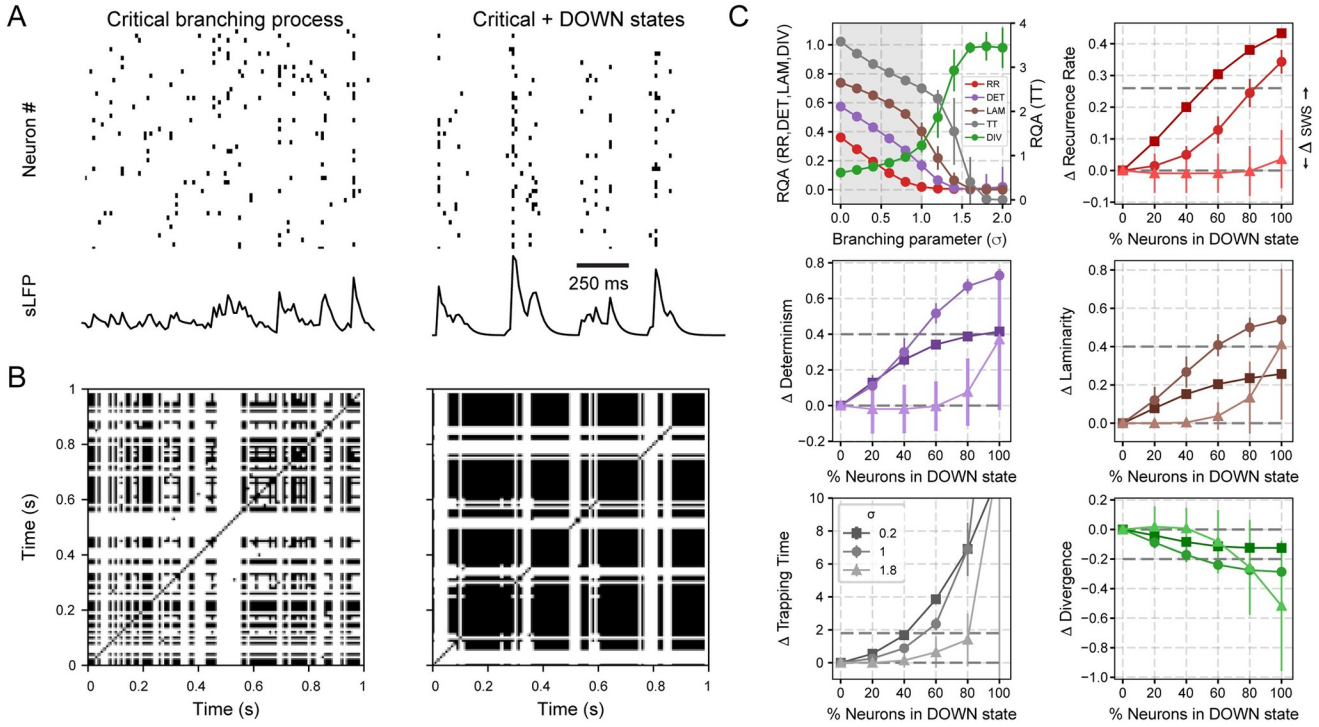

Fig 6. Critical branching model for neuronal activity during Wake and SWS. A Left: Population activity (raster plot) and synthetically generated local-field potential (sLFP, as in Fig 4) of a critical branching model with 50 interacting units. The branching parameter is set at $\sigma = 1$ (critical); an excitatory Poisson noise drive each unit independently. Right: DOWN states are generated by periodically silencing (4*Hz*) the noisy drive of a percentage of units. **B** Resultant recurrence plots for the data in **A**. **C** Average (± standard deviation) results from 100 simulations using different network connectivity and initial conditions. Each simulation consisted of 10^6 iterations in time. Top left: RQA metrics for the original model (i.e., without silencing) as function of σ; shaded [unshaded] area shows the sub-critical [super-critical] phase. Remaining panels: differences (Δ) between RQA metrics of the original model and the model with periodical silencing as a function of the percentage of neurons having their noise drive silenced (referred to as % of neurons in DOWN state). The horizontal dashed lines show the difference between the actual SWS RQA metrics (Fig 2C) and those of the critical branching model.

https://doi.org/10.1371/journal.pone.0290146.g006

the critical point $\sigma = 1$. The respective recurrence plots are shown in Fig 6**B**. For the modified branching model, we periodically silence the noise input arriving at a given set of units during a 250*ms* interval (similar to Ref. [44]) and call it Critical + DOWN. This external silencing is enough to synchronize the network to a state of inactivity (Fig 6**A**), trapping the population trajectory into recurrent square-like patterns (Fig 6**B**), similar to the experimental results from the neocortex and hippocampus (Fig 2).

We use RQA to quantify the differences between the original and modified branching models. The top left panel of Fig 6**C** displays RQA metrics for the branching model with 50 units as a function of σ, where the shaded area marks the sub-critical phase. For $\sigma = 1$, the model has RR $\simeq 0.02$, DET $\simeq 0.2$, LAM $\simeq 0.4$, DIV $\simeq 0.3$, and TT $\simeq 2.5$, which are comparable to the average RQA values of Fig 2**C** during Wake and REM sleep. The remaining panels show the change in the RQA metrics when the periodic noise-silencing is added to the model—changes are shown as a function of the percentage of units having their noise periodically silenced. The horizontal dashed lines show the difference between the SWS RQA metrics and those of the critical branching model. In other words, this relative SWS metric is found by taking the value obtained from the experimental average RQA metric shown in Fig 2**C** and subtracting the critical branching model RQA metric from the top left panel in Fig 6**C**. Using this, we can find the percentage of units with periodically-silenced noise that are needed to reproduce the experimental values found for SWS.

We find that as the number of units with a DOWN state increases (i.e., number of neurons with periodical silencing), the RQA metrics cross those observed during SWS from the *in-vivo* recordings (horizontal dashed line) (Fig 2**C**). When the model is at the critical point ($\sigma = 1$), a periodic noise-silencing to 40–60% of the units is enough to reproduce the RQA values during SWS (intersection of the Δ RQA metrics with the corresponding horizontal dashed lines), with the exception of RR, which requires 80%. On the other hand, both the sub- ($\sigma = 0.2$) and super-critical ($\sigma = 1.8$) models need a considerably larger percentage of silencing (80–100%) to reproduce the observed SWS values. Therefore, these results suggest that: i) the branching model needs to be close to $\sigma = 1$ (criticality) to reproduce the recurrent properties observed during Wake or REM sleep, and ii) that the inclusion of a periodic silencing of the noisy drive to 40–60% of the units reproduces the recurrent properties observed during SWS.

Discussion

Our main findings can be summarised in the following points. The complexity of neuronal dynamics in rats is reduced during SWS owing to spiking patterns repeating more often (i.e., greater recurrences). This spike pattern repetition occurs during DOWN states, thus bridging the decrease in complexity observed in the cellular and field recording levels (such as local field potentials or EEG). Moreover, we reveal a common behaviour in the population spike avalanches appearing across the sleep-wake states (which by definition exclude DOWN states). This scaling makes the sleep-wake states indistinguishable from each other, and demonstrates that the DOWN periods are responsible for the complexity reduction which characterises SWS. Finally, we reproduce these experimental results by numerical experiments employing a critical branching model, suggesting that criticality may favor transitions between states.

Recurrence quantification analysis improves the study of cortical population dynamics

Our study is based on the analysis of the spiking activity from *in- vivo* population recordings of the neocortex and hippocampus. To that end, we employ RQA, which leads to clear results and interpretations (see Fig 1), is robust to parameter tuning (e.g., changing the tolerance

parameter or time bin width; S1 Fig), and is computationally efficient (e.g., 10*s* windows are enough to distinguish states). Importantly, RQA allows analysing a population of neurons using various complementing non-linear metrics, such as randomness, entropy, or fractal dimension. This extends the typical characterisation of neuronal dynamics based on single neurons and single metrics (such as the basal firing rate, coefficient of variation, or rhythmicity).

We also compared our results with those provided by topological data analyses (S3 Fig). In particular, persistent homology analyses the topology of a high-dimensional cloud of points (manifold) in phase space [21, 53]. Interestingly, by using this analysis we find that the low-dimensional topology of the neocortical phase-space attractor appears to remain unchanged throughout the sleep-wake cycle (S3 Fig). This contrasts with results from the anterior nucleus of the thalamus which exhibits a ring-like structure during Wake and REM sleep, but not during SWS [53]. Thus, our observations suggest that the dynamical differences across states are still contained within the same manifold.

Population DOWN states reduce the complexity of cortical activity during SWS

In contrast to the unchanged attractor topology (S3 Fig), our results show that the evolution of neocortical and hippocampal spiking activity is significantly altered during SWS. We show that the cause for this alteration is (mainly) due to the appearance of synchronous DOWN states that disrupt the population spiking patterns and force them into a recurrent, deterministic state. We find a strong correlation between the duration of DOWN states and the number of recurrences in the population activity (Fig 3**B** and 3**C**). Then, we show that the decrease in complexity is lost once we discard the DOWN states from the SWS analysis (Fig 3**D** and 3**E**), making SWS spiking-patterns similar to those from REM sleep or wakefulness.

DOWN states appear to disrupt neuronal patterns in neocortical and hippocampal areas similarly, although both regions have different mechanisms for the generation of DOWN states [25, 35]. During SWS, hippocampal neurons oscillate between long, quiescent, stable periods (without clear membrane hyperpolarization [25]) and bursts of spiking activity (during sharp-wave ripples). In contrast, neocortical neurons oscillate between stable periods of spiking activity and unstable periods of quiescence (associated with hyperpolarization [25]). In spite of these differences, both populations have spiking patterns that are consistent with excitable UP/DOWN states [35].

For individual neocortical neurons, the complexity of firing patterns decreases during SWS [6]. In principle, this decrease could be expected due to the DOWN states, as their appearance causes neurons to remain silent during synchronous intervals. Here, however, when we analyse the firing patterns of individual neurons independently, we find that a considerable number maintain complex patterns even during SWS (S6 Fig). This can occur because either there are DOWN state active neurons, as previously shown in [54], or because the complexity reduction is a collective phenomenon that can only be studied at the population level. We support this latter argument by showing that the difference in complexity between Wake or REM sleep and SWS increases with the number of analyzed neurons (S2 Fig).

Measuring complexity from synthetic and experimental field recordings

The complex nature of brain recordings—and the decrease in complexity during unconscious states—has been reported using classical neuroscience approaches [55, 56]. For instance, the EEG power spectrum shows a power-law decay, $f^{-\alpha}$, for a broad range of frequencies, referred to as $1/f$ noise. Interestingly, the exponent α becomes greater than 1 (a more pronounced

decay) during sleep and anaesthesia [55, 56] since DOWN states and slow oscillations promote the appearance of low-frequency power, leading to a steeper spectral decay.

These observations match our sLFP analyses, which recover both the slow oscillations present in true LFPs during sleep (Fig 4C), and their entropy variations during the sleep-wake cycle (Fig 4C)—independently of the chosen entropy metric (i.e., permutation entropy [41], sample entropy [40], and Lempel-Ziv complexity [42]). Notably, the decrease in complexity during SWS is lost when we eliminate the DOWN states from the LFPs and sLFPs (Fig 4E), implying that DOWN states are responsible for reducing the complexity of field recordings during SWS. Consistent with our results, the slow-wave activity (0.1–4*Hz*) has been associated with the loss of complex neuronal interactions during sleep [32, 57, 58] and is caused by synchronous neuronal DOWN states [24–31]. Of note, the similarities in slow-wave activity [25, 28, 30, 31], and neural complexity [4, 5, 9, 15] between rodents and humans suggest that related mechanisms could also act in the latter during sleep.

It should be noted that estimating neural complexity directly from field recordings might lead to spurious results since there are major differences between the exponent variations in ECoGs and LFPs. For instance, we also find a $f^{-\alpha}$ behaviour in the power spectra of LFPs and ECoGs (S5 Fig) and get similar decay exponents during SWS and REM ($\alpha_{sleep} \simeq 2$). Nevertheless, for ECoGs, we find a significant difference in exponent values from Wake (when $\alpha_{wake} \simeq 1$), while, for LFPs, $\alpha_{sws} \simeq 2$ as during sleep. Thus, this could point to the presence of extra-neural sources during Wake that alter the ECoG power spectrum decay but do not influence the LFP recording level. Therefore, we argue that complementing field recordings with spiking activity is necessary to unveil and study genuine neural complexity.

Spiking periods show similar dynamics across states

An important result verified through complementing approaches (Figs 3–5) is that while spiking activity is occurring, SWS behaves similar to Wake or REM sleep. Thus, we suggest near-critical dynamics might be a necessary (but not sufficient) condition for neural complexity. We show that neuronal avalanches of length t contain an average of $g(t)$ spikes, where g is a scaling function independent of the sleep-wake state. This means that avalanches from the frontal cortex and hippocampus of rats across states follow a close behaviour that resembles a power law (Fig 5B and 5C), similar to previous results in the visual cortex [44]. We find that the exponents $\frac{1}{\sigma\nu z}$ and $\frac{\tau_t-1}{\tau-1}$ are relatively close in both areas (which follows the crackling noise relationship, claimed as a more stringent criticality test [45]). Specifically, for the neocortex, we have $\frac{1}{\sigma\nu z} = 1.11$ and $\frac{\tau_t-1}{\tau-1} = 1.19$, and for the hippocampus, we have $\frac{1}{\sigma\nu z} = 1.20$ and $\frac{\tau_t-1}{\tau-1} = 1.24$. These similar exponents are expected if the system is close to a critical point and have been reported for intermediate levels of spiking variability in anaesthetized rats and freely behaving mice [45]. Therefore, our results support the hypothesis that complex cortical activity arises from near-critical dynamics [43–47, 49, 50, 59–62].

DOWN states are sufficient to reproduce the complexity reduction in a critical model of the cortex

To complement our *in-vivo* results, we show that introducing DOWN states into a critical branching model is sufficient to generate an SWS-like state (Fig 6A and 6B). We achieve this by periodically silencing the noisy drive to a given percentage of units, thus mimicking the synaptic input reduction to pyramidal cells during SWS in the neocortex [63]. This reduction is likely caused by a pre-synaptic GABAb inhibition of the excitatory inputs arriving at the apical dendrites of principal cells [64], coordinated by the thalamus [65]. In contrast to neocortical

mechanisms, UP/DOWN states in the hippocampus are related to sharp-wave ripple generation, where low-spiking DOWN states predominate, and UP-states are initiated by recurrent excitation from CA3 neurons [66]. Therefore, in the hippocampus, the periodic silencing reproduces DOWN states occurring between sharp-wave ripples.

In our model, there is no need to silence the input to 100% of the neurons to reproduce the experimental results, consistent with the lack of hippocampal OFF-periods and minimal firing levels during DOWN states [35]. Additionally, we note that a similar strategy has been employed to model slow-wave oscillations during anaesthesia [44]. Moreover, we find that being near the critical point (Fig 6**C**) allows for more flexible transitions to the SWS-like state with respect to the sub- or super-critical model. Specifically, silencing the input to 40–60% creates a decrease in complexity similar to that observed experimentally. Notice further that, despite the subcritical model requiring less silenced neurons to achieve RR levels, it fails to capture LAM and DIV SWS values. These results further add to the idea of criticality in the brain, which would explain increased complexity [67], information processing and transmission [43], and dynamical range [60].

Conclusion

Complexity has been suggested as a necessary condition for cognition [14, 68]. Accordingly, it has been widely reported that during SWS the complexity of brain dynamics decreases [4–14]. However, the reason why brain signals are complex when animals are awake or why this complexity is lost during unconscious remains controversial [69]. In the present work, we conclude that DOWN states fully account for the complexity decrease during SWS, while a common underlying spiking regime describes all sleep-wake states in the neocortex and hippocampus.

Materials and methods

Datasets

Datasets We analyse 2 datasets: Watson et al. (neocortex, available at CRCNS.org/fcx) [70]; and Grosmark and Buzsaki (hippocampus, available at CRCNS.org/hc) [71]. The reader is referred to the original publications for details about experimental methods. We provide a summary below.

For the neocortex dataset [70], silicon probes were implanted in frontal cortical areas of 11 male Long Evans rats. Recording sites included medial prefrontal cortex (mPFC), anterior cingulate cortex (ACC), pre-motor cortex/M2, and orbitofrontal cortex (OFC). Recordings took place during light hours in the home cage (25 sessions, mean ± SD duration of 4.8 ± 2.2 h). We note that we exclude *BWRat19_032413* from the analysis since it did not contain REM sleep. Data was sampled at 20 *kHz*. To extract LFPs, recordings were low-pass filtered and re-sampled at 1.25 *kHz*. To extract spikes, data was high-pass filtered at 800 *Hz*, and then threshold crossings were detected. Spike sorting was accomplished by means of the Klusta-Kwik software. Sleep-wake states were identified by means electrophysiological and EMG analyses [70]. OFF periods were extracted as periods of population silence lasting at least 50*ms* and no more than 1250*ms*. Conversely, ON periods consisted of periods of population firing between OFF periods with at least 10 total spikes and lasting 200–4000*ms*.

For the hippocampus dataset [72], 7 silicon probes were implanted in the dorsal CA1 of 4 male Long Evans rats. LFP and spikes were extracted the same way as in the neocortex dataset; similar criteria were employed to identify the sleep-wake states. DOWN [UP] states were identified during SWS selecting the times when less [more] than 10% of neurons fired.

Recurrence quantification analysis

Prior to analyse the recurrences of the neuronal population [73–75], we bin the spike train of each neuron using 50*ms* non-overlapping spike count windows. The dynamics of the neuronal population is then described by the evolving firing counts of all neurons, which defines a trajectory (with a time resolution of 50*ms*) in the population phase space (that has N dimensions for N neurons).

A recurrence plot of the evolving firing counts is defined by the symmetric matrix

$$\begin{cases} R(i,j) = 1, & \text{if } \|\vec{x}(t_i) - \vec{x}(t_j)\| \leq \epsilon, \\ R(i,j) = 0, & \text{otherwise}, \end{cases} \tag{1}$$

where $\vec{x}(t_i)$ $[\vec{x}(t_j)]$ is the phase-space vector containing the firing counts of all neurons at the time bin t_i $[t_j]$, with $i = 1, \ldots, T$ (T being the number of 50*ms* bins that are available from the spike-train signals, e.g., $T = 200$ when using 10*s* windows) and $\epsilon > 0$ is the tolerance parameter defining closeness. We set $\epsilon = \sigma_P$, where σ_P is the standard deviation (across time) of the summed firing counts (across neurons) during wakefulness. $R(i, j) = 1$ corresponds to having the trajectory of the neuronal population at time t_i returning to the same region (up to ϵ) of phase space that it was at time t_j; that is, a recurrence happens after $t_i - t_j$.

To quantify the patterns arising from recurrences, we employ common measures from Recurrence Quantification Analysis (RQA) [73–75]. The metrics we use are: recurrence rate (RR), determinism (DET), laminarity (LAM), trapping time (TT) and divergence (DIV), which are defined by

$$RR = \frac{1}{N^2}\sum_{i,j=1}^{N} R_{i,j}, \quad DET = \frac{\sum_{l=l_{\min}}^{N} lP(l)}{\sum_{l=1}^{N} lP(l)}, \quad LAM = \frac{\sum_{v=v_{\min}}^{N} vP(v)}{\sum_{v=1}^{N} vP(v)},$$

$$TT = \frac{\sum_{v=v_{\min}}^{N} vP(v)}{\sum_{v=v_{\min}}^{N} P(v)}, \quad DIV = \frac{1}{Lmax},$$

where $P(l)[P(v)]$ indicates the probability of finding a diagonal [vertical] line of length $l[v]$, and $Lmax$ indicates the longest diagonal line excluding the identity line.

Synthetic LFPs and field complexity measures

We construct synthetic Local Field Potentials (sLFPs) by averaging the convolutions between spike counts in 80*ms* non-overlapping bins of each excitatory neuron and an exponentially decreasing kernel. Namely, $C_n(t) = S_n(t) \star \exp(-t/\tau)$, where $S_n(t)$ is the n-th neuron spike count time series, $\tau = 24ms$ is the characteristic time-scale of the kernel (typical mEPSP time for pyramidal neurons in the frontal cortex [76]), and $\star$ the convolution operator.

The resultant sLFP is then obtained from

$$sLFP(t) = \frac{1}{N}\sum_{n=1}^{N} C_n(t), \tag{2}$$

where N is the number of simultaneously recorded neurons.

For the frequency analysis, we compute the power spectrum of the sLFP using Welch's algorithm. We apply the `signal.welch` scipy python 3 function (scipy.org), with a 1*s* moving Hanning window (without overlap), and a 1*Hz* frequency resolution. For computing the sLFP-LFP coherence, we first downsample the LFP recordings to 125*Hz* and average them

across channels; we then employ the `signal.coherence` scipy function, using the same parameters as the power spectrum. We note that the 80*ms* spike count bin equals a 125 Hz sampling frequency.

For measuring sLFP and LFP complexity, we use Permutation Entropy (PE) [41], Sample Entropy (SE) [40], and Lempel-Ziv (LZ) [42] Complexity, implemented through the `antroPy` python 3 package (github/antropy). Prior to computing these measures, we also downsample the LFP recordings to 125*Hz* and average them across channels.

PE [41] requires dividing the sLFP or the average LFP signal, $\{x(t), t = 1, \ldots, T\}$, into $\lfloor (T - D)/D \rfloor$ non-overlapping vectors of D data points, with $D \ll T$ (shorter than the time-series length). Then, each vector is classified as a symbol α according to the number of permutations needed to order its D elements. We employ $\tau = 5$, where τ is the distance between consecutive time-stamps inside each vector containing $D = 3$ time points. Finally, the PE [41] is the Shannon entropy [77] of the resultant symbolic sequence; that is, $H = -\sum_{\alpha} p(\alpha) \log [p(\alpha)]$, where $p(\alpha)$ is the probability of finding symbol α in the signal.

Similar to PE, SE [40] consists of dividing a time-series into a series of D-sized vectors $(\vec{y}_D(i) = \{x(t_i), x(t_{i+1}), \ldots, x(t_{i+D-1})\})$ and is defined as $SE = -log\left(\frac{A}{B}\right)$, where A and B are, respectively, the number of times that $d[\vec{y}_{D+1}(i), \vec{y}_{D+1}(j)] < r$ and $d[\vec{y}_D(i), \vec{y}_D(j)] < r$ for all i, j vector pairs, and d is the Chebyshev distance and $r > 0$ is a tolerance parameter (0.1 * *SD* of the signal). In our case $D = 3$, and we downsample the signals by a factor of 5 in order to match τ from PE.

LZ [42] complexity is estimated by the `LZ-76` algorithm. We start by creating a binary sequence from the mean value of the sLFP or the average LFP recording—all points larger than the signal mean are converted to 1, and 0 otherwise. Then, we count the number of different binary sub-strings from beginning to end, *#substrings*. The LZ complexity is given by $LZ_w = (\#substrings)/(w/\log(w))$, where w is the length of the binary sequence.

Neuronal avalanches

We quantify neuronal avalanches following previous studies [44, 45]. First, population activity is binned employing the average inter-spike interval. Then, we measure the time (duration) and number (size) of spikes between one empty bin (0 spikes) to the following empty bin. We use the `powerlaw` (pypi.org/powerlaw) python 3 package to construct the probability distributions and obtain their exponents: τ_t and τ. We also compute the average number of spikes as a function of the avalanche duration, and obtain the exponent $\frac{1}{\nu\sigma z}$ by means of an ordinary least square fit on the log-log scale distribution.

Critical branching model

The critical branching model consists of 50 interacting units randomly connected in an Erdös-Rényi topology with a 0.03 attachment probability (i.e., each pair of units has a 0.03 probability of having a link). The time step was set as 1*ms*. Each unit has 3 possible states: resting, firing or refractory. The transition between resting and firing can either occur from the excitation coming from a connected neuron firing in the preceding time, or by the intrinsic Poisson noise that each neuron receives independently. The excitatory Poisson noisy drive is set by generating a random matrix whose values come from a [0, 1] uniform distribution, and then setting for each entry a spike if the value is less than $1 - e^{-\lambda}$ ($\lambda = 0.014$). We periodically silenced the Poisson noise for 250*ms* at a 4*Hz* frequency to create a SWS-like state. Once a neuron fires, it goes to the refractory state and it cannot be excited again. After one step in the refractory state, the neuron goes to the resting state and becomes excitable again. The propagation of spikes is controlled by the branching parameter σ, which regulates the overall excitability of the system.

For instance, if neuron i fires, the probability that a connected unit fires is defined as $P_{prop} = \sigma / \langle k_j \rangle$, where $\langle k_j \rangle$ is the average node degree across all units j.

Statistics

We present data as boxplots showing the median, the 1st and 3rd quartiles, and the whiskers corresponding to 1.5 times the inter-quartile range. Because of the non-Gaussian distributions of the complexity metrics, we employ non-parametric statistics. We use the Friedman test available with the `scipy.stats` from python 3 package to compare the results among states, i.e., Wake-SWS-REM (Wake-SWS-SWSup-REM, Fig 4**D**), with the Siegel post-hoc test applying the Benjamini-Hochberg false discovery rate correction available with the `scikitlearn` (scikit-learn.org). We set $p < 0.05$ for a result to be considered significant. In addition to p-values, we also report Cohen's d, which quantifies the magnitude of a result in terms of a standardised difference between conditions; an effect size is considered to be large if Cohen's d is > 0.8. For the power spectra and avalanche results, we present the data as the mean with the 95% confidence interval (obtained through bootstrap sampling). For the correlation analysis, we employ LOWESS regression to fit the best estimate to the scatter plot by means of the `regplot` python 3 function available at seaborn.pydata.org. As LOWESS regression has no associated p value, we employ a linear regression for each session and consider the result as significant only if $p < 0.05$ for all sessions. Additionally, to correlate the DOWN states to the recurrence sum, we employ the point-biserial correlation `pointbiserialr` function available at scipy.org.

Supporting information

S1 Fig. RQA differences among states are robust to parameter choice. A RQA metrics for different tolerance levels ϵ defining recurrence in phase space. We vary ϵ from 0 std to 4 std of the population firing counts. Setting ϵ to 0 means that a recurrence occurs between two times for the exact same neuronal firing pattern. The time bin is kept fix at 50 ms. **B** RQA metrics for different time binning of the population activity. Time bins are changed from 20 ms to 200 ms in order to define the firing counts for each neuron. The ϵ is kept fix at 1 std. The mean and its corresponding 95% confidence intervals are shown for each plot.
(TIF)

S2 Fig. RQA differences between states correlate with the number of neurons recorded. Absolute RQA differences between states as a function of the number of simultaneously recorded neurons. Each dot shows a recording session while the solid line the linear regression estimate with its 95% confidence interval. **A** shows the SWS-Wake difference, while **B** the SWS-REM difference.
(TIF)

S3 Fig. Persistent Homology cannot distinguish the sleep-wake states in the neocortex. Top panels: Point clouds obtained after dimensionality reduction. A representative animal is shown during Wake, SWS and REM sleep. Bottom panels: Betti 0 (HO) and Betti 1 (H1) barcodes for the same animal shown in the top panel. The length of each bar shows the level of persistence of each Betti 0 and 1 component.
(TIF)

S4 Fig. UP state recurrences are similar to Wake or REM sleep. A Recurrence plots constructed from a 10s interval of the population activity using. **B** 5 RQA metrics for the sleep-wake states; boxplots show results from the pool of 24 sessions across 12 animals (outliers are

not shown).
(TIF)

S5 Fig. Power spectrum slope differs among states. A LFP [ECoG] recordings coming from the frontal cortex [M1 cortex] during the states of Wake, SWS and REM sleep. The mean and its corresponding 95% confidence intervals are shown for each plot. **B** Power spectrum exponents calculated through ordinary least-squares fit on a log-log scale (OLS) or through the FOOOF parametrized spectra (FOOOF) [78] which only includes the aperiodic component.
(TIF)

S6 Fig. Single neurons deviate from the ensemble behaviour. Lempel-Ziv Complexity of single neuron firing pattern between Wake and SWS. Each bar shows the total number of neurons or sessions whose temporal complexity decreased or increased during sleep. Left: LFP recordings. Middle: sLFP recordings- Right: Single unit recordings.
(TIF)

S1 Text. Supplementary methods [9, 21, 53].
(PDF)

S1 File.
(ZIP)

Author Contributions

Conceptualization: Joaquín González, Adriano B. L. Tort, Pablo Torterolo, Nicolás Rubido.

Formal analysis: Joaquín González, Nicolás Rubido.

Funding acquisition: Joaquín González, Adriano B. L. Tort, Pablo Torterolo.

Investigation: Joaquín González.

Methodology: Joaquín González, Matias Cavelli.

Resources: Adriano B. L. Tort.

Software: Joaquín González.

Supervision: Adriano B. L. Tort, Pablo Torterolo, Nicolás Rubido.

Visualization: Joaquín González.

Writing – original draft: Joaquín González, Nicolás Rubido.

Writing – review & editing: Joaquín González, Matias Cavelli, Adriano B. L. Tort, Pablo Torterolo, Nicolás Rubido.

References

1. Koch C., Massimini M., Boly M. & Tononi G. Neural correlates of consciousness: progress and problems. Nat Rev Neurosci. 17, 307–321 (2016,5) https://doi.org/10.1038/nrn.2016.22 PMID: 27094080
2. Dement W. & Kleitman N. The relation of eye movements during sleep to dream activity: an objective method for the study of dreaming. J Exp Psychol. 53, 339–346 (1957,5) https://doi.org/10.1037/h0048189 PMID: 13428941
3. Siclari F., Baird B., Perogamvros L., Bernardi G., LaRocque J., Riedner B., et al. The neural correlates of dreaming. Nat Neurosci. 20, 872–878 (2017,6) https://doi.org/10.1038/nn.4545 PMID: 28394322
4. Ouyang G., Dang C., Richards D. & Li X. Ordinal pattern based similarity analysis for EEG recordings. Clin Neurophysiol. 121, 694–703 (2010,5) https://doi.org/10.1016/j.clinph.2009.12.030 PMID: 20097130

5. Nicolaou N. & Georgiou J. The use of permutation entropy to characterize sleep electroencephalograms. Clin EEG Neurosci. 42, 24–28 (2011,1) https://doi.org/10.1177/155005941104200107 PMID: 21309439

6. Abásolo D., Simons S., Silva R., Tononi G. & Vyazovskiy V. Lempel-Ziv complexity of cortical activity during sleep and waking in rats. J Neurophysiol. 113, 2742–2752 (2015,4) https://doi.org/10.1152/jn.00575.2014 PMID: 25717159

7. Schartner M., Pigorini A., Gibbs S., Arnulfo G., Sarasso S., Barnett L., et al. Global and local complexity of intracranial EEG decreases during NREM sleep. *Neurosci Conscious*. 2017, niw022 (2017) https://doi.org/10.1093/nc/niw022 PMID: 30042832

8. Bandt C.A New Kind of Permutation Entropy Used to Classify Sleep Stages from Invisible EEG Microstructure. *Entropy*. 19 (2017), https://www.mdpi.com/1099-4300/19/5/197 https://doi.org/10.3390/e19050197

9. González J., Cavelli M., Mondino A., Pascovich C., Castro-Zaballa S., Torterolo P. et al. Decreased electrocortical temporal complexity distinguishes sleep from wakefulness. *Sci Rep*. 9, 18457 (2019,12) https://doi.org/10.1038/s41598-019-54788-6 PMID: 31804569

10. González J., Cavelli M., Mondino A., Pascovich C., Castro-Zaballa S., Torterolo P. et al. Electrocortical temporal complexity during wakefulness and sleep: an updated account. *Sleep Science*. (2020).

11. Hou F., Zhang L., Qin B., Gaggioni G., Liu X. & Vandewalle G. Changes in EEG permutation entropy in the evening and in the transition from wake to sleep. *Sleep*. 44 (2021,4) https://doi.org/10.1093/sleep/zsaa226 PMID: 33159205

12. Mondino A., Hambrecht-Wiedbusch V., Li D., York A., Pal D., González J., et al. Glutamatergic Neurons in the Preoptic Hypothalamus Promote Wakefulness, Destabilize NREM Sleep, Suppress REM Sleep, and Regulate Cortical Dynamics. J Neurosci. 41, 3462–3478 (2021,4) https://doi.org/10.1523/JNEUROSCI.2718-20.2021 PMID: 33664133

13. Mateos D., Gómez-Ramírez J. & Rosso O. Using time causal quantifiers to characterize sleep stages. *Chaos, Solitons & Fractals*. 146 pp. 110798 (2021), https://www.sciencedirect.com/science/article/pii/S0960077921001508 https://doi.org/10.1016/j.chaos.2021.110798

14. Sarasso S., Casali A., Casarotto S., Rosanova M., Sinigaglia C. & Massimini M. Consciousness and complexity: a consilience of evidence. *Neuroscience Of Consciousness*. (2021,8), https://doi.org/10.1093/nc/niab023, niab023

15. González J., Mateos D., Cavelli M., Mondino A., Pascovich C., Torterolo P. et al. Low frequency oscillations drive EEG's complexity changes during wakefulness and sleep. *Neuroscience*. 494 pp. 1–11 (2022), https://www.sciencedirect.com/science/article/pii/S0306452222002214 https://doi.org/10.1016/j.neuroscience.2022.04.025 PMID: 35533963

16. Jordan D., Stockmanns G., Kochs E., Pilge S. & Schneider G. Electroencephalographic order pattern analysis for the separation of consciousness and unconsciousness: an analysis of approximate entropy, permutation entropy, recurrence rate, and phase coupling of order recurrence plots. Anesthesiology. 109, 1014–1022 (2008,12) https://doi.org/10.1097/ALN.0b013e31818d6c55 PMID: 19034098

17. Sitt J., King J., El Karoui I., Rohaut B., Faugeras F., Gramfort A., et al. Large scale screening of neural signatures of consciousness in patients in a vegetative or minimally conscious state. Brain. 137, 2258–2270 (2014,8) https://doi.org/10.1093/brain/awu141 PMID: 24919971

18. Sarasso S., Boly M., Napolitani M., Gosseries O., Charland-Verville V., Casarotto S., et al. Consciousness and Complexity during Unresponsiveness Induced by Propofol, Xenon, and Ketamine. Curr Biol. 25, 3099–3105 (2015,12) https://doi.org/10.1016/j.cub.2015.10.014 PMID: 26752078

19. Fagerholm E., Scott G., Shew W., Song C., Leech R., Knöpfel T. et al. Cortical Entropy, Mutual Information and Scale-Free Dynamics in Waking Mice. Cereb Cortex. 26, 3945–3952 (2016,10) https://doi.org/10.1093/cercor/bhw200 PMID: 27384059

20. Varley T., Sporns O., Puce A. & Beggs J. Differential effects of propofol and ketamine on critical brain dynamics. *PLoS Comput Biol*. 16, e1008418 (2020,12) https://doi.org/10.1371/journal.pcbi.1008418 PMID: 33347455

21. Varley T., Denny V., Sporns O. & Patania A. Topological analysis of differential effects of ketamine and propofol anaesthesia on brain dynamics. *R Soc Open Sci*. 8, 201971 (2021,6) https://doi.org/10.1098/rsos.201971 PMID: 34168888

22. Dasilva M., Camassa A., Navarro-Guzman A., Pazienti A., Perez-Mendez L., Zamora-López G., et al. Modulation of cortical slow oscillations and complexity across anesthesia levels. *Neuroimage*. 224 pp. 117415 (2021,1) https://doi.org/10.1016/j.neuroimage.2020.117415 PMID: 33011419

23. Liang Y., Liang J., Song C., Liu M., Pfel T., Gong P. et al. Complexity of cortical wave patterns of the wake mouse cortex. *Nat Commun*. 14, 1434 (2023,3) https://doi.org/10.1038/s41467-023-37088-6 PMID: 36918572

24. Steriade M., Nuñez A. & Amzica F. 1 Hz) neocortical oscillation and other sleep rhythms of the electroencephalogram. J Neurosci. 13, 3266–3283 (1993,8) https://doi.org/10.1523/JNEUROSCI.13-08-03266.1993 PMID: 8340807

25. Isomura Y., Sirota A., Ozen S., Montgomery S., Mizuseki K., Henze D. et al. Integration and segregation of activity in entorhinal-hippocampal subregions by neocortical slow oscillations. Neuron. 52, 871–882 (2006,12) https://doi.org/10.1016/j.neuron.2006.10.023 PMID: 17145507

26. Vyazovskiy V., Olcese U., Lazimy Y., Faraguna U., Esser S., Williams J. et al. Cortical firing and sleep homeostasis. Neuron. 63, 865–878 (2009,9) https://doi.org/10.1016/j.neuron.2009.08.024 PMID: 19778514

27. Cash S., Halgren E., Dehghani N., Rossetti A., Thesen T., Wang C. et al. The human K-complex represents an isolated cortical down-state. Science. 324, 1084–1087 (2009,5) https://doi.org/10.1126/science.1169626 PMID: 19461004

28. Nir Y., Staba R., Andrillon T., Vyazovskiy V., Cirelli C., Fried I. et al. Regional slow waves and spindles in human sleep. Neuron. 70, 153–169 (2011,4) https://doi.org/10.1016/j.neuron.2011.02.043 PMID: 21482364

29. Todorova R. & Zugaro M. Isolated cortical computations during delta waves support memory consolidation. Science. 366, 377–381 (2019,10) https://doi.org/10.1126/science.aay0616 PMID: 31624215

30. Massimini M., Huber R., Ferrarelli F., Hill S. & Tononi G. The sleep slow oscillation as a traveling wave. J Neurosci. 24, 6862–6870 (2004,8) https://doi.org/10.1523/JNEUROSCI.1318-04.2004 PMID: 15295020

31. Vyazovskiy V., Olcese U., Hanlon E., Nir Y., Cirelli C. & Tononi G. Local sleep in awake rats. Nature. 472, 443–447 (2011,4) https://doi.org/10.1038/nature10009 PMID: 21525926

32. Pigorini A., Sarasso S., Proserpio P., Szymanski C., Arnulfo G., Casarotto S. et al. Bistability breaks-off deterministic responses to intracortical stimulation during non-REM sleep. Neuroimage. 112 pp. 105–113 (2015,5) https://doi.org/10.1016/j.neuroimage.2015.02.056 PMID: 25747918

33. Cavelli M., Mao R., Findlay G., Driessen K., Bugnon T., Tononi G. et al. Sleep/wake changes in perturbational complexity in rats and mice. *IScience*. 26, 106186 (2023), https://www.sciencedirect.com/science/article/pii/S2589004223002638 https://doi.org/10.1016/j.isci.2023.106186 PMID: 36895652

34. Claar L., Rembado I., Kuyat J., Russo S., Marks L., Olsen S. et al. Cortico-thalamo-cortical interactions modulate electrically evoked EEG responses in mice. *ELife*. (2023,2), https://doi.org/10.7554/elife.84630.1 PMID: 37358562

35. Levenstein D., Buzsáki G. & Rinzel J. NREM sleep in the rodent neocortex and hippocampus reflects excitable dynamics. *Nat Commun*. 10, 2478 (2019,6) https://doi.org/10.1038/s41467-019-10327-5 PMID: 31171779

36. Destexhe A., Hughes S., Rudolph M. & Crunelli V. Are corticothalamic 'up' states fragments of wakefulness?. *Trends In Neurosciences*. 30, 334–342 (2007), https://www.sciencedirect.com/science/article/pii/S0166223607001002, July INMED/TINS special issue—Physiogenic and pathogenic oscillations: the beauty and the beast https://doi.org/10.1016/j.tins.2007.04.006 PMID: 17481741

37. Mochol G., Hermoso-Mendizabal A., Sakata S., Harris K. & Rocha J. Stochastic transitions into silence cause noise correlations in cortical circuits. Proceedings Of The National Academy Of Sciences. 112, 3529–3534 (2015) https://doi.org/10.1073/pnas.1410509112

38. Torres D., Makarova J., Ortuño T., Benito N., Makarov V. A., & Herreras O. (2019). Local and volume-conducted contributions to cortical field potentials. *Cerebral Cortex*, 29(12), 5234–5254. https://doi.org/10.1093/cercor/bhz061 PMID: 30941394

39. Buzsáki G., Anastassiou C. & Koch C. The origin of extracellular fields and currents–EEG, ECoG, LFP and spikes. Nat Rev Neurosci. 13, 407–420 (2012,5) https://doi.org/10.1038/nrn3241 PMID: 22595786

40. Pincus S.Approximate entropy as a measure of system complexity. Proc Natl Acad Sci U S A. 88, 2297–2301 (1991,3) https://doi.org/10.1073/pnas.88.6.2297 PMID: 11607165

41. Bandt C. & Pompe B. Permutation entropy: a natural complexity measure for time series. *Physical Review Letters*. 88, 174102 (2002) https://doi.org/10.1103/PhysRevLett.88.174102 PMID: 12005759

42. Lempel A. & Ziv J. On the complexity of finite sequences. IEEE Transactions On Information Theory. 22, 75–81 (1976) https://doi.org/10.1109/TIT.1976.1055501

43. Beggs J. & Plenz D. Neuronal avalanches in neocortical circuits. J Neurosci. 23, 11167–11177 (2003,12) https://doi.org/10.1523/JNEUROSCI.23-35-11167.2003 PMID: 14657176

44. Ribeiro T., Copelli M., Caixeta F., Belchior H., Chialvo D., Nicolelis M. et al. Spike avalanches exhibit universal dynamics across the sleep-wake cycle. *PLoS One*. 5, e14129 (2010,11) https://doi.org/10.1371/journal.pone.0014129 PMID: 21152422

45. Fontenele A., Vasconcelos N., Feliciano T., Aguiar L., Soares-Cunha C., Coimbra B. et al. Criticality between Cortical States. *Phys Rev Lett*. 122, 208101 (2019,5) https://doi.org/10.1103/PhysRevLett.122.208101 PMID: 31172737

46. Ponce-Alvarez A., Jouary A., Privat M., Deco G. & Sumbre G. Whole-Brain Neuronal Activity Displays Crackling Noise Dynamics. Neuron. 100, 1446–1459 (2018,12) https://doi.org/10.1016/j.neuron.2018.10.045 PMID: 30449656

47. Bellay T., Klaus A., Seshadri S. & Plenz D. Irregular spiking of pyramidal neurons organizes as scale-invariant neuronal avalanches in the awake state. *Elife*. 4 pp. e07224 (2015,7) https://doi.org/10.7554/eLife.07224 PMID: 26151674

48. Priesemann V., Munk M. & Wibral M. Subsampling effects in neuronal avalanche distributions recorded in vivo. BMC Neuroscience. 10, 1–20 (2009) https://doi.org/10.1186/1471-2202-10-40

49. Priesemann V., Valderrama M., Wibral M. & Le Van Quyen M. Neuronal avalanches differ from wakefulness to deep sleep–evidence from intracranial depth recordings in humans. *PLoS Comput Biol*. 9, e1002985 (2013) https://doi.org/10.1371/journal.pcbi.1002985 PMID: 23555220

50. Priesemann V., Wibral M., Valderrama M., Pröpper R., Le Van Quyen M., Geisel T., et al. Spike avalanches in vivo suggest a driven, slightly subcritical brain state. *Frontiers In Systems Neuroscience*. 8 pp. 108 (2014) https://doi.org/10.3389/fnsys.2014.00108 PMID: 25009473

51. Carvalho T., Fontenele A., Girardi-Schappo M., Feliciano T., Aguiar L., Silva T., et al. Subsampled Directed-Percolation Models Explain Scaling Relations Experimentally Observed in the Brain. *Front Neural Circuits*. 14 pp. 576727 (2020) https://doi.org/10.3389/fncir.2020.576727 PMID: 33519388

52. Mashour G., Roelfsema P., Changeux J. & Dehaene S. Conscious Processing and the Global Neuronal Workspace Hypothesis. *Neuron*. 105, 776–798 (2020), https://www.sciencedirect.com/science/article/pii/S0896627320300520 https://doi.org/10.1016/j.neuron.2020.01.026 PMID: 32135090

53. Chaudhuri R., Gerçek B., Pandey B., Peyrache A. & Fiete I. The intrinsic attractor manifold and population dynamics of a canonical cognitive circuit across waking and sleep. Nat Neurosci. 22, 1512–1520 (2019,9) https://doi.org/10.1038/s41593-019-0460-x PMID: 31406365

54. Valero M., Viney T., Machold R., Mederos S., Zutshi I., Schuman B., et al. Sleep down state-active ID2/Nkx2. 1 interneurons in the neocortex. *Nature Neuroscience*. 24, 401–411 (2021) https://doi.org/10.1038/s41593-021-00797-6 PMID: 33619404

55. Lendner J., Helfrich R., Mander B., Romundstad L., Lin J., Walker M., et al. An electrophysiological marker of arousal level in humans. *Elife*. 9 (2020,7) https://doi.org/10.7554/eLife.55092 PMID: 32720644

56. Colombo M., Napolitani M., Boly M., Gosseries O., Casarotto S., Rosanova M., et al. The spectral exponent of the resting EEG indexes the presence of consciousness during unresponsiveness induced by propofol, xenon, and ketamine. Neuroimage. 189 pp. 631–644 (2019,4) https://doi.org/10.1016/j.neuroimage.2019.01.024 PMID: 30639334

57. D'Andola M., Rebollo B., Casali A., Weinert J., Pigorini A., Villa R., et al. Bistability, Causality, and Complexity in Cortical Networks: An In Vitro Perturbational Study. Cereb Cortex. 28, 2233–2242 (2018,7) https://doi.org/10.1093/cercor/bhx122 PMID: 28525544

58. Rosanova M., Fecchio M., Casarotto S., Sarasso S., Casali A., Pigorini A., et al. Sleep-like cortical OFF-periods disrupt causality and complexity in the brain of unresponsive wakefulness syndrome patients. *Nat Commun*. 9, 4427 (2018,10) https://doi.org/10.1038/s41467-018-06871-1 PMID: 30356042

59. Chialvo D.Emergent complex neural dynamics. Nature Physics. 6 pp. 744–750 (2010) https://doi.org/10.1038/nphys1803

60. Kinouchi O. & Copelli M. Optimal dynamical range of excitable networks at criticality. Nature Physics. 2 pp. 348–351 (2006) https://doi.org/10.1038/nphys289

61. Meisel C., Olbrich E., Shriki O. & Achermann P. Fading signatures of critical brain dynamics during sustained wakefulness in humans. J Neurosci. 33, 17363–17372 (2013,10) https://doi.org/10.1523/JNEUROSCI.1516-13.2013 PMID: 24174669

62. Scott G., Fagerholm E., Mutoh H., Leech R., Sharp D., Shew W. et al. Voltage imaging of waking mouse cortex reveals emergence of critical neuronal dynamics. J Neurosci. 34, 16611–16620 (2014,12) https://doi.org/10.1523/JNEUROSCI.3474-14.2014 PMID: 25505314

63. Steriade M., Timofeev I. & Grenier F. Natural waking and sleep states: a view from inside neocortical neurons. J Neurophysiol. 85, 1969–1985 (2001,5) https://doi.org/10.1152/jn.2001.85.5.1969 PMID: 11353014

64. Funk C., Peelman K., Bellesi M., Marshall W., Cirelli C. & Tononi G. Role of Somatostatin-Positive Cortical Interneurons in the Generation of Sleep Slow Waves. J Neurosci. 37, 9132–9148 (2017,9) https://doi.org/10.1523/JNEUROSCI.1303-17.2017 PMID: 28821651

65. Hay Y., Deperrois N., Fuchsberger T., Quarrell T., Koerling A. & Paulsen O. Thalamus mediates neocortical Down state transition via GABAB-receptor-targeting interneurons. *Neuron*. (2021) https://doi.org/10.1016/j.neuron.2021.06.030

66. Buzsáki G. Hippocampal sharp wave-ripple: A cognitive biomarker for episodic memory and planning. Hippocampus. 25, 1073–1188 (2015,10) https://doi.org/10.1002/hipo.22488 PMID: 26135716

67. Timme N., Marshall N., Bennett N., Ripp M., Lautzenhiser E. & Beggs J. Criticality Maximizes Complexity in Neural Tissue. *Front Physiol*. 7 pp. 425 (2016) https://doi.org/10.3389/fphys.2016.00425 PMID: 27729870

68. Tononi G. & Edelman G. Consciousness and complexity. Science. 282, 1846–1851 (1998,12) https://doi.org/10.1126/science.282.5395.1846 PMID: 9836628

69. Pal D., Li D., Dean J., Brito M., Liu T., Fryzel A., et al. Level of Consciousness Is Dissociable from Electroencephalographic Measures of Cortical Connectivity, Slow Oscillations, and Complexity. J Neurosci. 40, 605–618 (2020,1) https://doi.org/10.1523/JNEUROSCI.1910-19.2019 PMID: 31776211

70. Watson B., Levenstein D., Greene J., Gelinas J. & Buzsáki G. Network Homeostasis and State Dynamics of Neocortical Sleep. Neuron. 90, 839–852 (2016,5) https://doi.org/10.1016/j.neuron.2016.03.036 PMID: 27133462

71. Grosmark A. & Buzsáki G. Diversity in neural firing dynamics supports both rigid and learned hippocampal sequences. Science. 351, 1440–1443 (2016,3) https://doi.org/10.1126/science.aad1935 PMID: 27013730

72. Grosmark A., Mizuseki K., Pastalkova E., Diba K. & Buzsáki G. REM sleep reorganizes hippocampal excitability. Neuron. 75, 1001–1007 (2012,9) https://doi.org/10.1016/j.neuron.2012.08.015 PMID: 22998869

73. Eckmann J., Kamphorst S. & Ruelle D. Recurrence Plots of Dynamical Systems. EPL. 4 pp. 973–977 (1987) https://doi.org/10.1209/0295-5075/4/9/004

74. Marwan N., Carmen Romano M., Thiel M. & Kurths J. Recurrence plots for the analysis of complex systems. *Physics Reports*. 438, 237–329 (2007), https://www.sciencedirect.com/science/article/pii/S0370157306004066 https://doi.org/10.1016/j.physrep.2006.11.001

75. Pitsik E., Frolov N., Hauke Kraemer K., Grubov V., Maksimenko V., Kurths J. et al. Motor execution reduces EEG signals complexity: Recurrence quantification analysis study. *Chaos: An Interdisciplinary Journal Of Nonlinear Science*. 30, 023111 (2020), https://doi.org/10.1063/1.5136246

76. Povysheva N., Gonzalez-Burgos G., Zaitsev A., Kröner S., Barrionuevo G., Lewis D. et al. Properties of excitatory synaptic responses in fast-spiking interneurons and pyramidal cells from monkey and rat prefrontal cortex. Cereb Cortex. 16, 541–552 (2006,4) https://doi.org/10.1093/cercor/bhj002 PMID: 16033926

77. Shannon C.A mathematical theory of communication. The Bell System Technical Journal. 27, 379–423 (1948) https://doi.org/10.1002/j.1538-7305.1948.tb00917.x

78. Donoghue T., Haller M., Peterson E., Varma P., Sebastian P., Gao R. et al. Parameterizing neural power spectra into periodic and aperiodic components. Nat Neurosci. 23, 1655–1665 (2020,12) https://doi.org/10.1038/s41593-020-00744-x PMID: 33230329

Bridging the scales through the analysis of neural complexity

Bridging scales with complexity

Joaquín González[1,2*], Nicolas Rubido[3], Ignacio Carrera[4], Alejandra Mondino[5], Giancarlo Vanini[6,7], & Pablo Torterolo[1]

1 – Departamento de Fisiología, Facultad de Medicina, Universidad de la República, Montevideo, 11800, Uruguay.

2 – Brain Institute, Federal University of Rio Grande do Norte, Natal, RN 59056, Brazil.

3 – Departamento de Química Orgánica, Facultad de Química, Universidad de la República, Montevideo, 11200, Uruguay.

4 – University of Aberdeen, King's College, Institute for Complex Systems and Mathematical Biology, Aberdeen, United Kingdom.

5 – Department of Clinical Sciences, College of Veterinary Medicine, North Carolina State University, Raleigh, NC, 27606, USA.

6 – Department of Anesthesiology, University of Michigan, Ann Arbor, Michigan 48109-5615.

7 – Center for Consciousness Science, University of Michigan, Ann Arbor, Michigan 48109.

* Correspondence: joaqgonzar@gmail.com

Abstract

Understanding brain activity across multiple scales is essential for unraveling the complexities of neural function. From the macroscopic to the microscopic level, the brain exhibits diverse dynamics, shaped by billions of neurons and their intricate synaptic connections. However, navigating across these scales presents significant challenges due to technical and conceptual limitations. Complexity analysis provides a promising framework to address these challenges, offering insights into how neural activity spans across scales and how alterations, such as those induced by drugs, impact brain function. This article explores the use of complexity analysis to study brain activity, emphasizing its role in navigating neural scales and elucidating the intricate relationship between microscopic neuronal dynamics and macroscopic brain function. Through this perspective, we aim to foster a deeper understanding of brain complexity and its implications for neuroscience research.

Keywords: EEG, LFP, sleep, REM, ibogaine, urethane, entropy

Introduction

A multitude of scales characterizes brain activity (Buzsáki, 2004; He and Raichle, 2009; Lewis et al., 2024, 2015). The brain comprises billions of neurons, each with thousands of synaptic connections, forming a vast and interconnected network (Binzegger et al., 2004; He and Raichle, 2009; Sporns et al., 2005). As a result, brain activity encompasses a myriad of scales ranging from the macroscopic to the microscopic (Fig. 1A). At the macroscopic level,

the activity of the different brain areas can be studied through the lens of functional magnetic resonance imaging (fMRI) (He and Raichle, 2009; Ogawa et al., 1990) or electroencephalography (EEG) (Berger, 1929; Biasiucci et al., 2019), capturing the collective dynamics of large populations of neurons. At the mesoscale level, we encounter neuronal circuits, where diverse groups of neurons give rise to intricate networks that allow specific computations to occur (Buzsáki et al., 2012; Buzsáki and Wang, 2012; Douglas and Martin, 2004; Gonzalez et al., 2023; Luo, 2021). These networks are usually studied through local field potentials (LFP) (Herreras, 2016) and calcium imaging (Tian et al., 2009). Finally, at the microscopic scale, the firing patterns of individual neurons can be studied through patch-clamp recordings (Sakmann and Neher, 1984) or multi-electrode arrays (Jun et al., 2017). These techniques allow us to study how the precise timing and frequency of the spike trains encodes the basic information employed for diverse computations across scales.

Navigating across the neural scales is a hard problem (Bohara et al., 2018; Gao and Ganguli, 2015; Huang et al., 2021; Munn et al., 2023; Paninski and Cunningham, 2018; Scholtens and van den Heuvel, 2018; Sejnowski et al., 2014; Williamson et al., 2019). The difficulties arise from both technical and conceptual limitations, hindering our ability to connect observations across different levels of analysis. While whole-brain imaging modalities like fMRI offer excellent spatial resolution, they often lack the temporal resolution necessary to capture the rapid dynamics of individual neurons firing. Conversely, electrophysiological methods excel in recording the millisecond-scale temporal dynamics of neuronal activity but are constrained by their limited spatial coverage, typically focusing on small populations of neurons or even single cells. Noteworthy, novel optical methods, such as calcium or voltage imaging, promise to offer both high spatial and temporal resolution (Abdelfattah et al., 2019; Grinvald and Hildesheim, 2004; Stringer et al., 2019a, 2019b), but these methods are still not as widely employed in research and clinical context as the abovementioned ones.

Moreover, the brain operates through a hierarchical organization of interconnected circuits, where information is processed and integrated across multiple levels (Friston, 2005; Kiebel et al., 2008). Therefore, to fully understand the brain, one needs to know how changes in activity at the level of individual neurons translates into emergent phenomena at the level of neural circuits, and whole-brain dynamics. Furthermore, the dynamic nature of brain activity adds another layer of complexity. Neural activity is highly context-dependent, influenced by factors such as behavioral state, sensory input, and neuromodulatory signals (Adamantidis et al., 2007; Lee and Dan, 2012; Nir and de Lecea, 2023; Steinmetz et al., 2019; Stringer et al., 2019a, 2019b). Integrating these dynamic factors across scales presents a significant challenge, as the relationship between neural activity and behavior can be nonlinear and multifaceted.

In this article, we will offer a perspective on how the analysis of neural complexity offers a novel approach to studying brain activity across different scales. The text will be organized as follows: 1) We provide an overview of brain activity at different scales.
2) We demonstrate how the analysis of neural complexity enables navigation across these scales. 3) We present an example of how psychedelic and anesthetic drugs affect neural complexity. 4) We provide a proof-of-concept illustrating how changes at the microscopic scale can impact the macroscopic scale.

Main text

Brain patterns occur simultaneously at different temporal and spatial scales

Neural oscillations span a wide range of frequencies (Fig. 1B). Brain rhythms, observed for instance through ECoG (electrocorticography) and LFP recordings, span from slow delta waves (0.5-4 Hz), prominent during deep Non-REM sleep or slow wave sleep (SWS) (Massimini et al., 2004), to faster gamma oscillations (30-150 Hz), associated during wakefulness with sensory processing and cognitive tasks (Buzsáki and Draguhn, 2004; Buzsáki and Wang, 2012; Fernández-Ruiz et al., 2021; Gonzalez et al., 2023; Tort et al., 2009). Notably, these frequency bands follow a scale-free power-law $P(f) = f^{-\beta}$, with an exponent (β) close to 1 (commonly referred as pink noise or 1/f decay) (Donoghue et al., 2020; González et al., 2023; Lendner et al., 2020; Miller et al., 2009). Note that the power-law behavior can be evidenced and quantified by plotting the power spectrum on a log-log scale and fitting a linear model to the data. This ~ 1/f decay is characteristic of a heavy-tail distribution, i.e., despite the contribution of the different bands decreasing with the frequency, high-frequency activity still contributes significantly to the field signal. Moreover, it is important to point out that frequency ranges (which delimit the frequency bands) increase as we move from the low to the high end of the spectrum (Buzsáki and Draguhn, 2004; González et al., 2020; Mondino et al., 2020), making the contribution of each band more similar in the overall recorded signal.

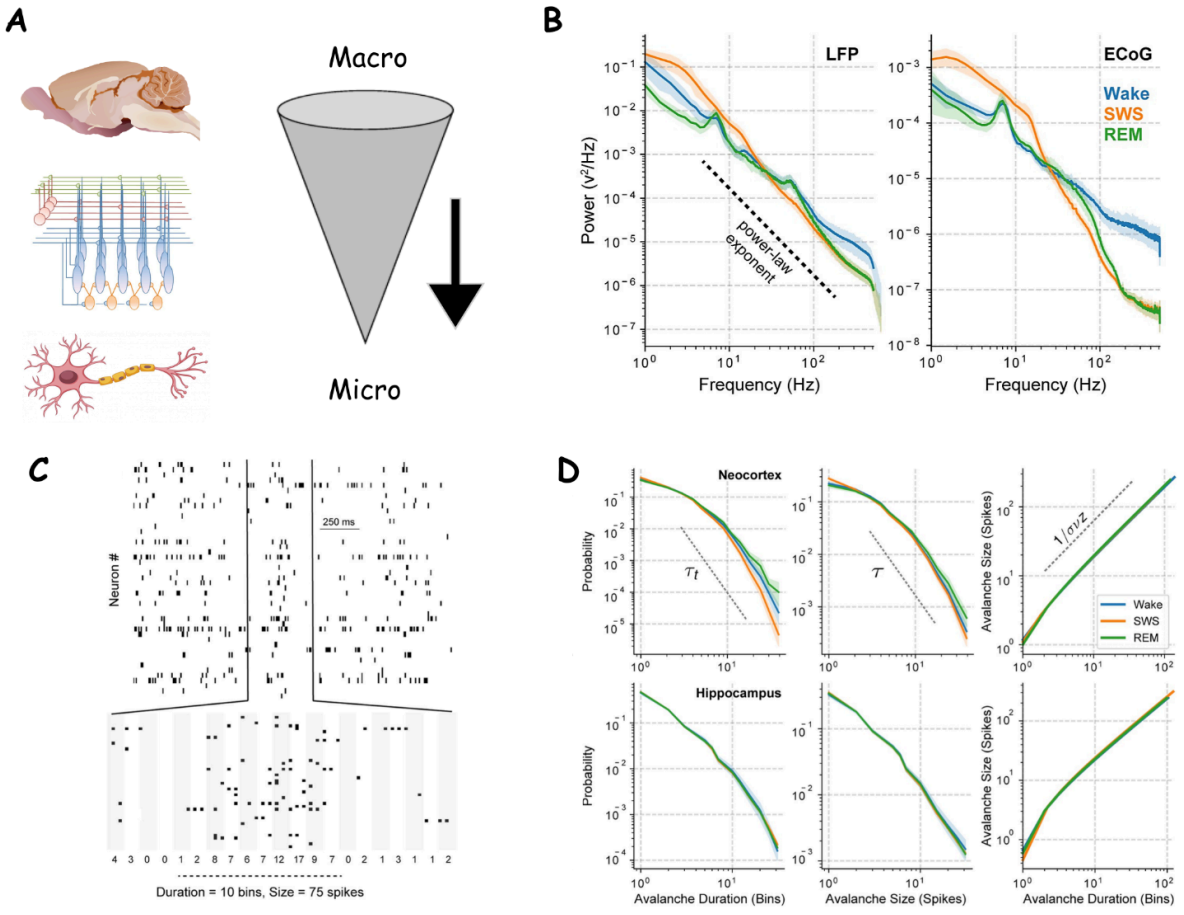

Figure 1. Different neural scales characterize brain activity. A Schematic representation of the different brain scales, from the macroscopic scale (the brain as an organ) to the mesoscopic (neural circuits in different brain areas) and to the microscopic (individual neurons). The brain image was obtained from https://neuroscience-graphicdesign.com/, the neural circuit was reproduced from (Stern et al., 2018), and the neuron was taken from Freepik.com. **B** LFP [ECoG] power spectrum from the frontal cortex [M1 cortex] during the states of Wake, SWS and REM sleep. The mean and its corresponding 95% confidence intervals are shown for each plot. **C** Example of a neuronal avalanche. The average inter-spike interval ISI is used to bin the raster plot (shaded rectangles), and the number of spikes per bin was counted. **D** Avalanche statistics for the neocortex (top) and hippocampus (bottom). Left: Distribution of avalanche duration. Middle: distribution of avalanche size. Right: avalanche size as a function of its duration. For each state (color coded), the mean distributions are shown in solid lines with a shaded area depicting the 95% confidence interval. Modified from (González et al., 2023).

Spiking activity in the brain also spans a wide temporal range (Fig. 1C). An example of this phenomena are neural avalanches, which describe spontaneous bursts of activity that propagate through neural networks, akin to the cascading effect of falling snowflakes in an avalanche (Beggs and Plenz, 2003; Bellay et al., 2015; Ribeiro et al., 2010). A neuronal avalanche starts after a time bin without spikes and finishes when another empty time bin is reached; these avalanches can occur at various temporal scales, from milliseconds to seconds (Fig. 1D), and involve the synchronized firing of large ensembles of neurons. Notably, avalanches exhibit scale-invariant properties, meaning that their size and duration distributions also behave as power-laws (Fig. 1D). Altogether, this scale-free behavior in oscillatory and spiking activity suggests that the brain operates near a critical point (Chialvo, 2010; Fontenele et al., 2019; Priesemann et al., 2014, 2013), where small perturbations can trigger large-scale cascades of activity, facilitating efficient information processing and integration.

Navigating the cortical scales by studying neural complexity

The previous section showed how brain activity (oscillations and spikes) exhibits a wide temporal arrangement and can be described by power-laws. This type of scaling often emerges in complex systems (Barabasi and Albert, 1999). Therefore, different tools have been devised over the decades to directly quantify the complexity of a system (Bandt and Pompe, 2002; Casali et al., 2013; Massimini et al., 2005; Tononi et al., 1994). In this section, we are going to show that by measuring neural complexity, it is possible to distinguish brain states across different recording scales.

Defining neural complexity can be a daunting challenge. Measuring it, on the other hand, often boils down to computing an entropy measure (e.g., permutation entropy, sample entropy, etc.) on a given brain activity time-series (Fig. 2). For instance, permutation entropy works by first converting the original time series into a sequence of ordinal patterns based on the relative ordering of data points within a defined window (Bandt and Pompe, 2002). Then, it calculates the probability distribution of these ordinal patterns. The Shannon entropy is then computed from this probability distribution, measuring the average uncertainty or randomness in the sequence of ordinal patterns. A higher permutation entropy value indicates greater complexity or irregularity in the time series, whereas a lower value suggests more regular and predictable behavior. Note that other metrics can also be applied

to a symbolic time-series to obtain complexity estimates, for instance, Lempel-Ziv, which measures data compressibility and often yields similar results to entropy-based measures (González et al., 2023; Lempel and Ziv, 1976; Mateos et al., 2020; Pascovich et al., 2022)

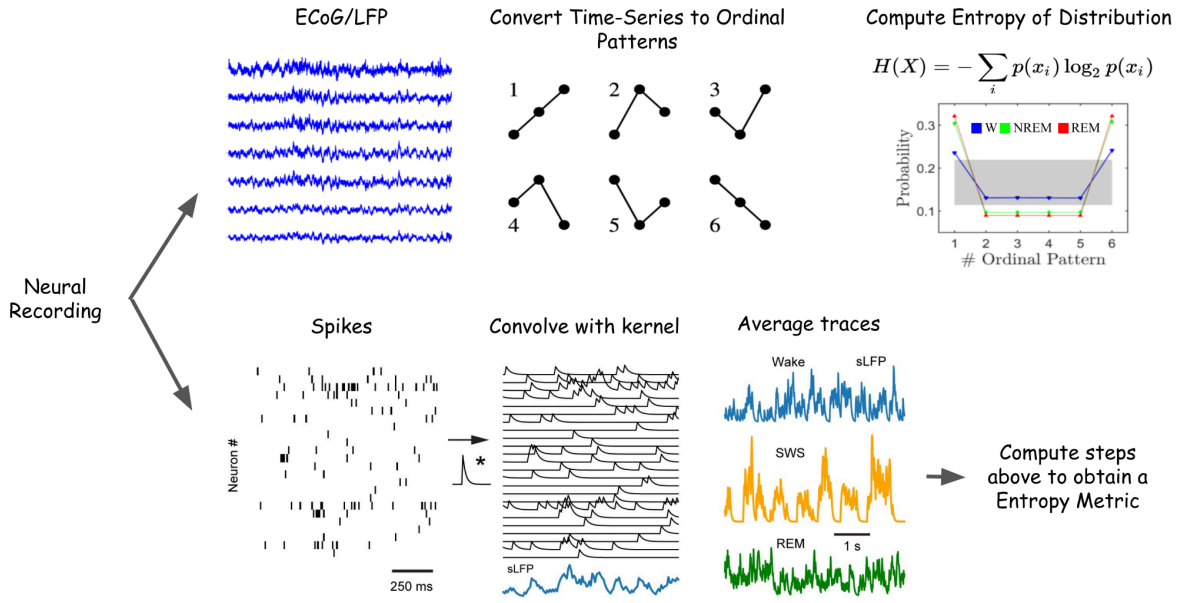

Figure 2. Measuring neural complexity. Top: The left panel shows an ECoG recording during wakefulness in a freely behaving rat. 5 seconds are shown; each trace corresponds to one cortical location. The middle panel exhibits the different possible ordinal patterns that can be obtained employing an embedding dimension = 3. That is all possible relative orderings of a single ECoG recording within a 3-point window. Thus, one transforms a continuous signal into a discrete sequence of ordinal patterns. The right panel shows the distribution of each ordinal pattern in a whole six-hour recording. Each color shows a different sleep state. Note that the purely increasing (1) or decreasing (6) ordinal patterns are the most common ones. The Shannon entropy is then computed from the ordinal pattern distribution. Modified from (González et al., 2019). **Bottom**: This panel shows how to obtain a synthetic LFP (sLFP). The sLFP is defined as the average of the convolutions between spike trains and a decaying exponential function. To the right we show examples of sLFP during Wake, SWS, and REM sleep population activity. The figures were modified from (González et al., 2023).

It is worth mentioning that most of these complexity metrics were developed for analyzing continuous 1-dimensional time-series. However, when dealing with spiking recordings from a neural population, we can transform the discrete, high-dimensional recordings into a 1-dimensional signal (as illustrated in the bottom panel of Figure 2). This transformation can be achieved by convolving the spikes from each neuron with an exponentially decaying kernel, mimicking a postsynaptic potential triggered by each spike. Subsequently, the convolved spikes can be averaged over the population of neurons for each time point, resulting in a synthetic 1-dimensional local field potential (sLFP) suitable for neural complexity analysis. An advantage of this approach is its ability to regulate the sources influencing the field potential, thus mitigating the impact of external variables unrelated to spiking activity, such as EMG contamination and volume-conducted signals (Buzsáki et al., 2012; Torres et al., 2019).

Having defined a way to measure neural complexity in field and spike recordings (Fig. 2), we can now show that this analysis bridges the different neural scales. To this end we compared ECoG (electrocorticography, also referred to as intracranial EEGs), LFPs and sLFPs recordings from frontal areas in freely behaving rats. By focusing on the low-frequency bands (filtering all signals between below 13 Hz), our results suggest that neural complexity differences remains relatively stable within each brain state, regardless of the scale at which it is analyzed (Fig. 3A). In other words, we found that the neural complexity differences across states were robustly maintained in all three recording scales. This result suggests that the intricacy of neural dynamics and its changes across the sleep-wake cycle are preserved across various levels of neuronal organization, from individual ensembles to broader cortical networks.

To gain a deeper understanding of why changes in neural complexity are consistent across different scales, we conducted an analysis of the microscopic (spiking) patterns underlying these changes. Our investigation revealed that periods of reduced firing, known as DOWN states (Isomura et al., 2006; Levenstein et al., 2019; Steriade et al., 1993) or OFF periods (Cavelli et al., 2023; Nir et al., 2011; Vyazovskiy et al., 2009), were responsible for the observed decrease in complexity in both synthetic local field potentials (sLFP) and traditional local field potentials (LFPs) during NREM sleep (Fig. 3B). This finding was evidenced by the observation that the removal of these periods prevented the decrease in complexity during NREM sleep. It is noteworthy that these DOWN states manifested as slow wave activity in LFPs and likely in ECoG recordings as well. Thus, our findings offer valuable insights into the propagation of microscopic activity across different scales.

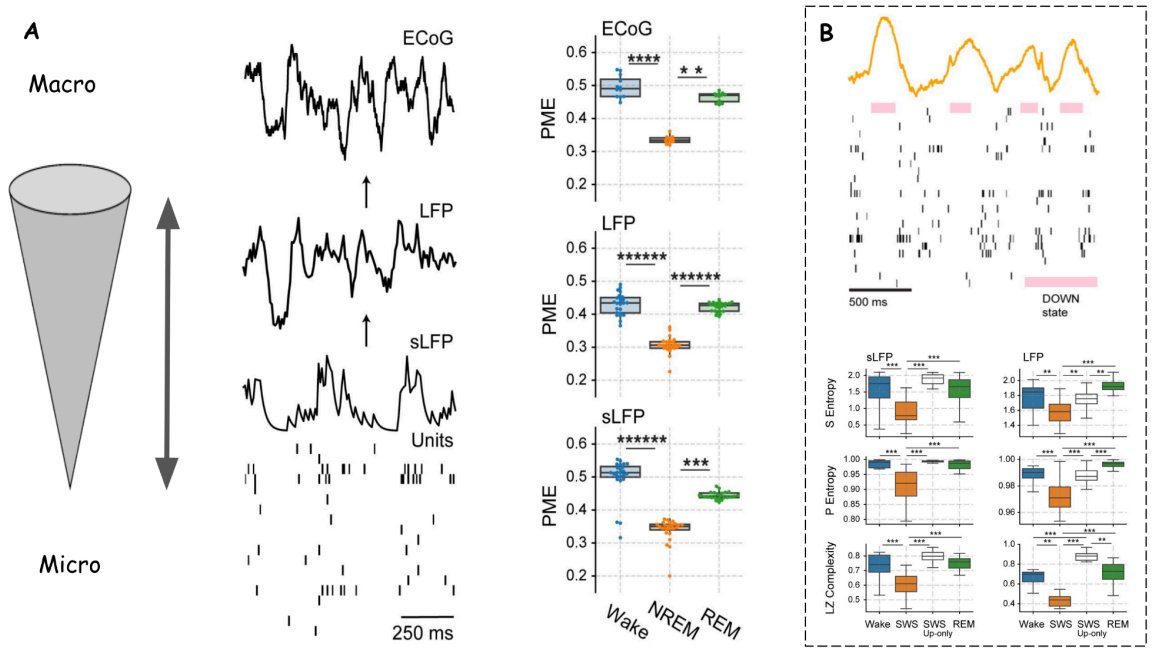

Figure 3. Bridging the scales through the use of complexity metrics. A Permutation Minimum-Entropy (PME) across recording scales. From top to bottom, ECoG, LFP, synthetic LFP (obtained by the convolution of the spike trains and a decreasing exponential kernel), and units (spikes from individual neurons recorded from the extracellular medium). ECoG data comes from our experiments, but the other recordings come from the work by (Watson et al., 2016) (data-set available

at: CRCNS.org). Note that we inverted both LFP and ECoG recordings for representation purposes. Box plots show PME values for the ECoGs, LFPs, and sLFPs data-sets. * Modified from (González et al., 2022). **B Top**: Example of LFP and spiking activity in the neocortex exhibiting DOWN states (shown by pink boxes) during SWS. **Bottom**: Boxplots of Sample Entropy (top), Permutation Entropy (middle), and Lempel-Ziv Complexity (bottom) of the sLFPs and LFPs in each state (N = 24 sessions). *p < 0.05, **p < 0.01, *** = p < 0.001. SWS Up-only was obtained by concatenating SWS UP periods only (excluding all down states). Modified from (González et al., 2023).

Drugs that alter consciousness disrupt neural complexity

In the previous section, we argued that the neural complexity differences between sleep-wake states are conserved across neural scales. To give further biological meaning to this quantity, we will next show that we can externally perturb neural complexity by administering drugs that alter consciousness. Moreover, we are going to argue how studying neural complexity can unveil functional convergence in the action of two unrelated drugs.

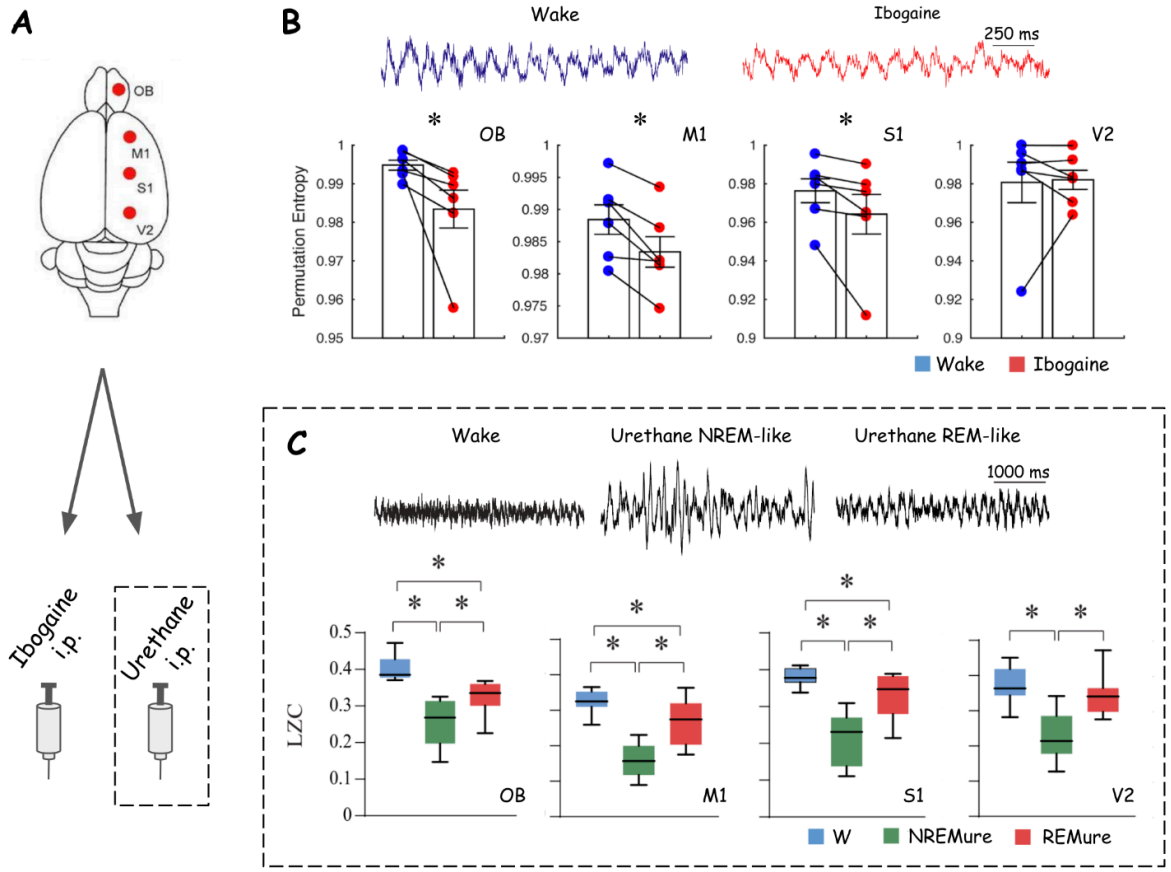

Figure 4. Ibogaine and urethane decrease neural complexity. A. Location of the analyzed intracranial electrodes in the right hemisphere (OB, olfactory bulb; M1, primary motor cortex; S1, primary somatosensory cortex; V2, secondary visual cortex). Either ibogaine (40 mg/Kg) or urethane (1.2-1.5 mg/Kg) were administered intraperitoneally. **B.** Top: Control (blue) and ibogaine (red) wake states (signal downsampled to 256 Hz) are shown. Bottom: Permutation entropy was employed to quantify the ECoG temporal complexity for ibogaine recordings. Each dot shows the average permutation entropy of an animal (n = 6). Bars represent mean ± S.E.M. *p < 0.05, paired t test. **C**. For the urethane experiments, LZC was computed for frequencies between 1 and 195 Hz during wakefulness (W) and the anesthetized states (NREM-like urethane, NREMure; REM-like urethane,

REMure) for each electrode localization in the right hemisphere. * indicates significant differences. Modified from (González et al., 2021) (Mondino et al., 2022).

On one hand, ibogaine, an atypical psychedelic, has gained popularity for its ability to induce long-lasting antiaddictive effects (Köck et al., 2022). However, its mechanisms of action remain incompletely understood and involve several neurotransmitter systems (Mash, 2023), including the action of an active metabolite (Baumann et al., 2000; Castro-Nin et al., 2023). Our findings indicate that systemic administration of ibogaine promotes a waking state characterized by a gamma frequency band (30-100 Hz) profile that resembles REM sleep (González et al., 2021, 2018). On the other hand, urethane is a commonly used anesthetic in animal research, which induces two alternating anesthetic states: NREMure and REMure (Hara and Harris, 2002). Although these states are often used as pharmacological models of sleep (Hay et al., 2021; Pagliardini et al., 2013), they differ significantly from natural sleep states (Mondino et al., 2022). Its mechanisms of action involve a wide array of targets but, unlike ibogaine, ultimately results in unconsciousness.

Crucially, despite the contrasting mechanisms and effects of the drugs (where ibogaine enhances gamma activity while urethane diminishes it), both ibogaine and urethane administration resulted in reduced neural complexity across the brain (Fig. 4). This finding suggests that brain activity becomes less diverse during the acute effects of both drugs. It's worth noting that urethane, especially in the synchronized state (referred to as NREMure in Fig. 4), seemed to induce more pronounced complexity changes compared to ibogaine. Hence, these examples illustrate how two drugs profoundly affecting cognition also disrupt neural complexity.

The way up: how microscopic changes affect global brain states.

Finally, we show by proof of concept how manipulating the microscopic level can impact macroscopic dynamics. These types of experiments and analyses can also help us understand which factors determine and influence neural complexity. For this example, we will see how a specific group of glutamatergic neurons in the preoptic area of the hypothalamus not only controlled sleep state transitions but also neural complexity in each state.

Noteworthy, the preoptic area of the hypothalamus is a crucial site for sleep generation, which projects diffusely into arousal centers across the brain (Vanini and Torterolo, 2021). While it has been historically considered an exclusive sleep promoting center, this notion has been challenged by theoretical models and experimental results. The emergent picture suggests that the preoptic area might play a dual role in sleep-wake control (Lombardi et al., 2020; Mondino et al., 2021; Vanini et al., 2020), initiating (but not maintaining) arousal to possibly prevent undesired REM sleep intrusions into NREM.

For this set of chemogenetic experiments (Mondino et al., 2021), the excitatory cre-dependent designer receptor hM3Dq was injected into the medial-lateral preoptic region of Vglut2-cre animals (Fig. 5A). As a result, only excitatory neurons expressed the designer receptor and could be activated by the systemic injection of a designer drug (in this case clozapine-n-oxide, CNO). When stimulated, this excitatory subgroup induced global state transitions and fragmented sleep. Remarkably, chemogenetic stimulation led to an increase

in neural complexity at the global cortical level (Fig. 5B). This increase in neural complexity occurred irrespective of the arousal state, as significant complexity increases were observed during both wakefulness and NREM sleep. In fact, complexity during NREM following chemogenetic stimulation reached similar levels to the unstimulated wakefulness. Hence, these findings suggest that changes at the microscopic level, such as alterations in the firing rate of a small subpopulation within a deep nucleus, can profoundly impact neural complexity at a different recording scale.

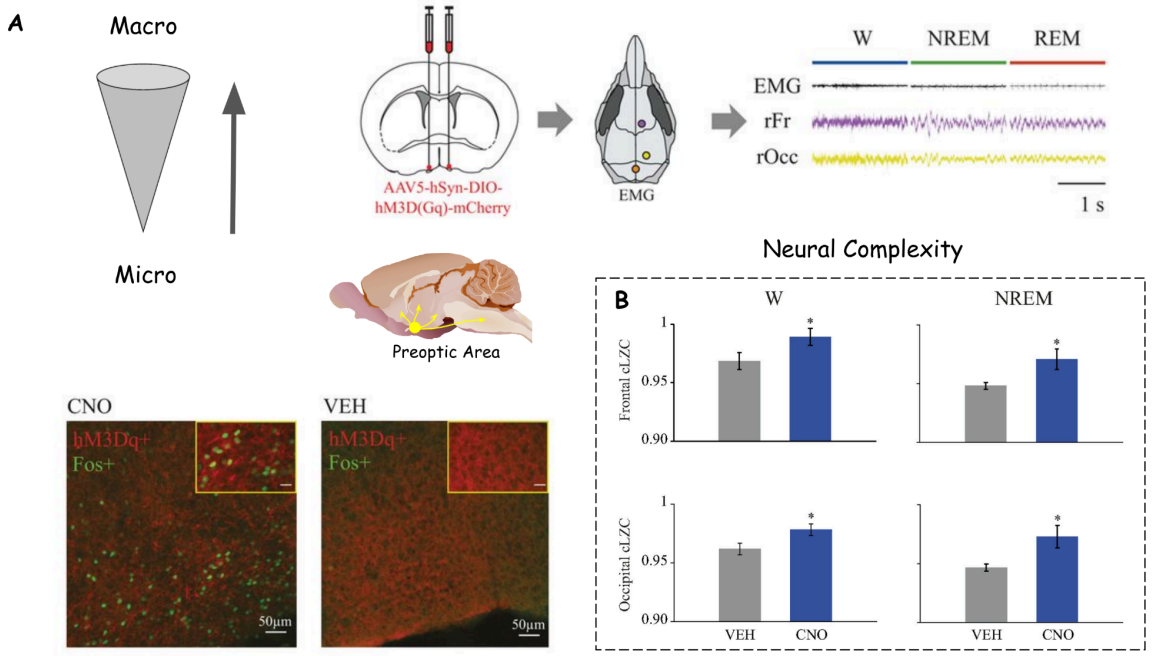

Figure 5. Going up: how microscopic changes affect global brain states. A Schematic representation of bilateral injections of a Cre-dependent adeno-associated virus for expression of the excitatory designer receptor hM3Dq into the medial-lateral preoptic region of Vglut2-Cre mice. Three weeks after the injection, mice were implanted with electrodes for recording the EEG from the right frontal (purple) and right occipital (yellow) cortex. A reference electrode was placed over the cerebellum (orange), and two electrodes were also implanted bilaterally in the neck muscles for recording the EMG. Representative EEG and EMG signals from a mouse during wakefulness, NREM sleep, and REM sleep. Below we show the cFos expression (green nuclei) in mCherry-positive (red) neurons in the medial-lateral preoptic region after CNO (1.0 mg/kg; n = 4 mice) and VEH (n = 4) administration. Brain image was modified from https://neuroscience-graphicdesign.com/. **B** Graphs plot showing neural complexity as assessed by corrected Lempel-Ziv complexity (cLZc) values during wakefulness (W) and NREM sleep for frontal and occipital regions. Data are mean ± SEM. Differences between VEH and CNO (1.0 mg/kg) in n = 10 mice were analyzed by two-tailed paired t tests. *Significant difference ($p < 0.05$) relative to control. Modified from (Mondino et al., 2021).

Conclusions

The brain exhibits activity across multiple scales, from the macroscopic to the microscopic, highlighting its complexity. Complexity analysis offers a novel perspective for studying brain activity across scales. It provides a framework for navigating the intricate dynamics of neural networks, allowing researchers to uncover patterns and emergent phenomena that may not be apparent with traditional analytical approaches. Studying the effects of drugs on neural complexity can offer insights into common mechanisms of action at the macroscopic level.

Finally, understanding how changes at the microscopic scale, such as the firing patterns of individual neurons, affect macroscopic brain activity is crucial for unraveling the mechanisms underlying brain function. Such insights can provide a deeper understanding of how neural circuits process information and generate behavior.

Declarations of interest

All other authors state no conflict of interest.

Author contributions

JG and PT wrote the initial draft. All authors reviewed and edited it. All authors have accepted responsibility for the entire content of this manuscript and approved its submission.

Acknowledgments

This research was supported by the CSIC-I+D grupos 2022- group ID-22620220100148 grant-Uruguay. We also thank Gill Brown for allowing us to reuse his illustration of the brain.

Data availability

The raw original data is available under request to the authors

References

Abdelfattah, A.S., Kawashima, T., Singh, A., Novak, O., Liu, H., Shuai, Y., Huang, Y.-C., Campagnola, L., Seeman, S.C., Yu, J., Zheng, J., Grimm, J.B., Patel, R., Friedrich, J., Mensh, B.D., Paninski, L., Macklin, J.J., Murphy, G.J., Podgorski, K., Lin, B.-J., Chen, T.-W., Turner, G.C., Liu, Z., Koyama, M., Svoboda, K., Ahrens, M.B., Lavis, L.D., Schreiter, E.R., 2019. Bright and photostable chemigenetic indicators for extended in vivo voltage imaging. Science 365, 699–704.

Adamantidis, A.R., Zhang, F., Aravanis, A.M., Deisseroth, K., de Lecea, L., 2007. Neural substrates of awakening probed with optogenetic control of hypocretin neurons. Nature 450, 420–424.

Bandt, C., Pompe, B., 2002. Permutation entropy: a natural complexity measure for time series. Phys. Rev. Lett. 88, 174102.

Barabasi, A.L., Albert, R., 1999. Emergence of scaling in random networks. Science 286, 509–512.

Baumann, M.H., Pablo, J.P., Ali, S.F., Rothman, R.B., Mash, D.C., 2000. Noribogaine (12-hydroxyibogamine): a biologically active metabolite of the antiaddictive drug ibogaine. Ann. N. Y. Acad. Sci. 914, 354–368.

Beggs, J.M., Plenz, D., 2003. Neuronal avalanches in neocortical circuits. J. Neurosci. 23, 11167–11177.

Bellay, T., Klaus, A., Seshadri, S., Plenz, D., 2015. Irregular spiking of pyramidal neurons organizes as scale-invariant neuronal avalanches in the awake state. Elife 4, e07224.

Berger, H., 1929. Über das Elektrenkephalogramm des Menschen. Archiv für Psychiatrie und Nervenkrankheiten 87, 527–570.

Biasiucci, A., Franceschiello, B., Murray, M.M., 2019. Electroencephalography. Curr. Biol. 29, R80–R85.

Binzegger, T., Douglas, R.J., Martin, K.A.C., 2004. A quantitative map of the circuit of cat primary visual cortex. J. Neurosci. 24, 8441–8453.

Bohara, G., West, B.J., Grigolini, P., 2018. Bridging Waves and Crucial Events in the Dynamics of the Brain. Front. Physiol. 9, 1174.
Buzsáki, G., 2004. Large-scale recording of neuronal ensembles. Nat. Neurosci. 7, 446–451.
Buzsáki, G., Anastassiou, C.A., Koch, C., 2012. The origin of extracellular fields and currents--EEG, ECoG, LFP and spikes. Nat. Rev. Neurosci. 13, 407–420.
Buzsáki, G., Draguhn, A., 2004. Neuronal oscillations in cortical networks. Science 304, 1926–1929.
Buzsáki, G., Wang, X.-J., 2012. Mechanisms of gamma oscillations. Annu. Rev. Neurosci. 35, 203–225.
Casali, A.G., Gosseries, O., Rosanova, M., Boly, M., Sarasso, S., Casali, K.R., Casarotto, S., Bruno, M.-A., Laureys, S., Tononi, G., Massimini, M., 2013. A theoretically based index of consciousness independent of sensory processing and behavior. Sci. Transl. Med. 5, 198ra105.
Castro-Nin, J.P., Serantes, D., Rodriguez, P., Gonzalez, B., Carrera, I., Torterolo, P., González, J., 2023. Noribogaine effects on wakefulness and sleep. bioRxiv. https://doi.org/10.1101/2023.07.26.550725
Cavelli, M.L., Mao, R., Findlay, G., Driessen, K., Bugnon, T., Tononi, G., Cirelli, C., 2023. Sleep/wake changes in perturbational complexity in rats and mice. iScience 26, 106186.
Chialvo, D.R., 2010. Emergent complex neural dynamics. Nat. Phys. 6, 744–750.
Donoghue, T., Haller, M., Peterson, E.J., Varma, P., Sebastian, P., Gao, R., Noto, T., Lara, A.H., Wallis, J.D., Knight, R.T., Shestyuk, A., Voytek, B., 2020. Parameterizing neural power spectra into periodic and aperiodic components. Nat. Neurosci. 23, 1655–1665.
Douglas, R.J., Martin, K.A.C., 2004. Neuronal circuits of the neocortex. Annu. Rev. Neurosci. 27, 419–451.
Fernández-Ruiz, A., Oliva, A., Soula, M., Rocha-Almeida, F., Nagy, G.A., Martin-Vazquez, G., Buzsáki, G., 2021. Gamma rhythm communication between entorhinal cortex and dentate gyrus neuronal assemblies. Science 372. https://doi.org/10.1126/science.abf3119
Fontenele, A.J., de Vasconcelos, N.A.P., Feliciano, T., Aguiar, L.A.A., Soares-Cunha, C., Coimbra, B., Dalla Porta, L., Ribeiro, S., Rodrigues, A.J., Sousa, N., Carelli, P.V., Copelli, M., 2019. Criticality between Cortical States. Phys. Rev. Lett. 122, 208101.
Friston, K., 2005. A theory of cortical responses. Philos. Trans. R. Soc. Lond. B Biol. Sci. 360, 815–836.
Gao, P., Ganguli, S., 2015. On simplicity and complexity in the brave new world of large-scale neuroscience. Curr. Opin. Neurobiol. 32, 148–155.
González, J., Cavelli, M., Castro-Zaballa, S., Mondino, A., Tort, A.B.L., Rubido, N., Carrera, I., Torterolo, P., 2021. EEG Gamma Band Alterations and REM-like Traits Underpin the Acute Effect of the Atypical Psychedelic Ibogaine in the Rat. ACS Pharmacol Transl Sci 4, 517–525.
González, J., Cavelli, M., Mondino, A., Pascovich, C., Castro-Zaballa, S., Torterolo, P., Rubido, N., 2019. Decreased electrocortical temporal complexity distinguishes sleep from wakefulness. Sci. Rep. 9, 18457.
González, J., Cavelli, M., Mondino, A., Rubido, N., Bl Tort, A., Torterolo, P., 2020. Communication Through Coherence by Means of Cross-frequency Coupling. Neuroscience 449, 157–164.
González, J., Cavelli, M., Tort, A.B.L., Torterolo, P., Rubido, N., 2023. Sleep disrupts complex spiking dynamics in the neocortex and hippocampus. PLoS One 18, e0290146.
González, J., Mateos, D., Cavelli, M., Mondino, A., Pascovich, C., Torterolo, P., Rubido, N., 2022. Low frequency oscillations drive EEG's complexity changes during wakefulness and sleep. Neuroscience 494, 1–11.
González, J., Prieto, J.P., Rodríguez, P., Cavelli, M., Benedetto, L., Mondino, A., Pazos, M., Seoane, G., Carrera, I., Scorza, C., Torterolo, P., 2018. Ibogaine Acute Administration in Rats Promotes Wakefulness, Long-Lasting REM Sleep Suppression, and a Distinctive Motor Profile. Front. Pharmacol. 9, 374.
Gonzalez, J., Torterolo, P., Tort, A.B.L., 2023. Mechanisms and functions of

respiration-driven gamma oscillations in the primary olfactory cortex. Elife 12. https://doi.org/10.7554/eLife.83044
Grinvald, A., Hildesheim, R., 2004. VSDI: a new era in functional imaging of cortical dynamics. Nat. Rev. Neurosci. 5, 874–885.
Hara, K., Harris, R.A., 2002. The anesthetic mechanism of urethane: the effects on neurotransmitter-gated ion channels. Anesth. Analg. 94, 313–8, table of contents.
Hay, Y.A., Deperrois, N., Fuchsberger, T., Quarrell, T.M., Koerling, A.-L., Paulsen, O., 2021. Thalamus mediates neocortical Down state transition via GABA-receptor-targeting interneurons. Neuron 109, 2682–2690.e5.
He, B.J., Raichle, M.E., 2009. The fMRI signal, slow cortical potential and consciousness. Trends Cogn. Sci. 13, 302–309.
Herreras, O., 2016. Local Field Potentials: Myths and Misunderstandings. Front. Neural Circuits 10, 101.
Huang, S.Y., Witzel, T., Keil, B., Scholz, A., Davids, M., Dietz, P., Rummert, E., Ramb, R., Kirsch, J.E., Yendiki, A., Fan, Q., Tian, Q., Ramos-Llordén, G., Lee, H.-H., Nummenmaa, A., Bilgic, B., Setsompop, K., Wang, F., Avram, A.V., Komlosh, M., Benjamini, D., Magdoom, K.N., Pathak, S., Schneider, W., Novikov, D.S., Fieremans, E., Tounekti, S., Mekkaoui, C., Augustinack, J., Berger, D., Shapson-Coe, A., Lichtman, J., Basser, P.J., Wald, L.L., Rosen, B.R., 2021. Connectome 2.0: Developing the next-generation ultra-high gradient strength human MRI scanner for bridging studies of the micro-, meso- and macro-connectome. Neuroimage 243, 118530.
Isomura, Y., Sirota, A., Ozen, S., Montgomery, S., Mizuseki, K., Henze, D.A., Buzsáki, G., 2006. Integration and segregation of activity in entorhinal-hippocampal subregions by neocortical slow oscillations. Neuron 52, 871–882.
Jun, J.J., Steinmetz, N.A., Siegle, J.H., Denman, D.J., Bauza, M., Barbarits, B., Lee, A.K., Anastassiou, C.A., Andrei, A., Aydın, Ç., Barbic, M., Blanche, T.J., Bonin, V., Couto, J., Dutta, B., Gratiy, S.L., Gutnisky, D.A., Häusser, M., Karsh, B., Ledochowitsch, P., Lopez, C.M., Mitelut, C., Musa, S., Okun, M., Pachitariu, M., Putzeys, J., Rich, P.D., Rossant, C., Sun, W.-L., Svoboda, K., Carandini, M., Harris, K.D., Koch, C., O'Keefe, J., Harris, T.D., 2017. Fully integrated silicon probes for high-density recording of neural activity. Nature 551, 232–236.
Kiebel, S.J., Daunizeau, J., Friston, K.J., 2008. A hierarchy of time-scales and the brain. PLoS Comput. Biol. 4, e1000209.
Köck, P., Froelich, K., Walter, M., Lang, U., Dürsteler, K.M., 2022. A systematic literature review of clinical trials and therapeutic applications of ibogaine. J. Subst. Abuse Treat. 138, 108717.
Lee, S.-H., Dan, Y., 2012. Neuromodulation of brain states. Neuron 76, 209–222.
Lempel, A., Ziv, J., 1976. On the complexity of finite sequences. IEEE Trans. Inf. Theory 22, 75–81.
Lendner, J.D., Helfrich, R.F., Mander, B.A., Romundstad, L., Lin, J.J., Walker, M.P., Larsson, P.G., Knight, R.T., 2020. An electrophysiological marker of arousal level in humans. Elife 9. https://doi.org/10.7554/eLife.55092
Levenstein, D., Buzsáki, G., Rinzel, J., 2019. NREM sleep in the rodent neocortex and hippocampus reflects excitable dynamics. Nat. Commun. 10, 2478.
Lewis, C.M., Bosman, C.A., Fries, P., 2015. Recording of brain activity across spatial scales. Curr. Opin. Neurobiol. 32, 68–77.
Lewis, C.M., Hoffmann, A., Helmchen, F., 2024. Linking brain activity across scales with simultaneous opto- and electrophysiology. Neurophotonics 11, 033403.
Lombardi, F., Gómez-Extremera, M., Bernaola-Galván, P., Vetrivelan, R., Saper, C.B., Scammell, T.E., Ivanov, P.C., 2020. Critical Dynamics and Coupling in Bursts of Cortical Rhythms Indicate Non-Homeostatic Mechanism for Sleep-Stage Transitions and Dual Role of VLPO Neurons in Both Sleep and Wake. J. Neurosci. 40, 171–190.
Luo, L., 2021. Architectures of neuronal circuits. Science 373, eabg7285.
Mash, D.C., 2023. IUPHAR - invited review - Ibogaine - A legacy within the current renaissance of psychedelic therapy. Pharmacol. Res. 190, 106620.

Massimini, M., Ferrarelli, F., Huber, R., Esser, S.K., Singh, H., Tononi, G., 2005. Breakdown of cortical effective connectivity during sleep. Science 309, 2228–2232.
Massimini, M., Huber, R., Ferrarelli, F., Hill, S., Tononi, G., 2004. The sleep slow oscillation as a traveling wave. J. Neurosci. 24, 6862–6870.
Mateos, D., Zozor, S., Olivares, F., 2020. Contrasting stochasticity with chaos in a permutation Lempel–Ziv complexity — Shannon entropy plane. Physica A: Statistical Mechanics and its Applications 554, 124640.
Miller, K.J., Sorensen, L.B., Ojemann, J.G., den Nijs, M., 2009. Power-Law Scaling in the Brain Surface Electric Potential. PLoS Comput. Biol. 5, e1000609.
Mondino, A., Cavelli, M., González, J., Osorio, L., Castro-Zaballa, S., Costa, A., Vanini, G., Torterolo, P., 2020. Power and Coherence in the EEG of the Rat: Impact of Behavioral States, Cortical Area, Lateralization and Light/Dark Phases. Clocks Sleep 2, 536–556.
Mondino, A., González, J., Li, D., Mateos, D., Osorio, L., Cavelli, M., Castro-Nin, J.P., Serantes, D., Costa, A., Vanini, G., Mashour, G.A., Torterolo, P., 2022. Urethane anaesthesia exhibits neurophysiological correlates of unconsciousness and is distinct from sleep. Eur. J. Neurosci. https://doi.org/10.1111/ejn.15690
Mondino, A., Hambrecht-Wiedbusch, V.S., Li, D., York, A.K., Pal, D., González, J., Torterolo, P., Mashour, G.A., Vanini, G., 2021. Glutamatergic Neurons in the Preoptic Hypothalamus Promote Wakefulness, Destabilize NREM Sleep, Suppress REM Sleep, and Regulate Cortical Dynamics. J. Neurosci. 41, 3462–3478.
Munn, B.R., Müller, E.J., Medel, V., Naismith, S.L., Lizier, J.T., Sanders, R.D., Shine, J.M., 2023. Neuronal connected burst cascades bridge macroscale adaptive signatures across arousal states. Nat. Commun. 14, 1–17.
Nir, Y., de Lecea, L., 2023. Sleep and vigilance states: Embracing spatiotemporal dynamics. Neuron 111, 1998–2011.
Nir, Y., Staba, R.J., Andrillon, T., Vyazovskiy, V.V., Cirelli, C., Fried, I., Tononi, G., 2011. Regional slow waves and spindles in human sleep. Neuron 70, 153–169.
Ogawa, S., Lee, T.M., Kay, A.R., Tank, D.W., 1990. Brain magnetic resonance imaging with contrast dependent on blood oxygenation. Proc. Natl. Acad. Sci. U. S. A. 87, 9868–9872.
Pagliardini, S., Funk, G.D., Dickson, C.T., 2013. Breathing and brain state: urethane anesthesia as a model for natural sleep. Respir. Physiol. Neurobiol. 188, 324–332.
Paninski, L., Cunningham, J.P., 2018. Neural data science: accelerating the experiment-analysis-theory cycle in large-scale neuroscience. Curr. Opin. Neurobiol. 50, 232–241.
Pascovich, C., Castro-Zaballa, S., Mediano, P.A.M., Bor, D., Canales-Johnson, A., Torterolo, P., Bekinschtein, T.A., 2022. Ketamine and sleep modulate neural complexity dynamics in cats. Eur. J. Neurosci. 55, 1584–1600.
Priesemann, V., Valderrama, M., Wibral, M., Le Van Quyen, M., 2013. Neuronal avalanches differ from wakefulness to deep sleep--evidence from intracranial depth recordings in humans. PLoS Comput. Biol. 9, e1002985.
Priesemann, V., Wibral, M., Valderrama, M., Pröpper, R., Le Van Quyen, M., Geisel, T., Triesch, J., Nikolić, D., Munk, M.H.J., 2014. Spike avalanches in vivo suggest a driven, slightly subcritical brain state. Front. Syst. Neurosci. 8, 108.
Ribeiro, T.L., Copelli, M., Caixeta, F., Belchior, H., Chialvo, D.R., Nicolelis, M.A.L., Ribeiro, S., 2010. Spike avalanches exhibit universal dynamics across the sleep-wake cycle. PLoS One 5, e14129.
Sakmann, B., Neher, E., 1984. Patch clamp techniques for studying ionic channels in excitable membranes. Annu. Rev. Physiol. 46, 455–472.
Scholtens, L.H., van den Heuvel, M.P., 2018. Multimodal Connectomics in Psychiatry: Bridging Scales From Micro to Macro. Biol Psychiatry Cogn Neurosci Neuroimaging 3, 767–776.
Sejnowski, T.J., Churchland, P.S., Movshon, J.A., 2014. Putting big data to good use in neuroscience. Nat. Neurosci. 17, 1440–1441.
Sporns, O., Tononi, G., Kötter, R., 2005. The human connectome: A structural description of

the human brain. PLoS Comput. Biol. 1, e42.
Steinmetz, N.A., Zatka-Haas, P., Carandini, M., Harris, K.D., 2019. Distributed coding of choice, action and engagement across the mouse brain. Nature 576, 266–273.
Steriade, M., Nuñez, A., Amzica, F., 1993. Intracellular analysis of relations between the slow (< 1 Hz) neocortical oscillation and other sleep rhythms of the electroencephalogram. J. Neurosci. 13, 3266–3283.
Stern, M., Bolding, K.A., Abbott, L.F., Franks, K.M., 2018. A transformation from temporal to ensemble coding in a model of piriform cortex. Elife 7. https://doi.org/10.7554/eLife.34831
Stringer, C., Pachitariu, M., Steinmetz, N., Carandini, M., Harris, K.D., 2019a. High-dimensional geometry of population responses in visual cortex. Nature 571, 361–365.
Stringer, C., Pachitariu, M., Steinmetz, N., Reddy, C.B., Carandini, M., Harris, K.D., 2019b. Spontaneous behaviors drive multidimensional, brainwide activity. Science 364, 255.
Tian, L., Hires, S.A., Mao, T., Huber, D., Chiappe, M.E., Chalasani, S.H., Petreanu, L., Akerboom, J., McKinney, S.A., Schreiter, E.R., Bargmann, C.I., Jayaraman, V., Svoboda, K., Looger, L.L., 2009. Imaging neural activity in worms, flies and mice with improved GCaMP calcium indicators. Nat. Methods 6, 875–881.
Tononi, G., Sporns, O., Edelman, G.M., 1994. A measure for brain complexity: relating functional segregation and integration in the nervous system. Proc. Natl. Acad. Sci. U. S. A. 91, 5033–5037.
Torres, D., Makarova, J., Ortuño, T., Benito, N., Makarov, V.A., Herreras, O., 2019. Local and Volume-Conducted Contributions to Cortical Field Potentials. Cereb. Cortex 29, 5234–5254.
Tort, A.B.L., Komorowski, R.W., Manns, J.R., Kopell, N.J., Eichenbaum, H., 2009. Theta-gamma coupling increases during the learning of item-context associations. Proc. Natl. Acad. Sci. U. S. A. 106, 20942–20947.
Vanini, G., Bassana, M., Mast, M., Mondino, A., Cerda, I., Phyle, M., Chen, V., Colmenero, A.V., Hambrecht-Wiedbusch, V.S., Mashour, G.A., 2020. Activation of Preoptic GABAergic or Glutamatergic Neurons Modulates Sleep-Wake Architecture, but Not Anesthetic State Transitions. Curr. Biol. 30, 779–787.e4.
Vanini, G., Torterolo, P., 2021. Sleep-Wake Neurobiology. Adv. Exp. Med. Biol. 1297, 65–82.
Vyazovskiy, V.V., Olcese, U., Lazimy, Y.M., Faraguna, U., Esser, S.K., Williams, J.C., Cirelli, C., Tononi, G., 2009. Cortical firing and sleep homeostasis. Neuron 63, 865–878.
Watson, B.O., Levenstein, D., Greene, J.P., Gelinas, J.N., Buzsáki, G., 2016. Network Homeostasis and State Dynamics of Neocortical Sleep. Neuron 90, 839–852.
Williamson, R.C., Doiron, B., Smith, M.A., Yu, B.M., 2019. Bridging large-scale neuronal recordings and large-scale network models using dimensionality reduction. Curr. Opin. Neurobiol. 55, 40–47.

Discusión

Resultados generales

Al comparar registros de la actividad cortical a distintas escalas (ECoG, LFPs y sLFPs de las áreas frontales en ratas en libre comportamiento) y centrarnos en las bandas de baja frecuencia (filtrando todas las señales por debajo de 13 Hz), nuestros resultados sugieren que las diferencias en la complejidad neural permanecen relativamente estables dentro de cada estado cerebral, independientemente de la escala en la que se analicen (Papers **1,2,4, 6**). En otras palabras, encontramos que las diferencias en la complejidad neural a través de los estados se mantenían robustamente en las tres escalas de registro. Este resultado sugiere que la complejidad de las dinámicas neuronales y sus cambios a lo largo del ciclo sueño-vigilia se conservan a través de varios niveles de organización, desde conjuntos individuales hasta redes corticales más amplias.

Patrones de descarga que determinan la complejidad neural

Para obtener una comprensión más profunda de por qué los cambios en la complejidad neural son consistentes a diferentes escalas, realizamos un análisis de los patrones microscópicos (espigas) subyacentes a estos cambios (Paper **5**). Nuestra investigación reveló que la complejidad de las dinámicas neuronales en ratas se reduce durante el sueño de ondas lentas debido a que los patrones de espigas se repiten con mayor frecuencia (es decir, mayores recurrencias). Esta repetición de patrones de espigas ocurre durante los estados DOWN, lo que explica la disminución de la complejidad observada tanto a nivel celular como en los registros de campo (como los potenciales de campo local o el EEG). Además, revelamos un comportamiento común en las avalanchas de espigas de la población que aparecen a lo largo de los estados de sueño-vigilia (que por definición excluye los estados DOWN). Esta universalidad hace que los estados de sueño-vigilia sean indistinguibles entre sí (mientras las neuronas descargan potenciales de acción) y demuestra que los períodos DOWN son responsables de la reducción de complejidad que caracteriza al sueño.

Durante el sueño de ondas lentas, las neuronas del hipocampo oscilan entre largos periodos de quietud y estabilidad (sin una hiperpolarización clara de la membrana [25]) y ráfagas de descarga de espigas (durante los ripples de onda aguda). En contraste, las neuronas neocorticales oscilan entre periodos estables de actividad y periodos inestables de silencio (asociados con la hiperpolarización [48]). A pesar de estas diferencias, ambas poblaciones presentan patrones de descarga neuronales que son consistentes con un régimen excitable UP/DOWN [49].

Para las neuronas neocorticales, la complejidad de los patrones de disparo disminuye durante el sueño de ondas lentas [50]. En principio, se podría esperar esta disminución debido a los estados DOWN, ya que su aparición provoca que las neuronas permanezcan en silencio durante intervalos sincrónicos. Sin embargo, al analizar los patrones de disparo de las neuronas individuales de manera independiente, encontramos que un número considerable mantiene patrones complejos incluso durante el SWS. Esto puede ocurrir porque existen neuronas activas durante los estados DOWN, como se mostró previamente en [51], o porque la reducción de complejidad es un fenómeno colectivo que solo puede

estudiarse a nivel de la población. Nuestros resultados apoyan este último argumento al mostrar que la diferencia en complejidad entre la vigilia o el sueño REM y el sueño de ondas lentas aumenta con el número de neuronas registradas en simultáneo.

Un modelo para reproducir la disminución en la complejidad neural durante el sueño

Para complementar nuestros resultados *in-vivo*, demostramos que la imposición de estados DOWN en un modelo de branching crítico es suficiente para generar un estado similar al sueño de ondas lentas (Paper **5**). Logramos esto silenciando periódicamente el impulso ruidoso a un porcentaje dado de unidades, imitando así la reducción del input sináptico a las células piramidales durante este estado en el neocórtex [52]. Esta reducción (en condiciones fisiológicas) es probablemente causada por una inhibición presináptica GABAb de las entradas excitatorias en las dendritas apicales de las células piramidales [53], coordinada por el tálamo [54]. En contraste con los mecanismos neocorticales, los estados UP/DOWN en el hipocampo están relacionados con la generación de Sharp-Wave Ripples, donde predominan los estados DOWN de baja actividad y los estados UP se inician por la excitación recurrente de las neuronas CA3 [55]. Por lo tanto, en el hipocampo, el silenciamiento periódico reproduce los estados DOWN que ocurren entre los ripples.

Importante, en nuestro modelo no es necesario silenciar la entrada al 100% de las neuronas para reproducir los resultados experimentales, lo cual es consistente con la ausencia de períodos de silencio completos en el hipocampo [49]. Además, notamos que se ha empleado una estrategia similar para modelar las ondas lentas durante la anestesia [56]. Asimismo, encontramos que estar cerca del punto crítico permite transiciones entre estados más flexibles en comparación con el modelo subcrítico o supercrítico. Específicamente, silenciar la entrada entre el 40% y el 60% crea una disminución en la complejidad similar a la observada experimentalmente. Estos resultados refuerzan la idea de la criticidad en el cerebro, lo cual explicaría el aumento de la complejidad [57], el procesamiento y transmisión de información [58], y el rango dinámico [59].

Alterando la complejidad neural exógenamente

En las secciones anteriores, argumentamos que las diferencias en la complejidad neural entre los estados de sueño y vigilia se conservan a través de diversas escalas neuronales. Para dar un significado biológico adicional a esta cantidad, nuestros resultados muestran que podemos perturbar externamente la complejidad neural (Papers **3** y **6**).

Nuestros hallazgos demuestran que tanto la ibogaína (psicodélico atípico) como el uretano (anestésico general) reducen la complejidad neural en todo el cerebro, lo que sugiere que la actividad cortical se vuelve menos diversa durante los efectos agudos de ambas drogas. Estos ejemplos ilustran cómo dos drogas que afectan profundamente la cognición también perturban la complejidad neural, esto ocurre a pesar de que los mecanismos y efectos de las drogas difieren (por ejemplo, la ibogaína aumenta la actividad gamma mientras que el uretano la disminuye).

Finalmente y de manera notable, la estimulación quimiogenética de un subgrupo de neuronas glutamatérgicas en el área preóptica, causó un aumento en la complejidad neural a nivel cortical global. Este aumento en la complejidad neural ocurrió independientemente

del estado de vigilia, ya que se observaron incrementos significativos en la complejidad tanto durante la vigilia como durante el sueño NREM. De hecho, la complejidad durante el sueño tras la estimulación quimiogenética alcanzó niveles similares a los de la vigilia sin estimulación. Por lo tanto, estos hallazgos sugieren que cambios a nivel microscópico, como alteraciones en la tasa de descarga de una pequeña subpoblación dentro de un núcleo profundo, pueden impactar profundamente la complejidad neural en una escala neural diferente.

Conclusiones

El cerebro exhibe actividad en múltiples escalas, desde el nivel macroscópico hasta el microscópico, resaltando que distintos procesos relevantes para el comportamiento ocurren en cada escala. El análisis de la complejidad ofrece una perspectiva novedosa para estudiar la actividad cerebral en diferentes escalas. Proporciona un marco para navegar por las dinámicas intrincadas de las redes neuronales, permitiendo descubrir patrones y fenómenos emergentes que pueden no ser evidentes con enfoques analíticos tradicionales. Además, estudiar los efectos de los fármacos en la complejidad neural puede ofrecer ideas sobre los mecanismos de acción comunes a nivel macroscópico. Finalmente, entender cómo los cambios a escala microscópica, como los patrones de disparo de las neuronas individuales, afectan la actividad cerebral macroscópica es crucial para desentrañar los mecanismos subyacentes de la función cerebral. Tales conocimientos pueden proporcionar una comprensión más profunda de cómo los circuitos neuronales procesan la información y generan comportamientos.

Referencias

1. Buzsáki G: **Large-scale recording of neuronal ensembles**. *Nat Neurosci* 2004, **7**:446–451.

2. Lewis CM, Hoffmann A, Helmchen F: **Linking brain activity across scales with simultaneous opto- and electrophysiology**. *Neurophotonics* 2024, **11**:033403.

3. Lewis CM, Bosman CA, Fries P: **Recording of brain activity across spatial scales**. *Curr Opin Neurobiol* 2015, **32**:68–77.

4. He BJ, Raichle ME: **The fMRI signal, slow cortical potential and consciousness**. *Trends Cogn Sci* 2009, **13**:302–309.

5. Binzegger T, Douglas RJ, Martin KAC: **A quantitative map of the circuit of cat primary visual cortex**. *J Neurosci* 2004, **24**:8441–8453.

6. Sporns O, Tononi G, Kötter R: **The human connectome: A structural description of the human brain**. *PLoS Comput Biol* 2005, **1**:e42.

7. Ogawa S, Lee TM, Kay AR, Tank DW: **Brain magnetic resonance imaging with contrast dependent on blood oxygenation**. *Proc Natl Acad Sci U S A* 1990, **87**:9868–9872.

8. Biasiucci A, Franceschiello B, Murray MM: **Electroencephalography**. *Curr Biol* 2019, **29**:R80–R85.

9. Berger H: **Über das Elektrenkephalogramm des Menschen**. *Archiv für Psychiatrie und Nervenkrankheiten* 1929, **87**:527–570.

10. Buzsáki G, Wang X-J: **Mechanisms of gamma oscillations**. *Annu Rev Neurosci* 2012, **35**:203–225.

11. Gonzalez J, Torterolo P, Tort ABL: **Mechanisms and functions of respiration-driven gamma oscillations in the primary olfactory cortex**. *Elife* 2023, **12**.

12. Luo L: **Architectures of neuronal circuits**. *Science* 2021, **373**:eabg7285.

13. Douglas RJ, Martin KAC: **Neuronal circuits of the neocortex**. *Annu Rev Neurosci* 2004, **27**:419–451.

14. Buzsáki G, Anastassiou CA, Koch C: **The origin of extracellular fields and currents--EEG, ECoG, LFP and spikes**. *Nat Rev Neurosci* 2012, **13**:407–420.

15. Herreras O: **Local Field Potentials: Myths and Misunderstandings**. *Front Neural Circuits* 2016, **10**:101.

16. Tian L, Hires SA, Mao T, Huber D, Chiappe ME, Chalasani SH, Petreanu L, Akerboom J, McKinney SA, Schreiter ER, et al.: **Imaging neural activity in worms, flies and mice with improved GCaMP calcium indicators**. *Nat Methods* 2009, **6**:875–881.

17. Sakmann B, Neher E: **Patch clamp techniques for studying ionic channels in excitable membranes**. *Annu Rev Physiol* 1984, **46**:455–472.

18. Jun JJ, Steinmetz NA, Siegle JH, Denman DJ, Bauza M, Barbarits B, Lee AK, Anastassiou CA, Andrei A, Aydın Ç, et al.: **Fully integrated silicon probes for high-density recording of neural activity**. *Nature* 2017, **551**:232–236.

19. Scholtens LH, van den Heuvel MP: **Multimodal Connectomics in Psychiatry: Bridging Scales From Micro to Macro**. *Biol Psychiatry Cogn Neurosci Neuroimaging* 2018, **3**:767–776.

20. Huang SY, Witzel T, Keil B, Scholz A, Davids M, Dietz P, Rummert E, Ramb R, Kirsch JE, Yendiki A, et al.: **Connectome 2.0: Developing the next-generation ultra-high gradient strength human MRI scanner for bridging studies of the micro-, meso- and macro-connectome**. *Neuroimage* 2021, **243**:118530.

21. Munn BR, Müller EJ, Medel V, Naismith SL, Lizier JT, Sanders RD, Shine JM: **Neuronal connected burst cascades bridge macroscale adaptive signatures across arousal states**. *Nat Commun* 2023, **14**:1–17.

22. Bohara G, West BJ, Grigolini P: **Bridging Waves and Crucial Events in the Dynamics of the Brain**. *Front Physiol* 2018, **9**:1174.

23. Paninski L, Cunningham JP: **Neural data science: accelerating the experiment-analysis-theory cycle in large-scale neuroscience**. *Curr Opin Neurobiol* 2018, **50**:232–241.

24. Williamson RC, Doiron B, Smith MA, Yu BM: **Bridging large-scale neuronal recordings and large-scale network models using dimensionality reduction**. *Curr Opin Neurobiol* 2019, **55**:40–47.

25. Gao P, Ganguli S: **On simplicity and complexity in the brave new world of large-scale neuroscience**. *Curr Opin Neurobiol* 2015, **32**:148–155.

26. Sejnowski TJ, Churchland PS, Movshon JA: **Putting big data to good use in neuroscience**. *Nat Neurosci* 2014, **17**:1440–1441.

27. Stringer C, Pachitariu M, Steinmetz N, Reddy CB, Carandini M, Harris KD: **Spontaneous behaviors drive multidimensional, brainwide activity**. *Science* 2019, **364**:255.

28. Stringer C, Pachitariu M, Steinmetz N, Carandini M, Harris KD: **High-dimensional geometry of population responses in visual cortex**. *Nature* 2019, **571**:361–365.

29. Grinvald A, Hildesheim R: **VSDI: a new era in functional imaging of cortical dynamics**. *Nat Rev Neurosci* 2004, **5**:874–885.

30. Abdelfattah AS, Kawashima T, Singh A, Novak O, Liu H, Shuai Y, Huang Y-C, Campagnola L, Seeman SC, Yu J, et al.: **Bright and photostable chemigenetic indicators for extended in vivo voltage imaging**. *Science* 2019, **365**:699–704.

31. Stern M, Bolding KA, Abbott LF, Franks KM: **A transformation from temporal to ensemble coding in a model of piriform cortex**. *Elife* 2018, **7**.

32. González J, Cavelli M, Tort ABL, Torterolo P, Rubido N: **Sleep disrupts complex spiking dynamics in the neocortex and hippocampus**. *PLoS One* 2023, **18**:e0290146.

33. Kiebel SJ, Daunizeau J, Friston KJ: **A hierarchy of time-scales and the brain**. *PLoS Comput Biol* 2008, **4**:e1000209.

34. Friston K: **A theory of cortical responses**. *Philos Trans R Soc Lond B Biol Sci* 2005, **360**:815–836.

35. Steinmetz NA, Zatka-Haas P, Carandini M, Harris KD: **Distributed coding of choice, action and engagement across the mouse brain**. *Nature* 2019, **576**:266–273.

36. Lee S-H, Dan Y: **Neuromodulation of brain states**. *Neuron* 2012, **76**:209–222.

37. Adamantidis AR, Zhang F, Aravanis AM, Deisseroth K, de Lecea L: **Neural substrates of awakening probed with optogenetic control of hypocretin neurons**. *Nature* 2007, **450**:420–424.

38. Nir Y, de Lecea L: **Sleep and vigilance states: Embracing spatiotemporal dynamics**. *Neuron* 2023, **111**:1998–2011.

39. Beggs JM, Plenz D: **Neuronal avalanches in neocortical circuits**. *J Neurosci* 2003, **23**:11167–11177.

40. Ribeiro TL, Copelli M, Caixeta F, Belchior H, Chialvo DR, Nicolelis MAL, Ribeiro S: **Spike avalanches exhibit universal dynamics across the sleep-wake cycle**. *PLoS One* 2010, **5**:e14129.

41. Miller KJ, Sorensen LB, Ojemann JG, den Nijs M: **Power-Law Scaling in the Brain Surface Electric Potential**. *PLoS Comput Biol* 2009, **5**:e1000609.

42. Barabasi AL, Albert R: **Emergence of scaling in random networks**. *Science* 1999, **286**:509–512.

43. Bandt C, Pompe B: **Permutation entropy: a natural complexity measure for time series**. *Phys Rev Lett* 2002, **88**:174102.

44. Tononi G, Sporns O, Edelman GM: **A measure for brain complexity: relating functional segregation and integration in the nervous system**. *Proc Natl Acad Sci U S A* 1994, **91**:5033–5037.

45. Massimini M, Ferrarelli F, Huber R, Esser SK, Singh H, Tononi G: **Breakdown of cortical effective connectivity during sleep**. *Science* 2005, **309**:2228–2232.

46. Casali AG, Gosseries O, Rosanova M, Boly M, Sarasso S, Casali KR, Casarotto S, Bruno M-A, Laureys S, Tononi G, et al.: **A theoretically based index of consciousness independent of sensory processing and behavior**. *Sci Transl Med* 2013, **5**:198ra105.

47. Lendner JD, Helfrich RF, Mander BA, Romundstad L, Lin JJ, Walker MP, Larsson PG, Knight RT: **An electrophysiological marker of arousal level in humans**. *Elife* 2020, **9**

48. Isomura Y., Sirota A., Ozen S., Montgomery S., Mizuseki K., Henze D. et al: **Integration and segregation of activity in entorhinal-hippocampal subregions by neocortical slow oscillations**. Neuron. 52, 871–882 (2006,12)

49. Levenstein D., Buzsaki G. & Rinzel J: **NREM sleep in the rodent neocortex and hippocampus reflects excitable dynamics**. Nat Commun. 10, 2478 (2019,6)

50. Abasolo D., Simons S., Silva R., Tononi G. & Vyazovskiy V: **Lempel-Ziv complexity of cortical activity during sleep and waking in rats**. J Neurophysiol. 113, 2742–2752 (2015,4)

51. Valero M., Viney T., Machold R., Mederos S., Zutshi I., Schuman B., et al: **Sleep down state-active ID2/ Nkx2. 1 interneurons in the neocortex**. Nature Neuroscience. 24, 401–411 (2021)

52. Steriade M., Timofeev I. & Grenier F.I: **Natural waking and sleep states: a view from inside neocortical neurons**. J Neurophysiol. 85, 1969–1985 (2001,5)

53. Funk C., Peelman K., Bellesi M., Marshall W., Cirelli C. & Tononi G: **Role of Somatostatin-Positive Cortical Interneurons in the Generation of Sleep Slow Waves**. J Neurosci. 37, 9132–9148 (2017,9)

54. Hay Y., Deperrois N., Fuchsberger T., Quarrell T., Koerling A. & Paulsen O: **Thalamus mediates neocortical Down state transition via GABAB-receptor-targeting interneurons.** Neuron. (2021)

55. Buzsaki G: **Hippocampal sharp wave-ripple: A cognitive biomarker for episodic memory and planning.** Hippocampus. 25, 1073–1188 (2015,10)

56. Ribeiro T., Copelli M., Caixeta F., Belchior H., Chialvo D., Nicolelis M. et al: **Spike avalanches exhibit universal dynamics across the sleep-wake cycle.** PLoS One. 5, e14129 (2010,11)(2021)

56. Ribeiro T., Copelli M., Caixeta F., Belchior H., Chialvo D., Nicolelis M. et al: **Spike avalanches exhibit universal dynamics across the sleep-wake cycle.** PLoS One. 5, e14129 (2010,11)

57. Timme N., Marshall N., Bennett N., Ripp M., Lautzenhiser E. & Beggs J: **Criticality Maximizes Complexity in Neural Tissue.** Front Physiol. 7 pp. 425 (2016)

58. Beggs J. & Plenz D: **Neuronal avalanches in neocortical circuits.** J Neurosci. 23, 11167–11177 (2003,12)

59. Kinouchi O. & Copelli M: **Optimal dynamical range of excitable networks at criticality.** Nature Physics. 2 pp. 348–351 (2006)

Lista de publicaciones no incluidas en la tesis (ordenadas por año)

1 Castro-Nin, J. P., Serantes, D., Rodriguez, P., Gonzalez, B., Carrera, I., Torterolo, P., & González, J. 2024. Noribogaine acute administration in rats promotes wakefulness and suppresses REM sleep. Psychopharmacology, 10.1007/s00213-024-06572-2.

2 Villalba, S., González, B., Junge, S., Bernardi, A., González, J., Fagúndez, C., Torterolo, P., Carrera, I., Urbano, F. J., & Bisagno, V. (2024). 5-HT2A Receptor Knockout Mice Show Sex-Dependent Differences following Acute Noribogaine Administration. International journal of molecular sciences, 25(2), 687. https://doi.org/10.3390/ijms25020687

3 Gonzalez J, Torterolo P, Tort ABL. Mechanisms and functions of respiration-driven gamma oscillations in the primary olfactory cortex. Elife. 2023;12:e83044. Published 2023 Feb 20. doi:10.7554/eLife.83044

4 González J, Cavelli M, Mondino A, et al. Breathing modulates gamma synchronization across species. Pflugers Arch. 2023;475(1):49-63. doi:10.1007/s00424-022-02753-0

5 Gallo D, González J, Rodriguez P, et al. Ibogaína: un psicodélico atípico con potencial antiadictivo. Rev Psiquiatr Urug. 2023; 2023;87(1). In press.

6 Serantes D, Cavelli M, González J, Mondino A, Benedetto L, Torterolo P. Characterizing the power spectrum dynamics of the NREM to REM sleep transition. bioRxiv. Published online 2023. doi:10.1101/2023.06.14.544943

7 Castro-Zaballa S, González J, Cavelli M, et al. Cortical high-frequency oscillations (≈ 110 Hz) in cats are state-dependent and enhanced by a subanesthetic dose of ketamine. bioRxiv. Published online 2023. doi:10.1101/2023.05.31.543142

8 Rognoni CP, Serantes D, Rodriguez A, et al. Dorsal and median raphe neuronal firing dynamics characterized by non-linear metrics. bioRxiv. Published online 2023. doi:10.1101/2023.05.23.541902

9 Torterolo P, Gonzalez J, Castro-Zaballa S, et al. Chapter 2 - Polysomnography in humans and animal models: basic procedures and analysis. In: Murillo-Rodriguez E, ed. Methodological Approaches for Sleep and Vigilance Research. Academic Press; 2022:17-32. doi:10.1016/B978-0-323-85235-7.00010-7

10 Mondino A, González J, Li D, et al. Urethane anaesthesia exhibits neurophysiological correlates of unconsciousness and is distinct from sleep [published online ahead of print, 2022 May 11]. Eur J Neurosci. 2022;10.1111/ejn.15690. doi:10.1111/ejn.15690.

11 Rivas M, Serantes D, Peña F, et al. Role of Hypocretin in the Medial Preoptic Area in the Regulation of Sleep, Maternal Behavior and Body Temperature of

Lactating Rats. Neuroscience. 2021;475:148-162. doi:10.1016/j.neuroscience.2021.08.034

12 Mondino A, Hambrecht-Wiedbusch VS, Li D, et al. Glutamatergic Neurons in the Preoptic Hypothalamus Promote Wakefulness, Destabilize NREM Sleep, Suppress REM Sleep, and Regulate Cortical Dynamics. J Neurosci. 2021;41(15):3462-3478. doi:10.1523/JNEUROSCI.2718-20.2021

13 Mondino A, Cavelli M, González J, Murillo-Rodriguez E, Torterolo P, Falconi A. Effects of Cannabis Consumption on Sleep. In: Monti JM, Pandi-Perumal SR, Murillo-Rodríguez E, eds. Cannabinoids and Sleep: Molecular, Functional and Clinical Aspects. Springer International Publishing; 2021:147-162. doi:10.1007/978-3-030-61663-2_11

14 Mondino A, Cavelli M, González J, Osorio L, Castro-Zaballa S, Costa A, Vanini G, Torterolo P. Power and Coherence in the EEG of the Rat: Impact of Behavioral States, Cortical Area, Lateralization and Light/Dark Phases. Clocks & Sleep. 2020; 2(4):536-556. https://doi.org/10.3390/clockssleep2040039

15 González J, Cavelli M, Mondino A, Rubido N, Bl Tort A, Torterolo P. Communication Through Coherence by Means of Cross-frequency Coupling. Neuroscience. 2020;449:157-164. doi:10.1016/j.neuroscience.2020.09.019

16 Cavelli M, Castro-Zaballa S, Gonzalez J, et al. Nasal respiration entrains neocortical long-range gamma coherence during wakefulness. Eur J Neurosci. 2020;51(6):1463-1477. doi:10.1111/ejn.14560

17 Osorio L, Mondino A, Cavelli M, González J, Torterolo P, Costa A. EEG power spectrum daily variations in sleep and wakefulness. Sleep Science. Published online 2020. doi: 10.5935/1984-0063.20200017

18 Peña F, Rivas M, González J, et al. Sleep and maternal behavior in the postpartum rat after haloperidol and midazolam treatments. Sleep Science. Published online 2020. doi: 10.5935/1984-0063.20200019

19 Cavelli M, Prunell G, Costa G, et al. Electrocortical high frequency activity and respiratory entrainment in 6-hydroxydopamine model of Parkinson's disease. Brain Res. 2019;1724:146439. doi:10.1016/j.brainres.2019.146439

20 Mondino A, Cavelli M, González J, et al. Acute effect of vaporized Cannabis on sleep and electrocortical activity. Pharmacol Biochem Behav. 2019;179:113-123. doi:10.1016/j.pbb.2019.02.012

21 Castro-Zaballa S, Cavelli M, González J, Monti J, Falconi A, Torterolo P. EEG dissociation induced by muscarinic receptor antagonists: Coherent 40 Hz oscillations in a background of slow waves and spindles. Behav Brain Res. 2019;359:28-37. doi:10.1016/j.bbr.2018.10.016

22 Castro-Zaballa S, Cavelli ML, Gonzalez J, et al. EEG 40 Hz Coherence Decreases in REM Sleep and Ketamine Model of Psychosis. Front Psychiatry. 2019;9:766. Published 2019 Jan 17. doi:10.3389/fpsyt.2018.00766

23 Torterolo P, Castro-Zaballa S, Cavelli M, Gonzalez J. Chapter 1 - Arousal and normal conscious cognition. In: Garcia-Rill E, ed. Arousal in Neurological and Psychiatric Diseases. Academic Press; 2019:1-24. doi:10.1016/B978-0-12-817992-5.00001-5

24 Cavelli M, Rojas-Líbano D, Schwarzkopf N, et al. Power and coherence of cortical high-frequency oscillations during wakefulness and sleep. Eur J Neurosci. 2018;48(8):2728-2737. doi:10.1111/ejn.13718

25 González J, Prieto JP, Rodríguez P, et al. Ibogaine Acute Administration in Rats Promotes Wakefulness, Long-Lasting REM Sleep Suppression, and a Distinctive Motor Profile. Front Pharmacol. 2018;9:374. Published 2018 Apr 27. doi:10.3389/fphar.2018.00374

26 Cavelli M, Castro-Zaballa S, Mondino A, González J, Falconi A, Torterolo P. Absence of EEG gamma coherence in a local activated cortical state: a conserved trait of REM sleep. In: ; 2017. https://api.semanticscholar.org /CorpusID:148783466